

# Manufacture, repair and recycling of thermoplastic composite boats

A thesis submitted for the degree of Doctor of Philosophy (Ph.D) at Newcastle University



Mariano E. Otheguy



School of Mechanical and Systems Engineering, Newcastle University,  
Claremont Road, NE1 7 RU, Newcastle upon Tyne, England, UK.

Supervisor: Prof. A. Geoff Gibson  
July 2010

To Lidia and Horacio, whose intense love fuels  
the engine which makes me stand up again, look ahead  
and let my feet guide me towards the horizon

Creative power, is that receptive attitude of expectancy which makes a mould into which the plastic and as yet undifferentiated substance can flow and take the desired form.

— Thomas Troward (1847-1916)

## **Abstract**

The design and construction of boats using thermoplastic composites (TPCs) is an emerging industry derived from the advantages these materials offer. Short manufacturing cycle times, virtually infinite shelf life, increased toughness, no volatiles emission, and the ability to be re-processed and recycled, lead to improved processes and open new and more sustainable manufacturing possibilities for boats and other structures. However, the manufacture, repair and actual recycling of TPCs still present a number of technical challenges. This thesis addresses the five most important of these challenges, from both the academic and industrial points of view.

The manufacturing of TPC structures involves the impregnation of reinforcing fibres with melted resin. This process, known as consolidation, is still to be fully understood. In order to contribute to this understanding, a consolidation model based on existing and newly developed sub-models was developed and applied to experimental data. The results obtained proved that the non-isothermal consolidation of laminates of a thickness typical of boatbuilding, can be approached by applying this model locally on a discretised laminate, fitting well experimental data.

The choice of a cost-effective moulding material is one of the factors currently preventing the widespread use of TPCs in boatbuilding. The vacuum forming of TPCs requires moulds which have considerable strength, and allow high service temperatures and the shape freedom which is typical of boat moulds. A review of commercial and experimental materials and laboratory experimentation on a novel glass-reinforced ceramic composite was carried out, showing that a range of metals and composites are useful for TPC-capable moulds, and that a cost-effective free-shape mould capable of processing any TPC is achievable.

After hull shell manufacturing stiffeners and other internal structure are often required. The manufacturing of such a reinforced and subdivided hull involves the use of a joining technology. Adhesive joining, widely used in thermosetting resin composite boats, cannot be easily used on TPCs due to their low energy surfaces. However, the re-melting ability of thermoplastic resins enables the use of welding, fusion bonding and other joining methods involving molecular diffusion at the bond line. Experiments carried out on lap and T-joints showed that vacuum-assisted local heating can be used for structural assemblies such as

reinforced boat hulls, obtaining strengths that are comparable to existing thermosetting designs.

A TPC boat manufactured and assembled in such way would still require a suitable repair technique that provides a long product life. An emergency repair method capable to return the boat to the water in less than 24 hours without using any mould was devised and tested on a prototype TPC rigid inflatable boat. This was achieved by fusion bonding the edges of a pre-manufactured flat panel to the hull. The flat panel adapted to the hull double curvature by means of vacuum pressure, delivering the required bond quality and strength.

Finally, the disposal of a TPC boat must be addressed after the end of its service life. Current policies and innovative business thinking are leading companies into reusing and recycling instead of landfilling materials. While the mechanical recycling of TPCs, achieved by means of resin re-melting, has been largely studied, the recycling of a real boat containing paint and core material raise questions on how these materials would affect the recycle. An experimental study on the recycling of a TPC real boat was carried out to answer these questions, revealing that despite the deleterious effect of core and paint, the final properties of injection moulded samples were in the region of those of virgin materials.

## Table of contents

Acknowledgements .....	1
Glossary .....	3
Symbols.....	7
Notes.....	10
Publications .....	11
<b>Chapter 1 – General background .....</b>	<b>12</b>
Composite boatbuilding .....	12
Composite materials.....	14
Fibres .....	14
Thermosetting resins.....	15
Thermoplastic resins.....	16
Thermoplastic composites .....	18
Fibre hybridisation.....	19
Manufacturing.....	21
<b>Chapter 2 - Current issues on TPC boatbuilding.....</b>	<b>22</b>
TPC boats .....	22
Current issues in TPC boatbuilding.....	25
Consolidation modelling.....	25
Tooling materials .....	25
Joining.....	25

Repair.....	25
Recycling.....	26
<b>Chapter 3 - State of the art review.....</b>	<b>27</b>
Consolidation modelling.....	27
Polypropylene - glass.....	29
Vacuum forming.....	30
Tooling.....	31
Joining.....	32
Repair.....	34
Non-destructive testing.....	34
Repair of composite boats.....	35
Recycling.....	36
Composite materials recycling.....	37
Recycling of real end-of-life structures.....	39
<b>Chapter 4 – A non-isothermal consolidation model for thick laminates.....</b>	<b>40</b>
Consolidation experiments.....	41
Data post-processing.....	42
Temperature distribution inside the laminate.....	45
Non-isothermal consolidation model.....	48
1-parameter model.....	48
Towards a comprehensive model.....	50

De-bulking.....	51
Impregnation .....	55
Viscosity .....	58
Pressure and permeability.....	59
Bundle permeability .....	60
The Kozeny constant .....	62
Evolution of the volume fraction.....	62
Impregnation length.....	67
Global consolidation .....	68
Summary.....	68
Mathematical solution .....	72
Results and discussion .....	75
Conclusions.....	79
<b>Chapter 5 – Tooling materials for TPC vacuum forming.....</b>	<b>80</b>
Mould requirements.....	80
Performance and cost .....	81
Polymer composite tools.....	82
Metallic tools .....	84
Ceramic tools .....	85
An affordable alternative .....	89
Experimental.....	91



Testing rig .....	91
Addressing the porosity.....	93
Sealing the moulding surface .....	93
Air-tightness test .....	96
Results.....	97
Sealing the back surface .....	100
Air-tightness tests.....	101
Consolidation tests .....	102
Results and discussion .....	102
Conclusions.....	104
<b>Chapter 6 – Fusion bonded T-joints .....</b>	<b>107</b>
Study on lap and T-joints.....	107
Lap shear.....	110
Results and discussion .....	111
T-joints .....	117
Design .....	117
Manufacturing .....	119
Testing .....	121
Results and discussion .....	123
Conclusions.....	128

Chapter 7 – Repair technology for thermoplastic composite boats.....	130
Controlled impact .....	131
NDE inspection .....	134
Fusion bonded patch repair .....	135
Repair procedure .....	138
Repair characterisation .....	143
Micrography .....	143
Tensile tests .....	145
Conclusions.....	149
Chapter 8 – Recycling of end-of-life TPC boats .....	150
Mechanical recycling .....	151
Materials.....	151
Recycling route and equipment .....	152
Results and discussion .....	158
Removed air.....	159
Strength .....	160
Elongation-to-break.....	162
Stiffness .....	164
Impact.....	165
Conclusions.....	167

Chapter 9 – Concluding remarks .....	169
Consolidation modelling.....	169
Tooling .....	170
Joining.....	171
Repair.....	172
Recycling.....	173
References .....	174

## Acknowledgements

This book contains the result of three years of work in thermoplastic composite materials and their application in boats, funded by the European Commission MOMENTUM Marie Curie Research Training Network (RTN), contract No. MRTN-CT-2005-019198. This work would not have been possible without the inspiration, help and support of a long list of people I am truly indebted to.

Firstly, I owe great gratitude to Roberto Palacín, director of the MOMENTUM RTN, who believed in me and hired me as Marie Curie Fellow on the project. His generosity and his flexible and unconditional help have been key to many of my achievements over the last three years.

Thanks also to Geoff Gibson, academic supervisor of this work, for his wise advice and for the freedom he gave me to develop new ideas.

I am especially grateful to Ed Findon, industrial supervisor at the research industrial partner BAE Systems Surface Ships, for his great dedication and support and for the opportunity to get involved in the UK Technology Strategy Board funded project “Lightweight Thermoplastic Composites for Made-to-order Structural Assemblies” and the EC funded project “CleanMould”.

I am also grateful to Bob Cripps (BAE Systems Surface Ships) for his help at different stages of my work.

I am very grateful to all staff at the School of Mechanical and Systems Engineering for helping out with all sorts of issues. I owe particular gratitude to the School Superintendent Ken Madden and all the technicians at the Mechanical Manufacturing Laboratory, who helped with the design and carried out the manufacturing of testing materials and rigs with great diligence, talent and friendliness.

I am also indebted to undergraduate students Tom Derbyshire for his good work on consolidation modelling, John Griffiths for his valuable preliminary work on lap and T-joints, and Holly Phillips for her good early work on recycling.

I also owe gratitude to a long list of professionals, including Christophe Ducret (OCV Reinforcements), Steven Austen (RNLI), Hans Knudsen (COMFIL ApS), PJ Feerick (ÉireComposites), Museok Kwak (The Welding Institute), Dr. Stephen Boyd (University of Southampton), Veronique Michaud and Jérôme Payet (EPFL), Jan Van Herck (Symbion NV) and especially Jan Wastiels (Vrije Universiteit Brussel).

Special thanks to William Waugh, Michael Danby, Teresa Driscoll, Melissa Savage, and Sam and Alice Keynes for their very valuable comments on my work.

Thanks to all who shared with me the office on the third floor of the School: Vincenzo Urso Miano, Gaetano La Delfa, Conor O'Neill, Craig Hudson, Dewan Islam, Cristian Ulianov, for their companionship, helpful comments and friendly working atmosphere.

And finally thanks to Yvonne Geven, a wonderful person who is with me in the sun and the storm, helps me see the light when it feels dark and nourishes my heart with sincere love.

## Glossary

APC-2	PEEK-carbon composite developed by Cytec Industries Inc.
Autoclave	Pressurised oven used to process advanced thermoplastic composites at typical pressures of 1.5 MPa.
Classification society	A classification society is a non-governmental organization in the shipping industry, often referred to as 'Class'. It establishes and maintains standards for the construction and classification of ships and offshore structures; supervises that construction is according to these standards; and carries out regular surveys of ships in service to ensure the compliance with these standards.
Consumables	Set of layered materials needed in certain composite manufacturing processes such as resin infusion or vacuum forming for instance.
CTE	Coefficient of thermal expansion.
Drapability	The ease of conforming to a complex surface, often applied to textiles and technical fabrics.
E-glass	A general purpose family of glasses with a typical composition of SiO <sub>2</sub> 54wt%, Al <sub>2</sub> O <sub>3</sub> 14wt%, CaO+MgO 22wt%, B <sub>2</sub> O <sub>3</sub> 10wt% and Na <sub>2</sub> O+K <sub>2</sub> O less than 2wt%. Also known as electrical glass, it is the most commonly used in composite reinforcement and also in electrical insulation due to its high resistivity.
FEP	Fluorinated Ethylene Propylene.
Isotropic	Exhibiting equal physical properties all directions.
LVDT	Linear variable differential transducer. A type of electrical transformer used for measuring linear displacement.

MDF	Medium density wood fibreboard.
NDE	Non-destructive evaluation, also known as NDT (Non-destructive testing).
Orientation	The direction at which the fibres are longitudinally pointing. Conventional notation of fibre orientation as used in the text, is $[+60^\circ, -60^\circ]_s = [+60^\circ, -60^\circ, -60^\circ, +60^\circ]$ , subscript "s" denoting that the stacking sequence is repeated symmetrically. The corresponding laminate has 4 layers, of which the first one forms $60^\circ$ anticlockwise with a convenient direction, usually significant for the moulded component. The second and the third layers form $60^\circ$ clockwise; and the last one $60^\circ$ anticlockwise again.
PA	Polyamide.
PBT	Polybutylene terephthalate
PEEK	Polyether ketone.
PEI	Polyetherimide
PEKK	Polyether ketone ketone
PET	Polyethylene terephthalate.
Plug	The mould used for the manufacturing of the final mould intended for component manufacturing. As moulds for composite boats are usually female, the plugs used to manufacture them are usually a male replica of the final hull, mostly manufactured by numerically controlled machining.
Polymer	A polymer is a large molecule composed of repeating structural units typically connected by covalent chemical bonds.

Polymerisation	The process of combining many small molecules known as monomers into a covalently bonded chain.
PP	Polypropylene.
PPS	Polyphenylene sulfide
Precursor material	Materials used to manufacture composite laminates. Precursors often contain resin and fibres, for example in the form of thermosetting or thermoplastic pre-pregs or commingled fabrics.
Prepreg	Precursor material which comprises fibres pre-impregnated with resin.
PS	Polystyrene
Resin infusion	Composite manufacturing process which attains dry fibre impregnation by allowing a liquid resin to flow into the cavity formed by a rigid mould and a flexible vacuum bag, driven by vacuum pressure.
RIB	Rigid inflatable boat.
S.G.	Specific gravity, i.e. the ratio of the density of a substance to the density of a reference substance, usually water.
Scantling	Measurement of prescribed size, dimensions, or cross sectional areas, normally used in boatbuilding.
SEM	Scanning Electron Microscopy is an imaging technique involving the scanning of the surface with a high-energy beam of electrons in a raster scan pattern. The electrons interact with the atoms that make up the sample producing signals that contain information about the sample's surface topography, composition and other properties.



Slamming	Impact of the bottom structure of a boat onto the sea surface.
$T_g$	Glass transition temperature.
$T_m$	Melting temperature.
TP PI	Thermoplastic Polyimide
TPC(s)	Thermoplastic composite(s).
Twintex®	Set of materials commercialised by Owens Corning Vetrotex, comprising PP or co-PBT and glass. Twintex® T PP 60, the material most used in the experiments described in the text, is a commingled fabric containing Polypropylene (PP) and 60wt.% of continuous glass fibres. Its natural color is white, but it is also available pigmented with carbon black.
VOCs	Volatile Organic Compounds are chemical organic compounds that have high enough vapor pressures to significantly vaporize at room temperature.
VUB	Vrije Universiteit Brussel (Free University of Brussels, Flemish-speaking, not to be confused with Université Libre de Bruxelles, French-speaking).

## Symbols

$\eta$	Resin viscosity.
$\eta_0$	Arrhenius constant for the resin viscosity.
$\lambda$	De-bulking compaction limit.
$\rho$	Density (of composite if not stated otherwise).
$\rho_{material X}$	Density of material X.
$a$	Coefficient of the consolidation rate X, in the formulation of the local volume fraction: $V_f = a \cdot X^b + c$ .
$A, B$	Fitting constants associated to the initial, solid-state de-bulking.
$A_i, B_i, m_i$	Fitting constants.
$b$	Exponent of the consolidation rate X, in the formulation of the local volume fraction: $V_f = a \cdot X^b + c$ .
$C$	Gebart constant of permeability.
$c$	Independent term in the formulation of the local volume fraction: $V_f = a \cdot X^b + c$ .
$C, D$	Provisional fitting constants.
$f$	Fitting factor.
$K$	Arrhenius exponent for the resin viscosity.
$k_0, (k_{ii})$	Kozeny constant (in the direction of the axis $i-i$ ).
$L$	Resin penetration distance to be covered.

$M_a$	Mass of constituent $a$ .
$M_i$	Mass of constituent $i$ .
$p$	Pressure applied during manufacturing.
$P$	Resin front pressure.
$r$	Depth of melt penetration, in the direction of the radius of a circular bundle.
$r_f$	Average fibre radius.
$S, (S_{ii})$	Permeability of the fibre bundle (in the direction of the axis $i-i$ ).
$S.G.$	Specific gravity.
$t$	Time.
$T$	Local absolute temperature.
$T_c$	Consolidation temperature
$T_g, T_g$	Glass transition temperature of the resin.
$T_m, T_m$	Melting temperature of the resin.
$V$	Volume occupied by the composite.
$V'_a$	Maximum glass volume fraction.
$v_a$	Volume occupied by constituent $a$ .
$V_f, (V_{f_i})$	Volume fraction of glass fibres (of constituent $i$ ).
$V_{f0}$	Glass volume fraction at the beginning of the liquid-state impregnation.
$V_{f0void}$	Void content at the beginning of the solid-state de-bulking.

$V_{fG}$	Nominal glass volume fraction.
$W_i$	Weight of constituent $i$ .
$W_{f_i}$	Weight fraction of the constituent $i$ .
$\bar{X}$	Global consolidation.
$\bar{X}$	Local consolidation.
$X$	Local impregnation degree.
$X_d$	Local consolidation degree due to de-bulking.
$X_i$	Consolidation degree in stage " $i$ ".
$X^i$	Scaled impregnation degree.

## Notes

All experimental work has been done at the School of Mechanical and Systems Engineering, Newcastle University, at approximately 20°C, 1000 mbar, unless stated otherwise.

Additional work was done at the facilities of BAE Systems Surface Ships. This shipyard changed its legal name whilst this work was being done. Former names were VT Halmatic, Portchester Shipyard and BVT Surface Fleet Support and BAE Systems Surface Ships, Small Boat Centre Of Excellence. The company will be referred as BAE Systems in the text for convenience. The publication of all images and data referring to BAE Systems has been authorised by courtesy of BAE Systems Surface Ships.

All charts and graphs error bars show 95% confidence values.

The image on the cover shows an epoxy-glass Atlantic 85 RIB, sister boat of the Twintex® experimental RIB. This image, as well as all other images of RNLI boats, is courtesy of the RNLI (Royal National Lifeboat Institution).

All tables and figures from the book Marine Composites, by Eric Greene Associates [1] (downloadable at [http://ericgreeneassociates.com/images/MARINE\\_COMPOSITES.pdf](http://ericgreeneassociates.com/images/MARINE_COMPOSITES.pdf)), have been reproduced with permission of the author.

Reproduction of Figures 4.13 and 4.14 courtesy of Professor Andrew Long, University of Nottingham.

Reproduction of Figures 4.10, 4.11 and 4.16 courtesy of Muhammad Ijaz.

Reproduction of Figures 4.12 and 4.17 courtesy of John Wiley and Sons.

## Publications

Some of the contents of this thesis have been published in the following journal articles:

Otheguy, M.E., Gibson, A.G., Robinson M. **“Fusion bonding of structural t-joints for thermoplastic composite boats”**, under peer-review for publication in the Journal of Thermoplastic Composite Materials as of June 2010.

Otheguy, M.E., Gibson, A.G., Findon, E., Cripps, R.M. **“Repair technology for thermoplastic composite boats”**, International Journal of Small Craft Technology (Royal institution of Naval Architects) International Journal of Small Craft Technology, Volume 152, Part B1, 2010, pp. 33-40.

Otheguy, M.E., Gibson, A.G., Findon, E., Cripps, R.M., Mendoza, A. Ochoa, Castro, M. T. Aguinaco. **“Recycling of end-of-life thermoplastic boats”**. Plastic, Rubber and Composites: Macromolecular Engineering, Volume 38, Numbers 9-10, December 2009, pp. 406-411.

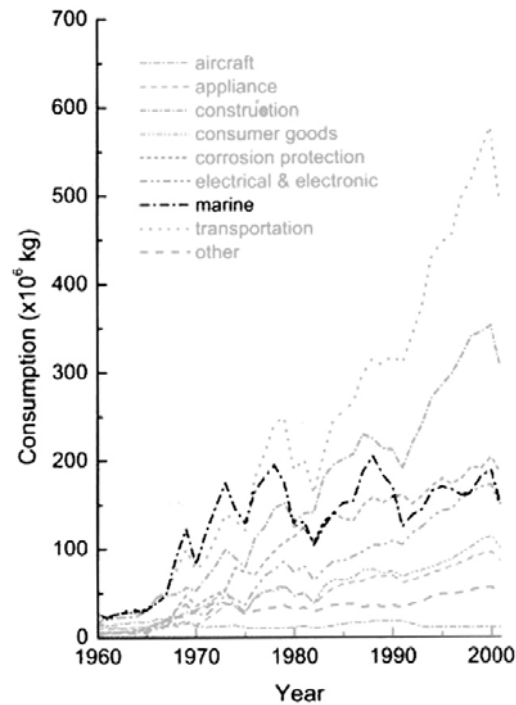
## **Chapter 1 – General background**

After 60 years of evolution, composite materials have become dominant in the construction of military and leisure boats. Recent developments in thermoplastic composites (TPCs) provide potential advantages over more traditional materials, making them suitable for small and medium-size boats. This chapter introduces a set of basic concepts on composite boatbuilding, composite materials and particularly TPCs. Such concepts are useful to understand why composites have succeeded in boatbuilding, the advantages of TPCs over traditional materials and the challenges to overcome. These challenges constitute the main motivation and work body of this thesis, and will be addressed in full in the following chapters.

### **Composite boatbuilding**

Fibre reinforced plastics (FRPs) have been increasingly used in boatbuilding since the early 1950s. After World War II, the U.S. Navy built a 9 m long composite craft based on its potential for reduced maintenance and production costs. Despite the difficulties of a newly developed material, the success of this project led to a rapid increase in the construction of composite small craft such as lifeboats and yachts [2]. In addition to virtually no maintenance and low cost, the flexibility of composite construction and the good finish of seamless hulls boosted their production, which in the U.S. alone multiplied sixfold in the next 15 years (Figure 1.1).

Additional advantages such as low weight, good vibration damping, high corrosion and impact resistance, and ease of fabrication, maintenance and repair led to the manufacture of increasingly longer boats [3, 4].



**Figure 1.1: Evolution in the use of polymer composites in the United States – source: Association of American Composite Fabricators, as in [5]**

Particularly, the 1980s and 1990s saw a rapid development in large composite naval ships, only limited by the comparatively reduced hull beam stiffness of glass reinforced plastics (GRP). Deformations on the hull beam limit the size of glass-reinforced composite ships to approximately 30 m long. Beyond this length, a compromise may be accepted between low stiffness and other characteristics, as the non-magnetic properties of composite mine counter measure vessels (MCMVs), reaching 55 m long. For larger ships, the much stiffer carbon fibre is needed, as demonstrated by the 72 m long Royal Swedish Navy corvette Visby, launched in June 2000. This successful design combined standard and innovative materials and construction techniques, obtaining a hull weight reduction of 30% with respect to steel, with remarkably low cost despite the use of expensive fibres. The low hull weight translated into increased range and reduced fuel consumption [5], which raised the interest in composites for large vessels. As a result, composite ships in the region of 100 m long are planned for construction between 2010 and 2020 [6].



## **Composite materials**

Composite materials are engineered materials made from two or more constituent materials with significantly different physical or chemical properties. These constituent materials, which remain separate and distinct within the finished structure, fall into two categories: matrix and reinforcement. The matrix material surrounds and supports the reinforcement materials, maintaining their relative positions, while the latter contribute with their mechanical and physical properties to enhance the matrix properties. Such synergism produces material properties unavailable from the individual constituent materials, while the wide variety of matrix and strengthening materials and configurations allow the designer of the structure to choose an optimum combination. In contrast to metals and other isotropic materials, these constituents are put together by the constructor, in such way that the final properties will depend on how exactly this is done. In particular, which constituents are used, how they are arranged and which fabrication process transforms them into a structure.

### **Fibres**

In boatbuilding, these constituents are usually a polymer matrix which binds together and transfers loads to reinforcing fibres. Traditionally, the fibres used in composite boats have been E-glass. However, a rapid diversification took place in the 1980s with the introduction of carbon, aramid and other types of glass fibres. Glass fibres are made of silicon dioxide and other minerals [7], melted and extruded into fibres between 5 and 25  $\mu\text{m}$  in diameter. This composition is related to their relatively good strength to weight characteristics and chemical resistance, ease of processability and relatively low price, reasons why glass fibres account for approximately 90% of the fibres used in reinforced plastics, and 80% in composite boats and ships [8]. However, their silicon dioxide base also makes these fibres to be sensitive to silicate-based compounds as certain ceramic matrices. As we will see in Chapter 5, this chemical incompatibility may have a negative impact on the cost-effectiveness of some tooling material alternatives.

## **Thermosetting resins**

The reinforcing fibres are bound together by means of the matrix, often a thermosetting polymer resin. Of all polymers, polyester resins are the most used in marine structures, again because of their low price and good mechanical and chemical properties. Vinyl ester has superior mechanical and chemical properties [10], but also higher cost. Epoxy resins complete the most common resins used in marine composites [4]. Epoxies are more difficult to process than the other two, but deliver better properties in composites incorporating glass and carbon fibres. At present, most applications in high performance composites make use of epoxy resins [8].

Thermosetting resins harden by means of a non-reversible chemical reaction, usually known as curing, the outcome of which is a cross-linked polymer. This micro-structural state implies that the long molecules of the resin are linked to each other by means of covalent bonds [9], forming a three-dimensional network in a huge single molecule [10] (Figure 1.3). The formability derived from this process and the good properties of the resulting composites have boosted their manufacture, contributing to lowering the prices of precursor materials. On the negative side, the irreversibility of the chemical reaction implies that these resins cannot be re-formed or re-manufactured. Their recyclability has been proven to be profitable only if it involves the recovery of carbon fibres [11]. Also, the setting reactions imply a limited shelf life and involve the release of volatile organic compounds (VOCs), representing a health risk in the working environment [12, 13].

The low viscosity of the first thermosetting resins allowed for relatively easy fibre impregnation, the first composite boats being fabricated by hand lay-up. Following this method, the resin was manually rolled on dry mats or fabrics laid up on the mould. More efficient methods were developed later as resin infusion and vacuum curing of pre-pregs, both involving a vacuum bag which encloses the whole component. This method cuts VOC emissions and also provides pressure and air extraction. These lead to a drop in void contents from 5% to 1%, leading to a significant improvement of the mechanical properties of manufactured parts.

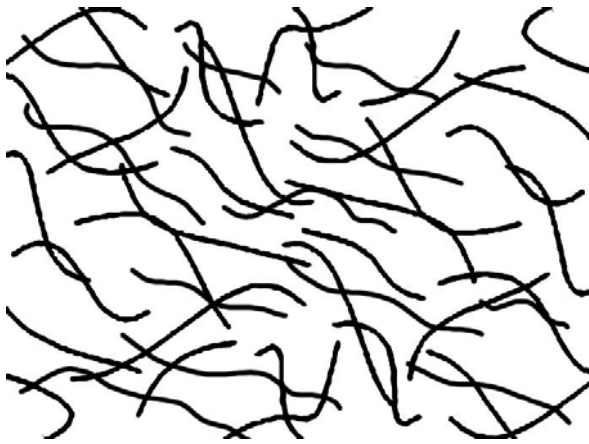


Figure 1.2: Polymer chains in a thermoplastic resin

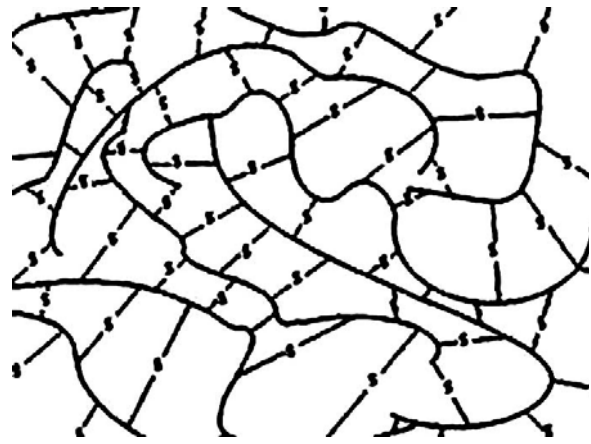


Figure 1.3: Cross-linked thermosetting resin

## Thermoplastic resins

Thermoplastic resins contain long polymer chains which are held together by means of weak electrostatic attraction [14] (Figure 1.2), also called Van der Waals bonds. When the polymer chains in the entangled regions are randomly arranged, the polymer is called amorphous. By contrast, if the chains fold next to each other into regular structures, it is known as crystalline. High crystallinity implies strong inter-atomic attractions, and leads to improved mechanical and physical properties. A typical crystalline polymer has up to 90% of its atoms in crystalline structures and the remainder in amorphous regions, which is why it is also known as semi-crystalline.

Van der Waals bonds are approximately 30 times weaker than the covalent bonds present in cross-linked thermosetting resins, allowing thermoplastic resins to behave as liquids at temperatures beyond their melting temperature,  $T_m$ . The temperature response of crystalline thermoplastics changes rapidly around their melting point, which is associated with the breakup of the crystalline regions and subsequent free movement of the polymer chains. By contrast, amorphous polymers do not have a distinct melting point, but a more gradual onset of free movement. This is characterised by increasing vibrations and rotations within the polymer chains that can be detected as transitions, the most important of which is called glass transition temperature,  $T_g$ .

The ability of thermoplastic resins to reflow beyond their melting point facilitates manufacturing processes free of chemical reactions, enabling manufacturing, re-

manufacturing and repair possibilities unattainable with thermosets. Some important thermoplastic resins and their melting temperatures are shown in Figure 1.4.

Another property of thermoplastics is their high toughness, derived from the weak chemical bonds amongst polymer chains. Tough materials are very useful for marine applications, because of their good response to the typically dynamic and sudden loads of the marine environment.

Conversely, the chemistry of thermoplastics naturally involves inert chemical groups, whose non-polarity leads to a low free energy surface [15]. This is the reason why thermoplastics are difficult to paint and bond with adhesives, usually requiring thorough and expensive surface treatments and primers prior to coating or adhesive joining.

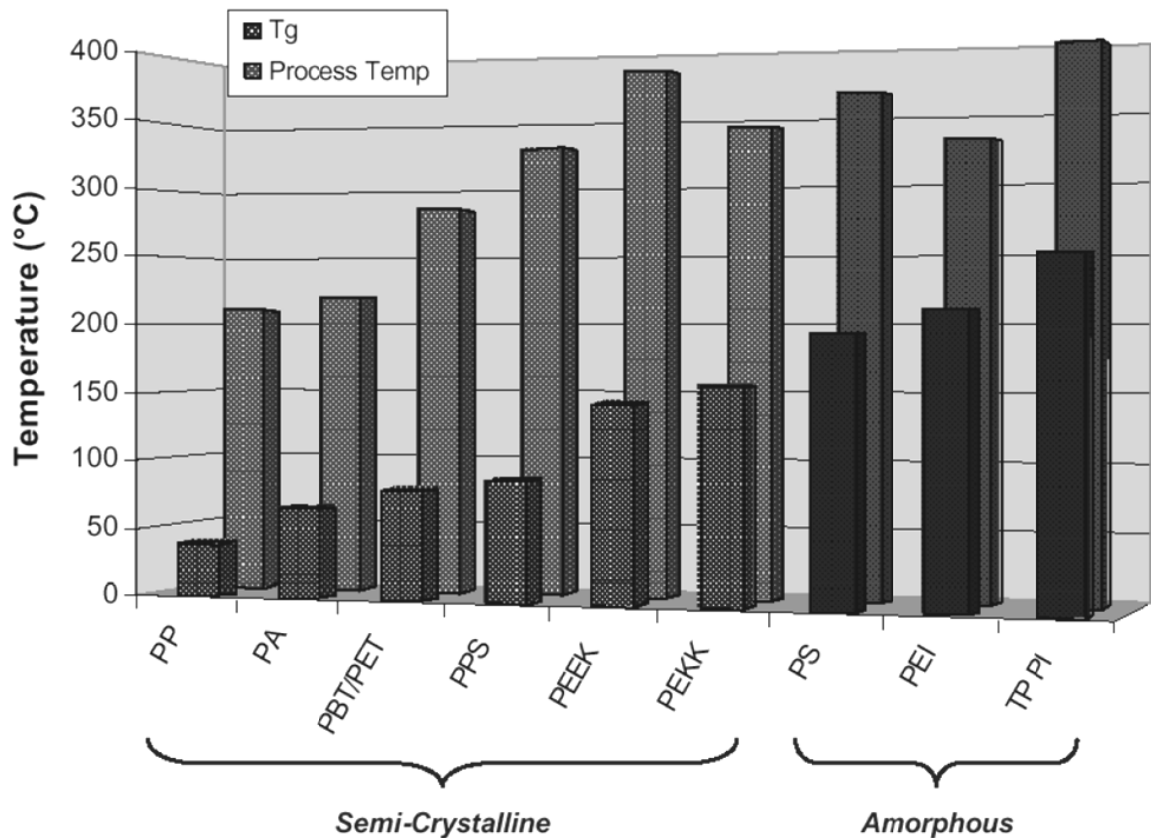


Figure 1.4: Glass transition and approximate processing temperatures for several thermoplastic resins (from[16]) – see Glossary for definitions

## Thermoplastic composites

Thermoplastic resins are widely used in a variety of industries, some of which enhance the resin properties with a reinforcement. Different manufacturing processes applied to resins reinforced with powder and fibres of various lengths produce a range of materials with different properties. Of these, continuous fibres reinforced thermoplastics (CFRT) best meet the properties required in small and medium-sized boats.

Whereas short reinforcement can be compounded together with the resin in convenient moulding pellets, continuous fibres require other impregnation processes. Unfortunately, the impregnation techniques useful for thermosets cannot be applied to thermoplastics, whose viscosity is typically 100 to 1000 times higher [17]. As a result, the impregnation of a standard bundle of fibres with such resin is equivalent to spreading a piece of chewing gum over 300 mm per fibre unit length [18], as shown in Figure 1.5. Additionally, the manufacturing of pre-pregs for boats is not as practical as with thermosets, because pre-consolidated TPC panels are much stiffer and lack the characteristic stickiness of thermosetting pre-pregs. This makes lay-up on a boat mould much more difficult. However, a number of recent developments facilitate continuous fibre impregnation for large panels, enabling their use in boatbuilding and other similar industries.

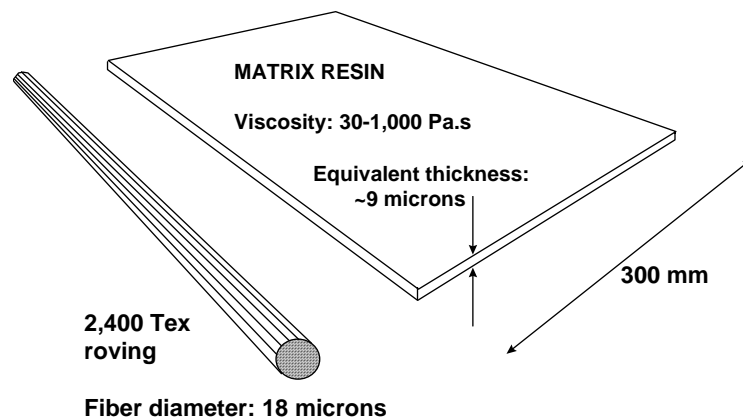


Figure 1.5: The impregnation of a bundle of 2,400 fibres with a diameter of 18  $\mu\text{m}$  is equivalent to spreading a 9  $\mu\text{m}$  thick layer of resin over a length of 300 mm

### ***Fibre hybridisation***

Fibre impregnation can be achieved by reducing the distance to be covered by the resin in order to impregnate the fibres [18]. In the example of Figure 1.5, this would be equivalent to spreading smaller pieces of chewing gum, each over a smaller surface. This can be achieved by combining polymer and reinforcing fibres in such way that, after melting, the resin only needs to cover a distance equivalent to few times the fibre diameter. Several methods have been used to reduce the distance between polymer and reinforcing fibres, such as stacking layers of fibres and resin film, or coating fibre bundles with resin powder. While these methods may be appropriate for the manufacturing of small panels with a hot press, their reduced drapability and sensitivity to lay-ups other than horizontal make them impractical for boat construction.

As an alternative to film stacking and powder coating, polymer fibres can be mixed with reinforcing fibres, leading to a hybrid yarn. This method, called fibre hybridisation, stands out because of the high drapability of the resulting precursor materials. Also, because of the ease of fibre impregnation attained, as such fibre arrangement requires a very short resin penetration distance to achieve complete impregnation. Of all methods of fibre hybridisation, which are listed in Figure 1.6, commingled fabrics have been favoured for their use in boats due to their drapability, robustness and good properties of the final components. For this reason, the work contained in this thesis is focussed in the use of commingled PP-glass fabrics.

It is worth mentioning that the actual dispersion of polymer and reinforcing fibres is limited by how exactly they are hybridised. For example, the air texturing method (Figure 1.7) is relatively simple and inexpensive, hence widely used. However, it delivers commingled yarns (Figure 1.8) which typically suffer from a certain degree of glass fibre misalignment and segregation of resin and glass fibres. As it will be shown and discussed in later chapters, this still allows for appropriate mechanical properties at macroscopic level. However, its influence on microscopic phenomena cannot be neglected, particularly regarding consolidation modelling.


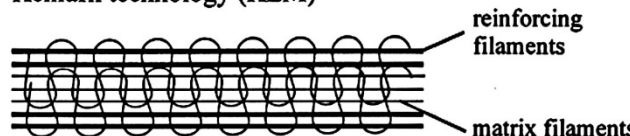


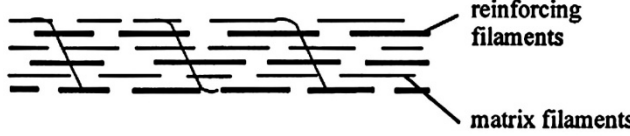
Technology	Geometry of fibre arrangement
<p>Parallel winding of reinforcing and thermoplastic matrix filaments (side-by-side, SBS)</p>  <p>reinforcing filaments</p> <p>matrix filaments</p>	<p>parallel arrangement of reinforcing and matrix filaments</p>
<p>Kemafil technology (KEM)</p>  <p>reinforcing filaments</p> <p>matrix filaments</p>	<p>parallel arrangement of matrix fibres surrounded by parallel reinforcing fibres in the core, sheathed by matrix fibres in the skin</p>
<p>Air texturing (COM)</p>  <p>reinforcing filaments</p> <p>matrix filaments</p>	<p>reinforcing and matrix fibres are commingled; the arrangement of reinforcing fibres is out of yarn axis</p>
<p>Friction spinning (FS)</p>  <p>reinforcing filaments</p> <p>matrix filaments</p>	<p>parallel arrangement of reinforcing fibres in the core and spun fibres in the skin</p>
<p>Schappe technology (SCH)</p>  <p>reinforcing filaments</p> <p>matrix filaments</p>	<p>mixture of discontinuous reinforcing and matrix fibres surrounded by continuous matrix filaments</p>

Figure 1.6: Hybrid yarn structures and corresponding production technologies, from [19]

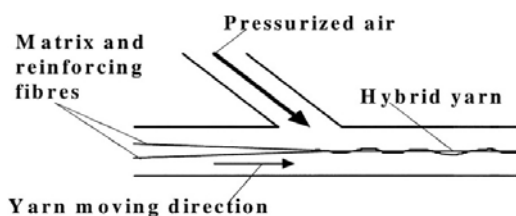


Figure 1.7: Air texturing method of fibre hybridising, from [19]

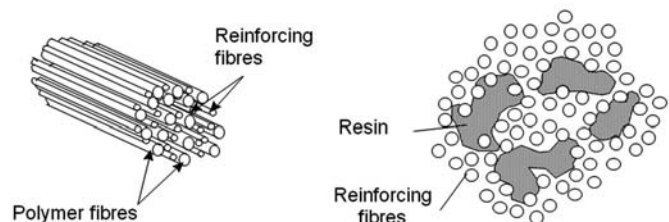


Figure 1.8: Commingled fibre bundles facilitate the impregnation by reducing the distance covered by the resin melt

## ***Manufacturing***

In order to obtain laminates of the desired characteristics, the commingled fabrics undergo a process known as consolidation. By means of heating and pressure, the resin fibres first soften and then melt down, impregnating the reinforcing fibres. Ideally just after complete impregnation and void elimination, the part is cooled down to room temperature, ready to be used or joined to other parts. While a high heating rate is usually preferred for faster production cycles, a low cooling rate leads to a high degree of crystallinity, improving the final properties of the laminates [20].

The consolidation of commingled fabrics can be achieved by several methods. Amongst them, vacuum forming best matches the manufacturing needs of boatbuilding, because of the relative low cost and simplicity of moulds and machinery needed. The TPC plies to be vacuum formed are laid-up on the mould tool and covered with a bagging film which is sealed to the mould tool. The air-tight cavity formed is subjected to vacuum, which leads to the application of the atmospheric pressure ( $\sim 100$  kPa) onto the entire laminate. The whole set is then heated to the processing temperature until full consolidation has taken place, and subsequently cooled at the desired rate. Intermediate layers of consumables facilitate a well distributed vacuum pressure (breather) and the release of breather and bag after processing (release film). The moulds used with this method can be much simpler and cheaper than those needed for compression moulding, because of the lower pressures they need to withstand. All the mouldings manufactured in this research work have been produced by vacuum forming.



## **Chapter 2 - Current issues on TPC boatbuilding**

The properties of TPCs allow a faster fabrication of tougher composite parts with no volatiles emissions, easier material storage and enhanced recyclability. These advantages have already been captured by the first generation of TPC boats. However, a number of aspects of the construction of boats with these materials require further development, especially towards the construction of large and complex assemblies. These aspects constitute key research areas in TPC boatbuilding, which are introduced in this chapter and investigated in depth in chapters 3 to 8.

### **TPC boats**

The construction of small boats with thermoplastics was first done by rotational-moulding, consisting of a boat-size metallic mould which is filled with pellets containing resin and powder of short fibre reinforcement. With this method, the whole mould is heated and rotated so that the reinforced resin spreads all over its inner surface and coalesces, producing a one-piece hull. The associated cost of this method has so far restricted this manufacturing process to series production of boats of up to 7 m long [21, 22].

The development in the 1980s of continuous fibre reinforced TPCs provided a set of strong materials capable of toughness and temperature resistance beyond the limits of the existing thermosets [23]. Rapidly adopted by the automotive and aerospace industries, many thermoplastic resins were nevertheless unsuitable for boats due to part size and boatbuilding market constraints. However, the low cost, low processing temperatures and adequate strength and toughness of Polypropylene (PP) led to the development in the 1990s

of air-textured commingled PP-glass fabrics suitable for boatbuilding and other applications. These new materials offer the composite boat builders a number of potential advantages against thermosets which are summarised in Table 2.1.

**Table 2.1: Comparison between thermoplastic and thermosetting composites in the context of boatbuilding, edited from [24]**

Thermoplastic composites	Thermosetting composites
+ No chemistry involved, no emission of VOCs	– Harden by a chemical reaction, involving
+ Unlimited shelf life	– Limited shelf life due to ongoing setting reactions, pre-pregs usually needing storage at temperatures well below 0°C [25]
+ Short processing cycles	– Long curing cycles
+ Re-processable and recyclable	– Setting reactions non-reversible
+ High toughness	– Poor toughness
+ High chemical resistance	– Poor chemical resistance
– Novel or experimental technology	+ Established technology
– Low energy surface prevents ease of adhesive joining and painting	+ Adhesives and coatings are a well established technology
– High viscosity when melted	+ Ease of fibre impregnation due to low viscosity

In view of these advantages, recent experimentation was carried out for the manufacture of boats with this material, delivering the first TPC rigid inflatable boat (RIB, Figure 2.1) in 2000 as a demonstrator of the European Commission (EC)-funded project EnviroComp. BAE Systems, the industrial partner in the project, used the newly developed technology for the manufacturing of very cost-effective, simple-shaped assault boats (Figure 2.2) and other experimental RIBs as the Twintex® Atlantic 85 (Figures 2.3 and 2.4), tested in service by the Royal National Lifeboat Institution (RNLI). Other companies recently started to use commingled PP-glass for boats, such as the Irish manufacturer ÉireComposites, who developed the process of a monocoque catamaran (Figure 2.5), launched commercially in 2005 [26], and the German boat builder Mega Sports Vertriebs, who presented a set of TPC

canoes in 2008 (Figure 2.6) [27].



Figure 2.1: Pacific 22 MK II, manufactured by BAE Systems, winner of a JEC Award in 2000



Figure 2.2: Production assault boat (BAE Systems), British Royal Navy



Figures 2.3 and 2.4: Twintex® Atlantic 85, developed by BAE Systems for the RNLI



Figure 2.5: Twincat, 4.60 m long catamaran manufactured by ÉireComposites for French boatbuilder 2win, winner of a JEC Award in 2006



Figure 2.6: Open canoe, 3 m long, manufactured by Mega Sports Vertriebs

## **Current issues in TPC boatbuilding**

The successful pioneering cases described above, while proving the suitability of TPCs for boatbuilding, also highlighted the need for further development in various areas. As a starting point for this research work, it was decided to identify the most important of these areas from the industry point of view. A series of fruitful meetings with engineers from BAE Systems and other collaborating companies led to a list of five research areas:

### ***Consolidation modelling***

The mechanisms involved in the consolidation of commingled TPCs under vacuum are not fully understood. Whereas other manufacturing processes have been subject of extensive research, there literature available on vacuum forming is very limited. Hence, further work on consolidation modelling would benefit the understanding and also provide the basis for practical tools useful for the boatbuilding industry.

### ***Tooling materials***

Suitable mould materials have low service temperature limits, provide limited formability or are still very expensive. Hence, a cost-effective suitable material for free-formable moulds capable of processing a range of thermoplastic composites (TPCs) suitable for marine structures is still to be found.

### ***Joining***

The joining of manufactured parts is still an issue. The chemistry of thermoplastic resins provides a low energy surface which prevents adhesives from attaining as good results as those observed on thermosets. They require thorough and expensive surface preparation and strengths attained are still low. This is preventing the manufacturing of large assemblies, hence the design and fabrication of medium-size boats. Therefore, the development of a joining technique is an important issue to be addressed.

### ***Repair***

At present, small repairs of simple geometries are carried out by vacuum-assisted fusion bonding, taking advantage of the re-melting ability of thermoplastic resins. Also, the re-

consolidation of the entire structure has been proven to heal the UV degradation and small damages and is being used to deliver an as-new repaired boat. However, the repair of double curvature panels in boats with internal structure, especially in the absence of a suitable mould presents another issue whose solution would enable the development of more complex and larger marine structures and their maintenance.

### ***Recycling***

There is an increasing concern regarding the environmental impact of products and their end-of-life disposal management. Recent legislation regulates the disposal of consumer durables, in particular restricting the landfilling of composites and requiring after-life product recovery as in the case of automotive industry. Reuse and recycling of materials can be a profitable alternative to landfilling, although the recyclability of thermosetting composites is limited. Thermoplastic resins, due to their ability to re-melt, offer additional possibilities for composite recycling. However, thermoplastic boats may incorporate other materials such as sandwich core and paint, which may make their recycling more difficult. Hence, a study on the recyclability of real end-of-life TPC boats would significantly contribute to the development of new material management strategies.

## **Chapter 3 - State of the art review**

In the five key research areas identified at the end of the previous chapter, a general lack of literature available was acknowledged. The reason for this is twofold. On one hand, the developments needed towards a feasible, repeatable and high quality TPC boat construction are of very practical nature, often the result of industrial applied research. The eventually successful results of such research are seldom published in the public domain because they constitute a serious commercial advantage for the companies involved. Hence the scarcity of available literature on recent developments in the fields of tooling materials and repair for instance. On the other hand, TPC commingled fabrics are relatively young materials and many of the existing developments in this area are related to compression moulded automotive parts rather than vacuum formed large structures as boats. Therefore, limited or no information was available on consolidation models relating to vacuum forming, or bulk heating fusion bonding applied to joints and repairs. However, it was necessary to determine the state of the art towards a scientific contribution on TPC boatbuilding. With this objective, a comprehensive review was carried out, combining the traditional literature review where it provided sufficient background, and the gathering of industrial expertise provided by BAE Systems and other companies where it did not.

### **Consolidation modelling**

Vacuum forming, recently developed in comparison to compression moulding, is affected by variations in two process parameters: time and temperature. By contrast, compression moulding also requires control of the applied pressure. Given the reduced scope for variations and possibilities and relative novelty of vacuum forming, the available literature

about consolidation models focussed on compression moulding [20, 28-36] is abundant in comparison with the relatively scarce information available on consolidation under vacuum [37, 38].

In the 1980's, before the development of the first consolidation models applicable to TPCs, the impregnation of a dry fibre bed was studied with syrups, oils and thermosets. These studies aimed to explain the penetration of a liquid through an aligned fibre bed and find the permeabilities for a given fibre arrangement. Gutowski et al. [39] produced a model of the transverse permeability of unidirectional carbon fibre bundles, based on the characteristics and orientation of the reinforcing fibres only. This model, which has achieved unmatched fitting with experimental data [40], has been applied extensively in later works on the impregnation of fibre networks of various types by thermosetting and thermoplastic resins.

A year later, Lee and Springer [20] published the first comprehensive consolidation model for TPCs, focused on PEEK-carbon. This model comprised three stages during the manufacturing of thermoplastic composites: impregnation, consolidation and crystallisation. The impregnation stage assumed resin laminar flow along the fibres and transverse flow according to Darcy's empirical law for flow through porous media, which will be discussed later in this chapter. Darcy's law is affected by the transverse permeability of the fibre bed, which Lee and Springer approximated using viscous flow through an array of cylinders. The subsequent consolidation stage involved the coalescence and also molecular diffusion of already impregnated bundles. This stage was later found to be equivalent to less than 1% of the total consolidation [34]. For the final stage, the model included the effects of varying the cooling rate on the resin crystallinity. The model achieved acceptable correlation with experimental data in all three consolidation stages.

Van West et al. [31] proposed a more elaborate model for the consolidation of compression-moulded PEEK-carbon composites. The model comprised inter-bundle compaction related to material softening, followed by intra-bundle impregnation. The impregnation of the fibres was modelled using the Gutowski sub-model of the fibre bed permeability, allowing for fibre movement during resin flow. The resin was assumed to flow only across the fibres until full impregnation. This model was later modified to enable application to non-Newtonian fluids [33] and integrated with a model of fabric deformation in an attempt to model the

consolidation of PP-glass fabrics. The non-Newtonian approach was recently applied by Gennaro et al. [28], on the basis that polymer melts show such behaviour, showing a non-linear relationship between stress and shear rate. Polymers actually show Newtonian behaviour for low resin flow velocities, changing to non-Newtonian if this velocity increases [35]. Hence, for low resin velocities it is reasonable to assume a Newtonian behaviour as found in most of the available results on compression moulding consolidation models. This assumption is particularly relevant to vacuum forming, because occurring resin velocities are much lower than in compression moulding.

### ***Polypropylene - glass***

The first study on the consolidation of PP-glass laminates was published in 1994 by Klinkmüller et al. [30]. The impregnation of Twintex® PP-glass unidirectional yarns was modelled using existing sub-models for resin viscosity (Arrhenius) and flow (Darcy), and fibre bed permeability (Gutowksi), with good correlation to experimental results. The values of fitting constants were very useful for further works on the same materials. Contemporaneously, Ye et al. [32] progressed works on the consolidation of PEEK-carbon commingled composites. As they reported, polymer and reinforcing fibres are not evenly distributed in the actual commingling process, leading to a two-stage consolidation process. This concept, which has become predominant in later publications, consists of resin coalescence both within and outside of the reinforcing tows, subsequent resin pool formation around the tows and final liquid impregnation back into the fibre bundles. The model was fitted to experimental data, concluding that the degree of commingling was approximately 75%. The value set for the Kozeny constant, a fitting constant related to the permeability sub-model, was 3-4 orders of magnitude higher than the usual values found in the literature. This may have been intended to absorb other inaccurate assumptions within the model.

Bernet et al. [34] adopted the same two-stage consolidation process, taking into account an air pressure increase due to closing voids within fibre bundles. Trapped air in closed voids in the resin and its possible dissolution by means of increasing pressure are typical phenomena in compression moulding. Nevertheless, theoretical absence of air and reduced pressures prevent the occurrence of either phenomenon in vacuum forming. Bernet and co-workers



implemented a permeability sub-model proposed by Gebart [41], based on the advantage that it does not have any associated fitting constant. However, precisely because of lacking a fitting ability, it gives the same permeability for perfectly aligned and somewhat misaligned fibre bundles, which is an arguable assumption.

An innovative statistical approach was undertaken by Bernhardsson et al. [29] to model the consolidation of compression-moulded warp-knitted PP-glass laminates. Using the Darcy and Gutowski sub-models mentioned above, they found that, in relation with short-span flexural properties, changes in temperature had a much larger influence than pressure variations for a given processing time. This conclusion is in line with the low void content observed in vacuum-formed laminates [42], despite the fact that the process pressure is up to 15 times lower than that of autoclave-moulding.

Wysocki et al. [43] developed an alternative mathematical formulation for the consolidation of compression-moulded Twintex® PP-glass, based on two-phase continuum mechanics. Ultimately, they obtained results somewhat similar to other authors by using Darcian flow, Arrhenius viscosity as published by Klinkmüller and the Gebart permeability sub-model.

While resin viscosity has mostly been modelled according to an Arrhenius exponential formulation, some authors have used other sub-models such as the Williams-Landel-Ferry (WLF) formula [36]. This formula has the advantage of estimating the viscosity at any temperature using universal coefficients, given the viscosity at  $T_g$ . However, most authors reporting results on Twintex® PP-glass refer to the viscosity sub-model published by Klinkmüller.

### ***Vacuum forming***

Gibson, Ijaz et al. were amongst the first authors to specifically investigate the consolidation of laminates during vacuum forming [38, 44]. Their experiments made use of one further difference between compression moulding and vacuum forming: that the latter does not force the movement of the laminate microstructure, enabling the observation of the compaction process without coercively modifying it. Using this property, the results published by Ijaz showed a two-stage consolidation of composites incorporating a crystalline polymer matrix. The first stage occurred around  $T_g$  and the latter at  $T_m$ , signifying an initial

solid-state de-bulking followed by a liquid-state melt impregnation. The resulting consolidation curve was fitted with a version of the Kamal equation [45], which correlated very well with the experimental data but involved 7 fitting constants of no clear physical meaning. Hence, the pursuit of a useful model with significant physical meaning was found to be one important motivation for the work to be done in consolidation modelling. Furthermore, the Darcian flow approach, widely used by most investigators, was reported to not fit the data under Ijaz's approach. One possible reason for this is that the model worked out the consolidation rate using the temperature of a single point in the laminate. Hence, the model assumed that the whole laminate reached the same temperature simultaneously.

This assumption is a common limitation to all the described models, which will be termed "isothermal" models. In this context, this means that the temperature of the laminates is uniform across their thickness. This simplification may be acceptable for rapid processing of thin laminates. However, while vacuum forming is still a fast manufacturing method compared with the processing of thermosetting composites, it is considerably slower than compression moulding. This is particularly true for laminates with a thickness in the region of 10 mm, as it is the case for structures such as boats. Hence, the inadequacy of an isothermal approach may prevent the implementation of a consolidation model with full physical meaning. This was another important motivation for the development of a non-isothermal consolidation model for thick TPC laminates, which was subsequently addressed. The results of the original work in this research area carried out by the author are explored in detail in Chapter 4.

## **Tooling**

Any investigation on laminate consolidation assumes the availability of a mould that provides suitable dimensional stability, part finish and durability. However, the manufacture of such a mould is one of the most critical aspects and difficult issues in composite manufacturing. Traditionally, the most important issue to consider in selecting mould materials for composite manufacturing has been thermal expansion, since composite manufacturing involves significant temperature changes [46]. This is particularly true for TPCs, with processing temperatures of up to 400°C as seen in Figure 1.4. To avoid inaccuracies in composite component dimensions and prevent unnecessary residual

stresses, the coefficient of thermal expansion (CTE) of the mould should be as closely matched to that of the component as possible.

In addition, TPC vacuum forming requires mould air-tightness. Any porosity in the mould material would lead to an insufficient vacuum level inside the bag. This would lead to high void contents and low component quality. The manufacturing of TPCs also requires dimensional stability at processing temperatures. These temperatures, much higher than those needed for thermosetting composites, make most thermosetting moulding materials unsuitable for most TPC precursors. These constraints restrict the range of mould materials for TPC vacuum-forming. Industrial experience to date shows that metals and ceramic composites can be used as such; however, further development of the latter would contribute to finding new applications for TPCs.

Research on the performance of mould materials for industrial applications is of a very practical industrial nature. Composite fabricators tend to develop their own technologies which if successful become a commercial advantage, often treated as an industrial secret. For this reason, published information about the performance of moulding materials is somewhat limited. With the aim of structuring the available alternatives for tooling materials, a review was carried out including metals, commercial polymer composites and experimental ceramic composites. It was found that ceramic composites have the potential to enable vacuum forming of any shape and any thermoplastic resin. However, their inherent porosity needs to be addressed. Review and the results of the experimental work are reported and discussed in Chapter 5.

## **Joining**

Even if improvements in consolidation understanding and development of suitable tooling materials are achieved, further developments in TPC boatbuilding cannot progress without an efficient joining technique capable of sufficient strength.

The joining of TPCs can, in principle, be achieved by mechanical fastening, adhesive bonding, or fusion bonding. Mechanical fasteners have advantages such as high strength in peel loading, high degradation resistance and easy inspection and disassembly, especially useful for repair and even re-consolidation of parts of the hull. The high toughness of TPCs reduces

the risk of cracks due to stress concentrations, to which bolted or riveted thermosetting composites are very sensitive due to their brittleness. For these reasons, mechanical fasteners are being used in relatively simple (BAE Systems, Figure 2.2; Mega Sports Vertriebs, Figure 2.6) or experimental (BAE Systems, Figures 2.3 and 2.4) TPC boats.

Adhesive joining has a lower cost and weight, better appearance, has no requirement for drilling, and has lower stress concentrations. Therefore it has largely displaced mechanical fastening in boatbuilding. Nevertheless, adhesives still exhibit some drawbacks when used with TPCs, because it is intrinsically difficult to bond chemically inert matrices such as PP, and they often require extensive surface preparation and long cure cycles compared with other methods.

Fusion bonding offers the greatest potential for fast processing, high strength and water-tight joints [47-49]. Fusion bonding is possible with thermoplastics but not thermosets, as it involves the physical melting or re-melting of the resin in the composite, which is characteristic of TPCs. There is a variety of fusion bonding methods for thermoplastics and their composites, usually classified by the type of heating used. Various means can be used to supply heat to the interface, including hot plates, hot gas, friction, ultrasonic methods and resistance welding.

Resistance welding involves resistive metallic inserts which heat up only the bonding lines, and has the potential for use with thermoplastic composite boats. Its main advantage is that it potentially enables an easy and clean disassembling of the structure by re-circulating energy along the embedded resistances, highly advantageous for repair and possible remanufacturing. However, this method is still under development and the inserts could adversely affect the corrosion resistance and mechanical recyclability of the composite structure.

An alternative fusion-bonding technique is co-consolidation. By locally heating the parts near the bond line from one or both sides, the thermoplastic matrix can melt and inter-diffuse, forming a potentially high quality joint. Co-consolidation is also known as bulk-heating because although it is localised to the in-plane joint area, it involves the through-thickness heating of the whole part. This leads to longer heating and cooling cycles to allow the critical

spots to be fully processed, and also possible laminate warping due to local release of residual stresses generated in the manufacturing process [50].

This method has the advantage of adding no extra weight or foreign materials into the bond line region, requiring little surface preparation apart from general cleanliness, and has the potential to give bond strength equal to that of the parent material [51]. Comparative studies on fusion bonded PEEK-graphite show that co-consolidation provide higher quality joints than resistance welding and adhesives, as seen in Table 3.1 [47]. In addition, it has shown satisfactory results on boat repair [52] and aerospace joints [53].

**Table 3.1: Comparative studies on lap shear strength of various joining methods applied to PEEK-graphite (from [47])**

	Average lap shear strength, MPa		
	Maguire [54]	Todd [55]	Silverman [56]
Adhesive	15.7	30	17.4 – 41.6
Resistance	23.8	36	25.5
Co-consolidation	-	40	35.6*

\* with resin

For these reasons, the development of a fusion bonding technique for lap and T-joints suitable for boats was addressed and experiments carried out, the results of which are presented and discussed in Chapter 6.

## Repair

For all construction techniques of all conceivable products, the restoration of functionality following damage is a key requirement, as it ensures a long product life and higher value for cost. Available repair techniques differ according to the material to be repaired, although in all cases previous damage assessment is needed.

### *Non-destructive testing*

Damaged laminates are usually identified using non-destructive testing (NDT), because the heterogeneous nature of composites implies an inherent difficulty to identify internally

damaged areas. NDT techniques commonly used in damage assessment on composite boats include tap testing, ultrasonics and laser shearography [57-59].

Tap testing was the first technique used, based on the sound response to tapping the laminate with a small hammer. Internal delaminations and other common failures in composites are often hidden by an apparently normal external appearance. However, the presence of defects inside laminates do change the sound obtained by tapping the damaged area, which can be recognised by the trained ear.

Ultrasonic NDT is based on the emission of a very short pulse wave into the material by means of a small transducer. The wave is reflected by internal defects on the other side of the laminate, and usually received back by the same transducer, typically through a coupling agent such as oil or water. The time taken by the reflected wave indicates the distance of the boundary causing the reflection, which if lower than the laminate thickness, signifies the detection of damage. This NDT method can assist in the detection of smaller defects and damages and it is widely used in quality control and damage assessment of composite boats.

Finally, defects can be detected with laser shearography by means of subtracting interferometric images of the material surface, taken before and after loading the material by means of heat or vacuum. Portable shearography hoods, although more expensive than other methods, allow for rapid inspection of large areas in composite boats [6, 60], and provide better results with advanced sandwich materials.

### ***Repair of composite boats***

Following the identification and removal of damaged material, several repair methods can be implemented depending on the materials involved. For thermosetting composite boats, adhesive bonding is the preferred technique [61]. Minor damages can be removed and repaired with a compatible putty or adhesively bonded patch, whereas major damage in complex shaped panels requires a mould or a sister boat to make a replacement piece which is adhesively joined to the hull [60].

The repair of TPC structures has been studied [48, 62] for applications such as tanks and containers, usually taking advantage of the re-melting ability of the resin by fusion bonding. However, a technique suitable for boats is yet to be in the public domain.

For simple geometries such as the assault boats manufactured by BAE Systems (Figure 2.2), vacuum-assisted healing and co-consolidation are being successfully used [63]. The bolted joints of these boats are disassembled, allowing for local repairs or full re-processing of the entire structure. Small damaged flat panels are patched by adding unprocessed fabrics which are locally co-consolidated under vacuum using a thin metallic flat tool to keep the shape of the repair (Figure 3.1). UV degradation and possible delamination healing, as well as repairs of complex geometries (Figure 3.2) are done by re-processing the whole structure as if it were a new build. This effective repair method minimises environmental impact and maximises resource efficiency by reusing the materials many times, aligning the interests of constructor and user; however, it requires the boat to be transported into a repair yard.

An industrial interest was acknowledged regarding the development of an emergency repair technique which enables rapid in-the-field repairs of complex geometry TPC hulls. In response to that interest, a damage and repair experiment was carried out on a Twintex® Atlantic 85 (Figures 2.3 and 2.4), as reported and discussed in Chapter 7.



Figure 3.1: Flat panel repair on a simple geometry TPC boat (BAE Systems, Figure 2.2)

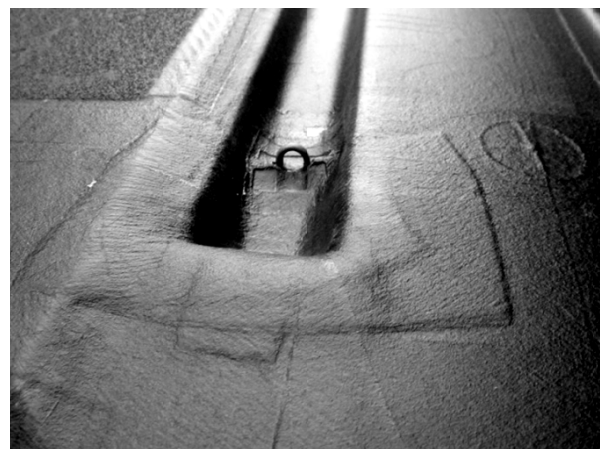


Figure 3.2: Patched repairs of complex geometries, consolidated by re-processing the entire structure

## Recycling

The above mentioned outstanding properties of composite materials and construction developments have led to an increasing production of composite boats, which in 2000 amounted for 191,400 tonnes distributed over some 327,000 boats in the U.S. alone [64].

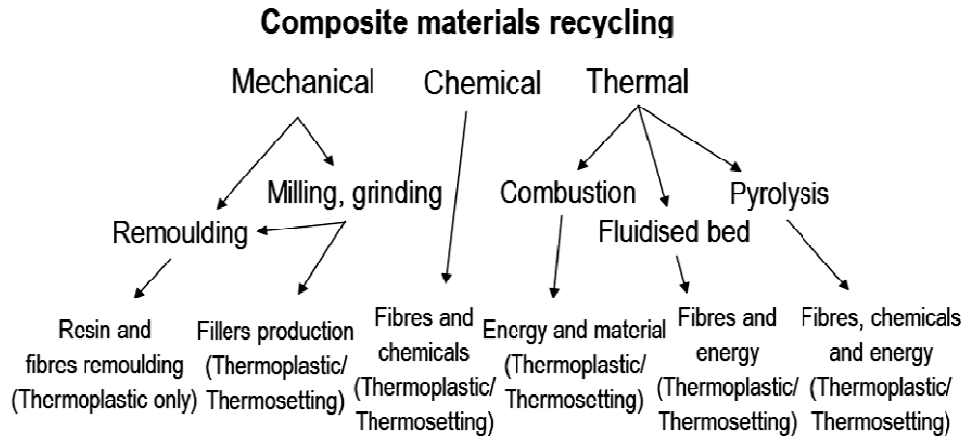
This market dominance on military and leisure boats leads to an ongoing accumulation of materials which have limited reusability and recyclability.

The recyclability aspect of composites, alongside with VOC emissions and carbon footprint has recently attracted remarkable institutional attention in boatbuilding and other industries [65, 66]. As a result, it has become a formal directive in the EU to develop end-of-life strategies that avoid landfill (2004). This follows the example set in the automotive industry by the End of Life Vehicles Directive (ELVD, 2003), which after January 2015 requires 95% of the mass of each vehicle manufactured to be reused or recovered. These new rules have led many car manufacturers to redesign their vehicles to facilitate disassembly, as well as to carefully select materials to promote recycling and reuse.

### ***Composite materials recycling***

The energy required for transportation and reprocessing of materials makes the direct reuse of the object or structure preferable where possible, by means of repair or transformations and upgrading. As seen in the previous section, TPCs already offer additional repair possibilities compared with thermosets. Also, the ability of the matrix to re-flow potentially enables enhanced re-manufacturing and upgrading. This makes TPCs a set of materials useful to close the manufacturing-disposal loops, which is a necessary step towards sustainable industries [67, 68]. Where reuse or re-manufacturing is not possible, recycling is the next best material management option. The recycling of materials can be classed as primary (reprocessing into a similar product), secondary (reprocessing into a lower quality product), tertiary (reprocessed into chemicals) and quaternary (energy recovery). While thermosets accept secondary to quaternary recycling only, TPCs can also potentially be recycled into the same materials [69] (Figure 3.3). All these ways to recycle composites comprise mechanical, thermal and solvent routes.





**Figure 3.3: Recycling processes for thermoplastic and thermosetting composites**

The mechanical recycling of composites has been explored and applied in the recent past, notably by the ERCOM project and by Phoenix Fibreglass [11]. Laminates were ground, milled, and then used as fillers in new composite products. These early initiatives, while being technically viable, did not achieve economic profit in the mid term, due to the lack of suitable markets for products containing recycled material. There was also the economic problem that on the business scale it was implemented, the cost of the recycled filler exceeded that of virgin fillers, such as calcium carbonate.

Thermal processes are aimed at fibre, material and energy recovery through controlled combustion of the organic portion of the composite scrap. Combustion with energy recovery can make use of the calorific value of the resin for heating or energy applications. However, the glass fibres are heated along with the resin, and thus absorb part of the useful heat that can be extracted.

Research on processes such as cement manufacture has shown that hot ashes may have some use in the product. However, the handling of hazardous combustion products may be a significant problem. One thermal and material recovery technique worth mentioning is the fluidised bed. This process for composite scrap operates at 400-700°C and involves blowing air through a silica sand bed. The fibres are recovered by filtering the hot gas stream emerging from the bed. The gas can then be combusted in an afterburner to recover heat. Any metallic inserts in the composite can be recovered from the sand. The glass fibres recovered with this technique are short and show a strength loss of about 25%. Also,

composites can be heated in the absence of air, again resulting in short fibres, along with gaseous and liquid decomposition products from the resin. Unfortunately, the current glass fibre price makes it unprofitable to recover fibres using these methods. By contrast, carbon fibre appears to be expensive enough to allow this recovery method which is profitably used by companies such as Adherent Technologies Inc. (US) [70, 71], Recycled Carbon Fibre Ltd. (former Milled Carbon, UK) and Hadeg Recycling GmbH (Germany), which employ proprietary catalysed processes that use lower temperatures, thus protecting the properties of carbon fibres.

Other technically viable recycling methods include chemical decomposition with solvents or supercritical fluids [72]. However, the chemicals used can constitute an environmental hazard and the resulting chemical mixtures require complex processing to recover useable products.

### ***Recycling of real end-of-life structures***

The re-flowing capability of thermoplastic resins offers additional possibilities for secondary recycling, for instance by injection moulding. The recycling of TPC materials has been largely investigated in the laboratory [73-82]. However, the recycling of real end-of-life structures, such as the hull of a the Twintex® Atlantic 85 (BAE Systems, Figures 2.3 and 2.4), involves the management of several “contaminant” materials in addition to PP-glass. For instance the hull laminate is painted with a primer-topcoat system, and the internal structure comprises a sandwich configuration including a balsa core. An investigation on the outcome of the direct mechanical recycling of the mixture of materials was found to be one important research question worth addressing. Aiming at assessing the effect of the contaminant materials on the properties of the recycled composite, material from the hull was granulated and diluted with additional PP. The resulting mixture was injection moulded into test bars which were tested under tension, obtaining interesting results that are discussed in detail in Chapter 8.

## **Chapter 4 – A non-isothermal consolidation model for thick laminates**

An understanding of the processes involved in the manufacturing of TPC laminates is needed prior to investigating other aspects of TPC boatbuilding. To contribute to this understanding, a theoretical and experimental study was conducted on the possibility to model the thermal and mechanical processes affecting commingled PP-glass during manufacturing. Such a model could enable precise adjustments of the manufacturing of TPC boat hulls, bulkheads and other components. In particular, the expertise gathered at BAE Systems shows that oven-processed PP-glass large assemblies may suffer from local resin squeeze-out due to excessive heating, affecting the dimensions of the components. At the same time, other insufficiently heated zones may show low a consolidation degree [83]. Therefore, a model capable of identifying such phenomena has the potential to support the moulding of complex TPC assemblies.

Most of the available models published to date can be classed as “isothermal”, signifying that the laminates exhibit the same temperature across their thickness. This assumption may be acceptable for fast heating rates and small thicknesses as is common in compression moulding. However, it is far from the actual processing conditions for laminates used to date in TPC boatbuilding, which can be around 10 mm thick. For this reason, a model capable of explaining such process needs to be addressed, from both theoretical and experimental points of view.

The model published by Ijaz et al. [38, 44] addressed the consolidation of vacuum formed PET-glass and PP-glass attaining good agreement with experimental data. However, the

mathematical approach used lacked physical meaning to a certain extent, requiring 7 fitting constants. It was believed that the reason why more meaningful sub-models did not fit the experimental data was that the model was iso-thermal, assuming that the consolidation occurred simultaneously through the thickness of the laminate. This was the driving motivation to address the research work described on the following.

## **Consolidation experiments**

During manufacturing, void content in commingled fabrics is eliminated up to a certain limit value close to zero, and the laminate thickness is significantly reduced. The final outcome of this process is what will be called hereafter fully consolidated laminate, still at processing temperature. The subsequent cooling ramp will have a certain influence on the final mechanical properties, mainly regarding re-crystallisation [20, 37] at microscopic level, although possibly involving other ongoing macroscopic mechanisms such as resin axial flow. However, these effects fall out of the scope of this work, which will concentrate on the consolidation process as defined above.

Consolidation experiments were carried out on a purpose-built testing rig. The rig consisted of a heavily insulated chamber incorporating a bed of electric heaters. Temperatures at various points and the laminate thickness were measured with thermocouples and a linear variable differential transducer (LVDT), respectively. The rig had the additional objective to test the performance of an experimental ceramic composite, identified as a promising mould material suitable for the manufacturing of TPC boats. Both these tests and the rig are described in detail in Chapter 5. In the rig, the tools were heated from underneath only, so that the laminate bottom would be significantly hotter than the top. This is particularly convenient for the investigation of the consolidation process of thick laminates, where not all the layers are impregnated simultaneously, because the temperature of the laminate varies not only with time but also through the laminate thickness. To emphasize this fact we will refer to such consolidation process as *non-isothermal* consolidation.

It is known that commingled TPCs undergo a remarkable thickness reduction during consolidation, as the air evacuates and the fibres and resin are compacted under pressure at high temperatures. As void content reaches a minimum limit value, thickness remains

constant unless affected by resin squeeze-out. However, resin evacuation due to axial flow can be reasonably assumed to occur after full consolidation. This way, the thickness of the laminate can be identified with its degree of consolidation, as has been assumed in the literature related to compression [31] and vacuum moulding [37]. All tests comprised heating cycles only, assuming that the micro-structure of the material is completely determined before the cooling cycle starts.

A material commonly used in TPC boats was used in the consolidation experiments: a multi-axial  $[+60^\circ, -60^\circ]_s$  non-woven Twintex<sup>®</sup> fabric with an areal weight of  $2,150 \text{ g/m}^2$ . Six layers of this precursor material provided a final laminate thickness of approximately 9 mm. Temperature measurements comprised the heaters, top and bottom of the mould, three points inside the laminates (Figure 4.1), the top of the consumables and air inside the heating chamber. All these data were logged together with the laminate thickness into a PC, connected to the rig.



**Figure 4.1: Ceramic tool with 6 layers of multi-axial Twintex<sup>®</sup> and thermocouples for thermal measurements on bottom, middle and top layers**

## **Data post-processing**

Data obtained this way needed post-processing, since some parts of the rig moved due to thermal expansion and this movement could affect the thickness variation measurements.

With this purpose, three “dry runs” with no composite consolidation taking place were carried out in order to best understand these background movements and enable their removal from further recorded datasets. These comprised a complete heating cycle applied on the mould plus all the consumables but without any TPC laminates, during which temperatures and vertical movements were recorded.

As seen in Figure 4.2, the typical obtained measurement indicates that a movement downwards is recorded first, followed by a movement back upwards. This can be interpreted as a flat tool bending downwards, because of the expansion of its heated side.

As the temperature difference between the bottom and the top of the mould declines, the mould bends back upwards, with a possible remaining deformation due to hysteresis in bending. Following this reasoning, the tool bending depends on the temperature difference across its thickness.

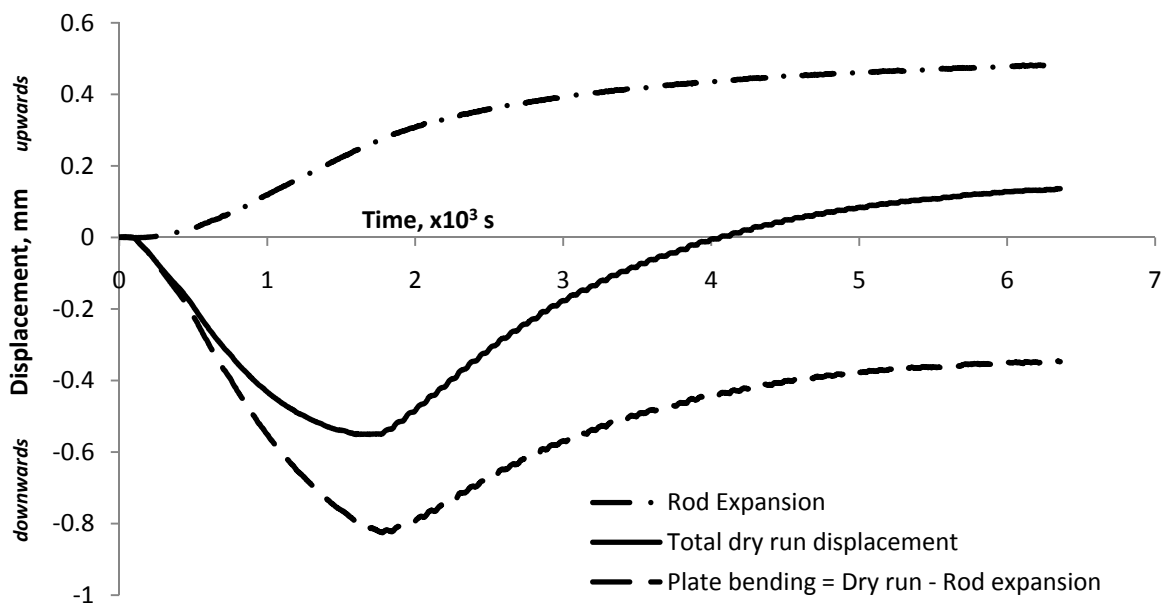
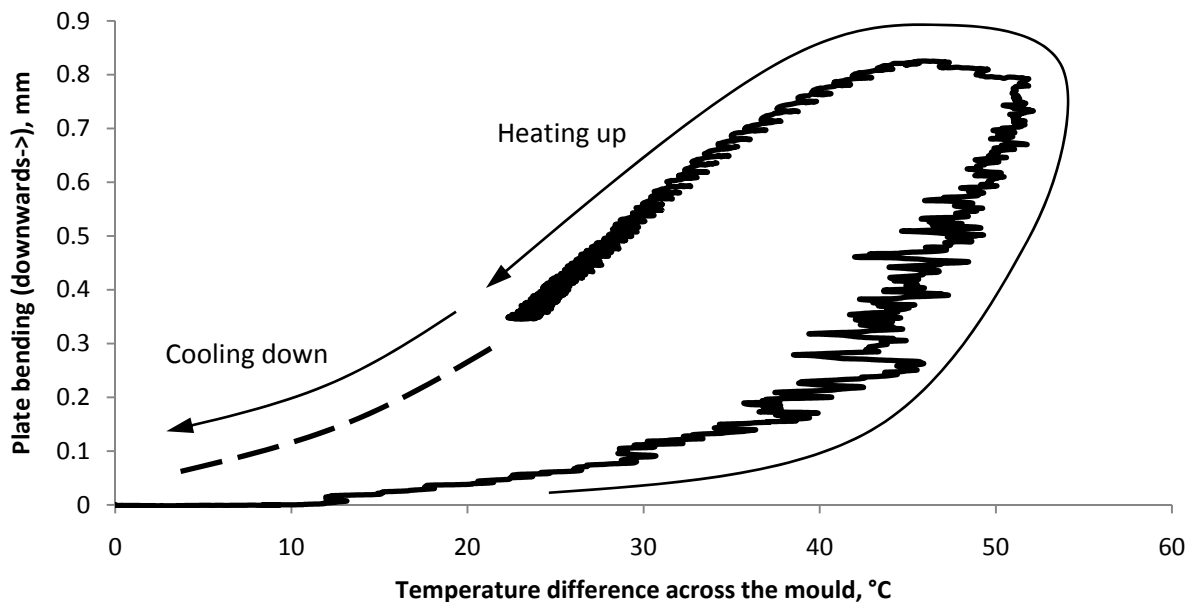


Figure 4.2: Recorded displacements during a dry run (without composite) in the rig

Another source of movement is the LVDT rod, which is subjected to thermal expansion. This expansion is proportional to the temperature of the rod, which in turn follows the air temperature within the heating chamber. Heat conduction between the top of the bag and the rod was neglected due to the small contact surface and the occurrence of further convection.

The robust make of the rig reasonably constrained all the remaining sources of movement “contamination” to negligible values. Therefore, all the background movement could be reduced to the addition of rod expansion and tool bending.

The mould bending, calculated as the total vertical displacement minus the rod expansion, was plotted against the temperature difference across the mould (Figure 4.3), and modelled with two polynomials. This enabled an estimation of the thermal bending effect for any given temperature difference across the mould, then subtracted from the consolidation data to eliminate this movement source. The rod expansion was also subtracted from the consolidation data, providing a reliable consolidation dataset.



**Figure 4.3: Plate bending downwards movement during a dry run, plotted against temperature difference across the mould**

Six manufacturing cycles were run with Twintex® with little variation among each other. One representative dataset was post-processed as described above, obtaining the final curve shown in Figure 4.4. The original data was logged every 2 seconds, obtaining approximately 3100 points. This dataset was sampled down to 199 points for ease of data handling during the modelling process. It must be noted that there is a final long consolidation plateau that covers approximately the last 0.5% consolidation over a time equivalent to the achievement of the previous 50%.

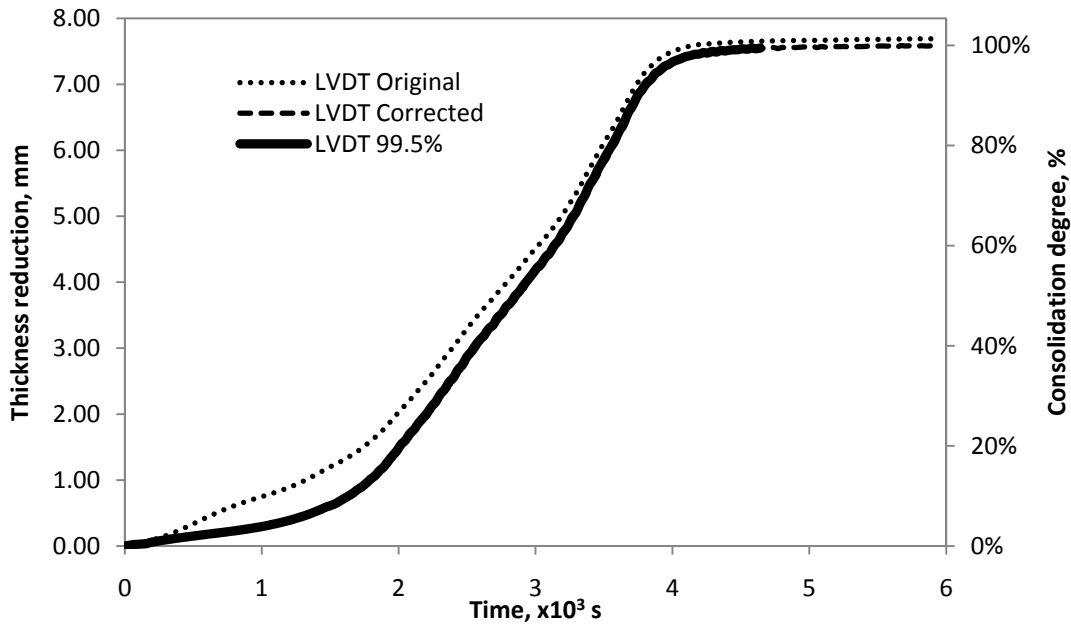


Figure 4.4: Original, corrected and 99.5% consolidation curves

According to the literature, the minimum void content expected in vacuum-consolidated laminates is in the order of 0.5% [42]. As seen on Figure 4.4, the thickness reduction during consolidation is approximately 7.6 mm, leading to a final 9 mm laminate. Assuming that this thickness decrease is entirely driven by void disappearance, the approximate void content of the unprocessed fabrics under vacuum is 45%. Since void content decreases from 45% to 0.5-1% as consolidation does from 0% to 100%, the last 0.5% of consolidation corresponds to a reduction in void content of approximately 0.23%. Being not trivial that a difference of 0.23% void content in this region would have a measurable impact the final mechanical properties of a moulded part [42], it was decided to consider that the consolidation was complete at 99.5% of the total normalised movement, as also shown in Figure 4.4. This criterion also leads to a notable energy saving in an industrial context, as equally good quality mouldings can be manufactured with significantly less energy in a shorter time.

### Temperature distribution inside the laminate

A model capable of simulating non-isothermal consolidation must be able to evaluate the local consolidation at each point of the laminate. With this objective, the laminate was divided into a number of layers within which temperature and consolidation degree were assumed to be uniformly distributed, and corresponding to that of its middle point (Figure



4.5). This assumption is not true, and may lead to an error, possibly preventing the application of known appropriate sub-models. However, an increase in the number of layers leads to a layer thickness decrease, reducing the error incurred. The number of points and thus, layers, was determined to match the size of the basic unit of consolidation in the material.

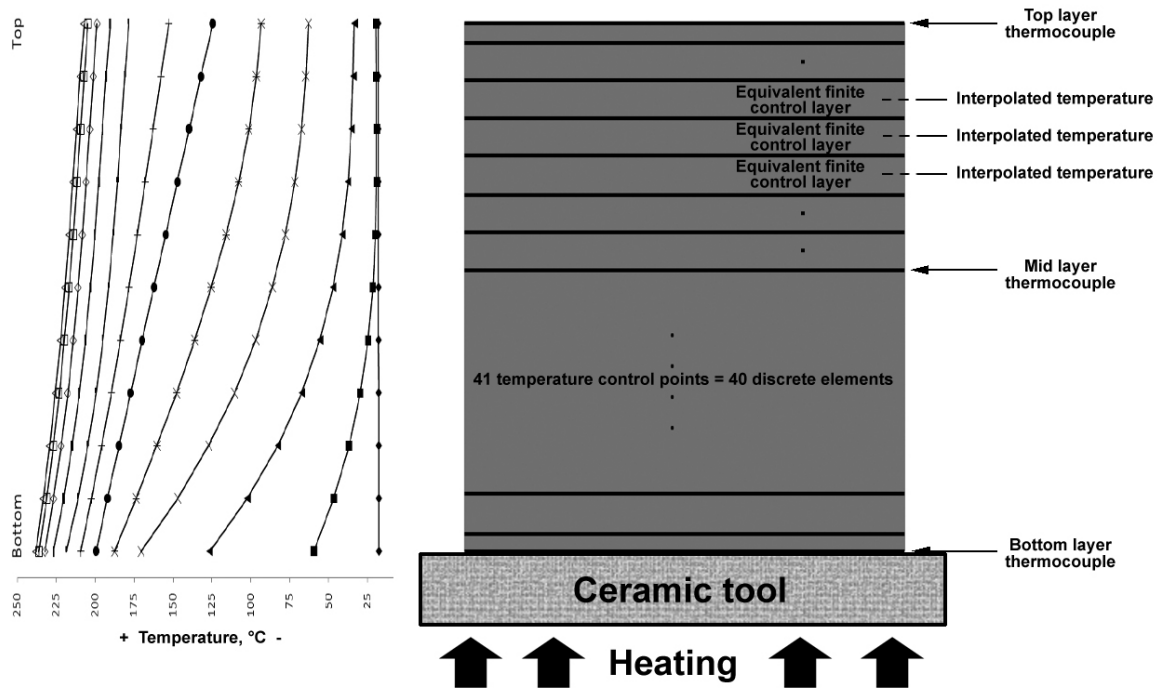


Figure 4.5: Laminate discretization and temperature map during its consolidation

A useful basic unit, discussed in detail in the sections below, can be the dry fibre bundle. The average size of dry fibre bundles was measured in Twintex<sup>®</sup> PP-glass by Klinkmüller et al. [30], being approximately 0.28 mm. As seen in Figure 4.4, the thickness of the laminate varied between 16.6 and 9.0 mm, hence a laminate discretisation into 41 control points, leading to 40 layers, would lead to a layer thickness variation between 0.41 and 0.22 mm along the consolidation process, well in the region of the chosen basic unit of consolidation. Of all layers, those at the top and bottom of the laminate had half of the nominal thickness, because the top and bottom temperatures were measured on the surface of the laminate, which coincided with the middle point of the corresponding layer. Therefore, the resulting 40 full thickness layers actually corresponded to 39 full-thickness and 2 half-thickness layers,

in which the temperature and consolidation degree were assumed to be uniform and simultaneous.

Based on the three measured temperatures on top, middle and bottom of the laminates, 22 values of the temperatures of the remaining 38 points were interpolated with cubic polynomials, obtaining the temperature internal profiles shown in Figures 4.6 and 4.7. For clarity, these figures show only 11 of the actual control points and 10 of the temperature values. Their location is indicated by means of thickness fraction, meaning that 0.0 corresponds to the laminate bottom, in touch with the heated tool, and 1.0 to the top, covered by the consumables.

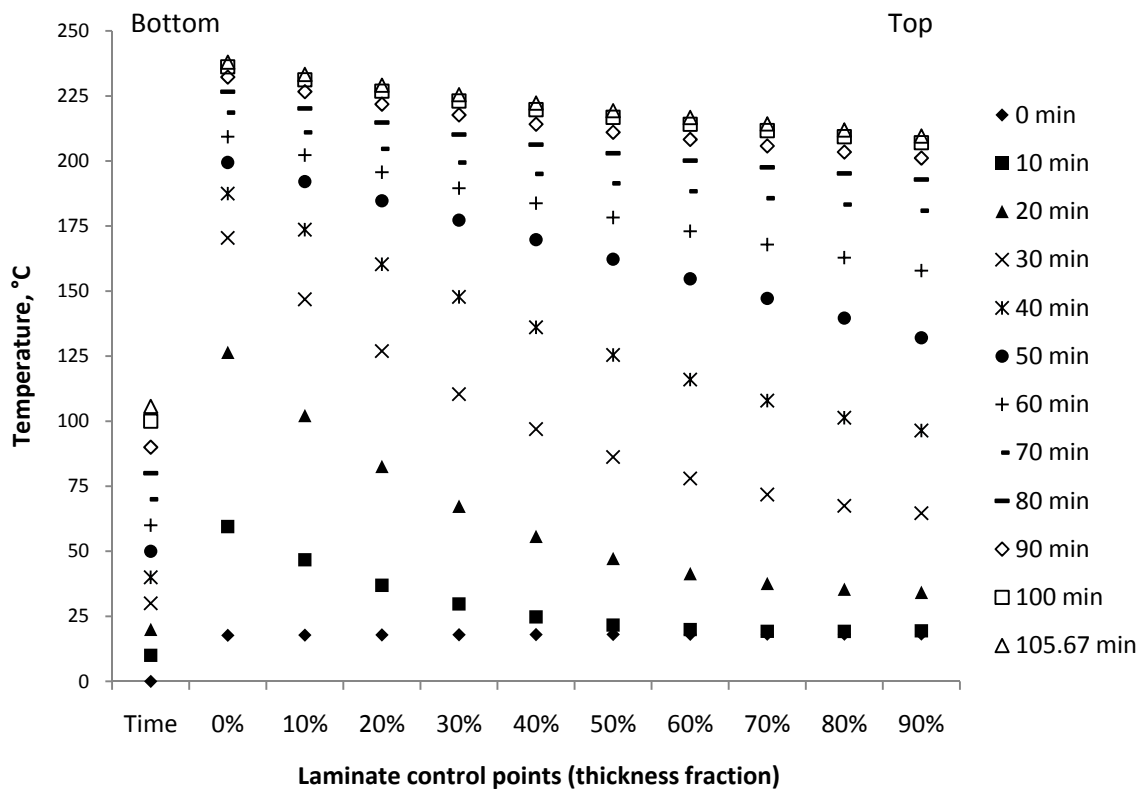


Figure 4.6: Detail of the temperature map shown in Figure 4.5 – measured temperatures correspond to control points at 0, 0.5 and 1.0 thickness fractions only – figure shows only 11 of the actual 41 control points

With regard to the interpolation, the choice of a 3<sup>rd</sup> degree polynomial allowed to tailor the derivative on the cool end (top of the laminate, thickness fraction 1.0) to provide a coherent fitting of the interpolating curves at all points. The appearance of the temperature maps shows that they are reasonably reliable, leaving small room for any significant variation.

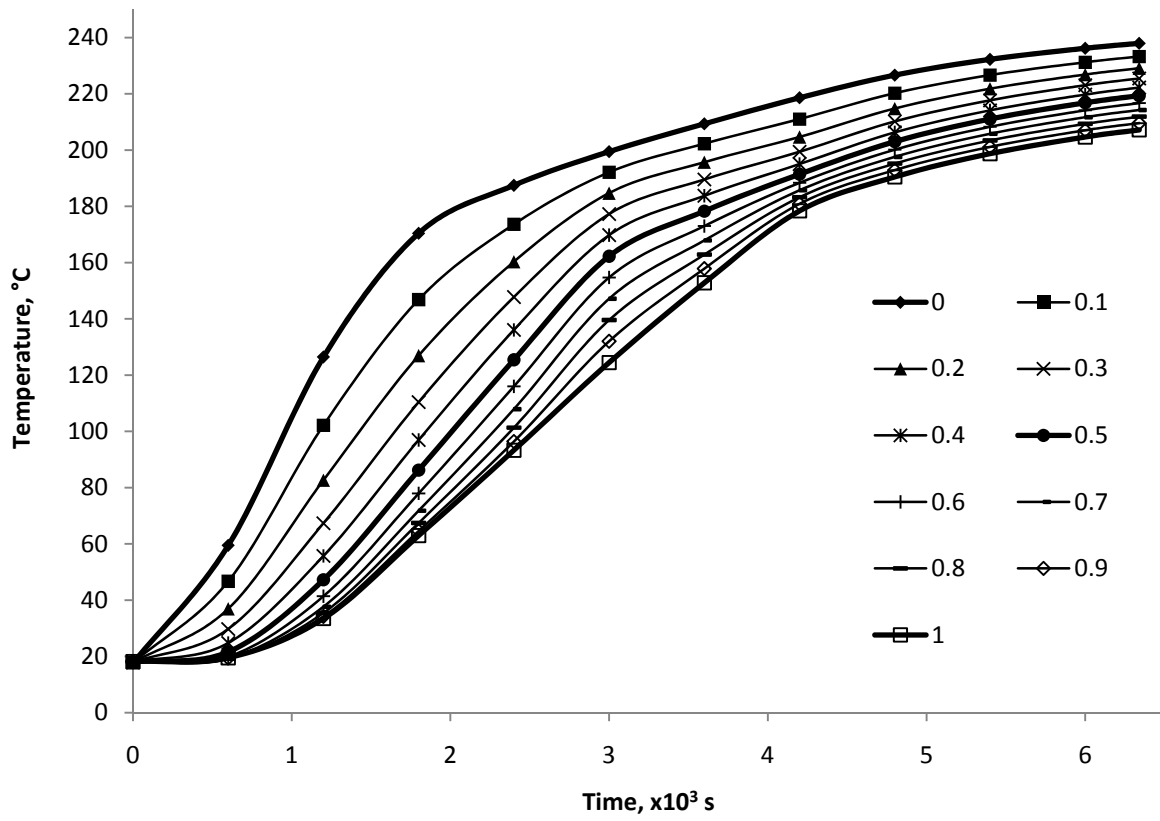


Figure 4.7: In-laminate measured (thick lines) and interpolated temperatures (thin lines) – legend indicates thickness fraction corresponding to control points location within the laminate – A heating rate drop can be seen near the melting point of the PP resin, approximately 170°C

## Non-isothermal consolidation model

### 1-parameter model

A simple model which takes into account the temperature difference among the discrete layers, was constructed assuming that full consolidation instantly occurs as soon as the material reaches the consolidation temperature,  $T_c$ . The time to full local consolidation in each point was found by cubic interpolation in the temperature maps calculated above, and plotted against its correspondent control point location. As shown in Figure 4.8, despite its simplicity, this model provides a consolidation rate not far from the measured values. For the case of  $T_c = 190$ , the estimated time to full global consolidation is approximately equal to the measured time. This in its turn is approximately the usual processing temperature for

PP-glass laminates, which underlines the usefulness of this model, despite that it fails to accurately predict the consolidation starting and final stages.

The delay observed at the starting point can be attributable to material softening before it reaches the melting temperature, which cannot be captured by such simple model. This phenomenon has been reported to constitute an initial solid state de-bulking that accounts for up to 40% of the total thickness reduction, hence the consolidation process, of various glass reinforced TPCs [37, 38, 44].

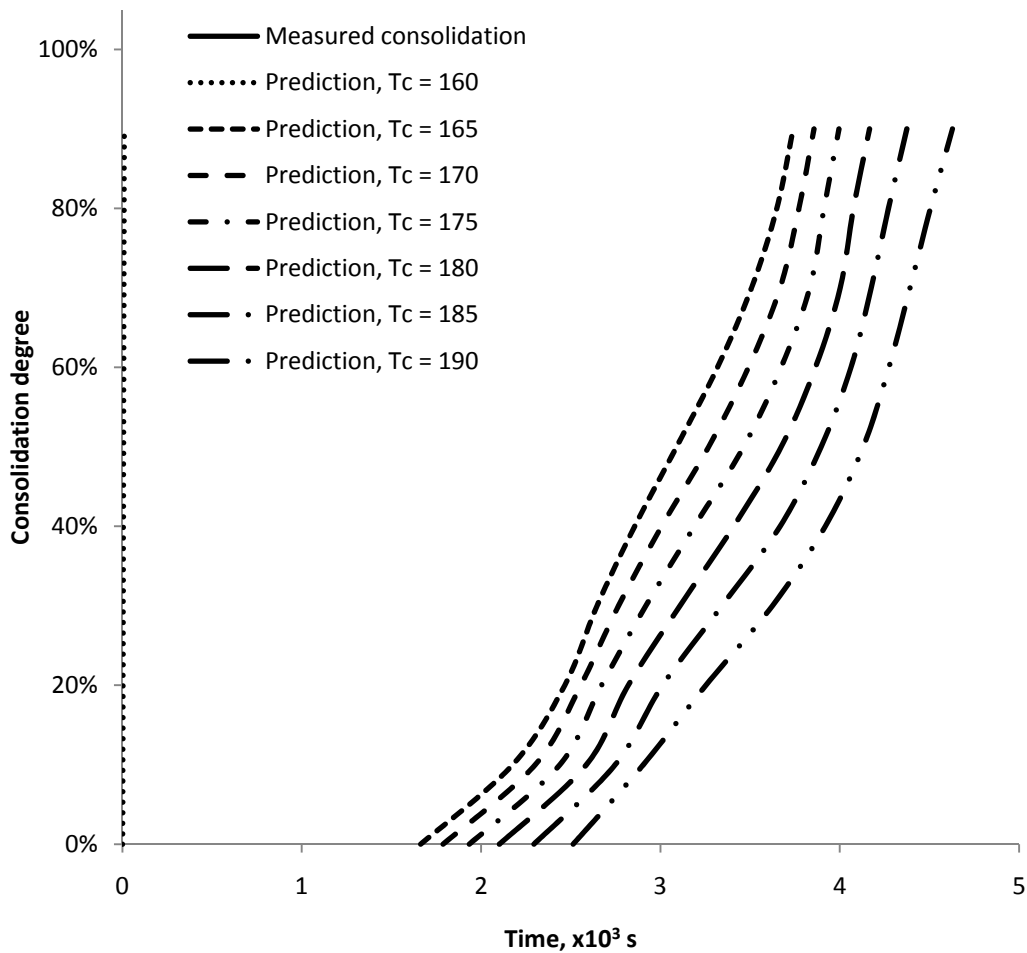


Figure 4.8: Predicted consolidation by the 1-parameter model, for a set of Tc values

From that point onwards the consolidation rate described by the model is fairly accurate. Of particular interest is the evolution of the consolidation rate, which is both measured and predicted to increase as consolidation process progresses. This phenomenon may be due to the non-isothermal nature of the consolidation of thick laminates, magnified by the single-

side heating used in the testing rig, which melt the lower layers first and the upper layers last. Hence, a cumulative effect may be expected, so that the last bit of consolidation occurs at a faster rate than the first, because an increasing number of layers may be simultaneously shrinking due to resin melt and impregnation. In addition, more heat is continuously added to the laminate, and its temperature still increases when the last layer starts consolidating. Hence, the resin viscosity decreases more and more, increasing fibre impregnation and void filling, and possibly accelerating the overall laminate thickness reduction. Following this interpretation, the local layer compaction may well look like a “consolidation wave”, starting at the hot bottom of the laminate and ending at the top. The amplitude and shape of this wave determines the degree to which the ongoing consolidation underneath affects the compaction of the whole laminate while the upper layers consolidate.

There is a final sudden decrease in the consolidation rate which remains not captured by the model either. As discussed below, it probably corresponds to a final stage of fibre wetting, impregnation and void filling, characterised by very low fibre bundle permeability.

This simple model has the ability to predict the consolidation rate at its maximum values with reasonable accuracy, although it fails to correctly simulate the first and last stages of consolidation. On the following, a comprehensive attempt to explain and accurately predict the whole consolidation is addressed and discussed.

## **Towards a comprehensive model**

Following the laminate discretisation described above, two different consolidation variables are needed, namely local and global consolidation degrees. The local consolidation degree  $\bar{X}$  corresponds to the instantaneous consolidation state of each local layer, which depends on the local absolute temperature  $T$ . The global consolidation  $\bar{\bar{X}}$ , which corresponds to the consolidation state of the whole laminate, is computed at any time of the process as the sum of the local consolidation states affected by the local layer weight with respect to the whole laminate, as follows:

$$\bar{\bar{X}} = \sum_1^{41} \bar{X} \cdot (\text{local layer weight}) \quad (4.1)$$

where *local layer weight* =  $\frac{\text{local layer thickness}}{\text{total laminate thickness}} = \frac{1}{80}$  for top and bottom layers, or =  $\frac{1}{40}$  for the rest of the layers.

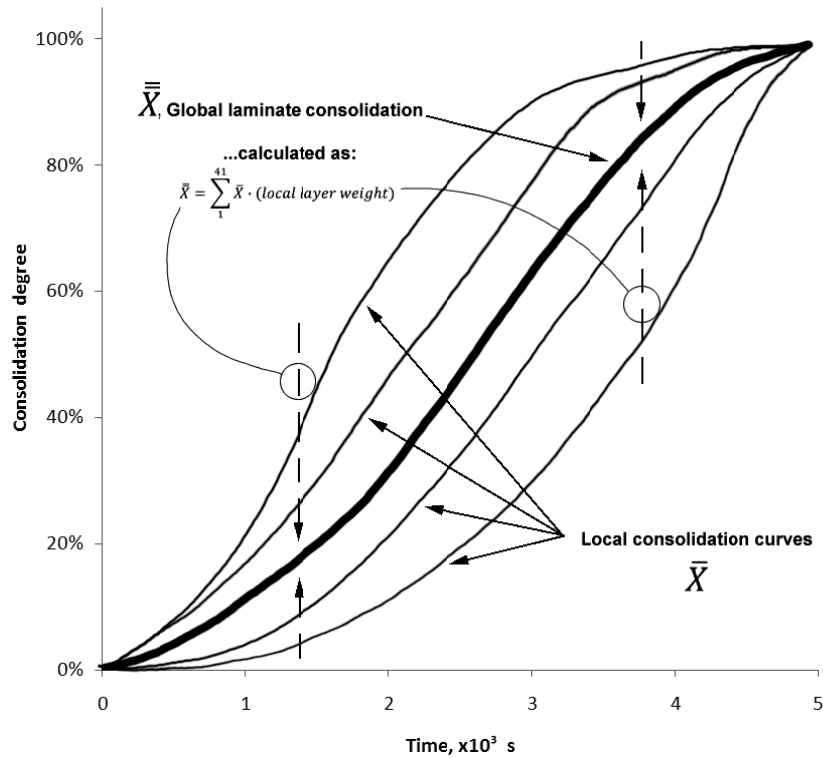


Figure 4.9: The global consolidation is modelled as the average of the local consolidation of each discrete layer

## De-bulking

Gibson, Ijaz and collaborators, [37, 38, 44] recently reported that the consolidation of commingled TPC laminates appears to occur in two stages: an initial de-bulking below melting temperature, followed by a rapid impregnation of the fibres with the melted resin, which slows down as it approximates full consolidation (Figure 4.10). Ijaz included data and calculations on PP-glass in his PhD thesis, which however do not show this two-stage process so clearly. Instead, a consolidation curve equivalent to that of the second stage observed on PET-glass is observed as in Figure 4.11.

It must be noted that the PET-glass first consolidation stage occurs above  $T_g$ . In the case of PP, this temperature is in the region of  $0^\circ\text{C}$ . Therefore, the material will be well inside this first stage when subjected to pressure at room temperature, and particularly between room temperature and  $T_m$ , which is approximately  $165^\circ\text{C}$ . This is the reason why PP does not show the two-stage consolidation behaviour seen for PET-glass.

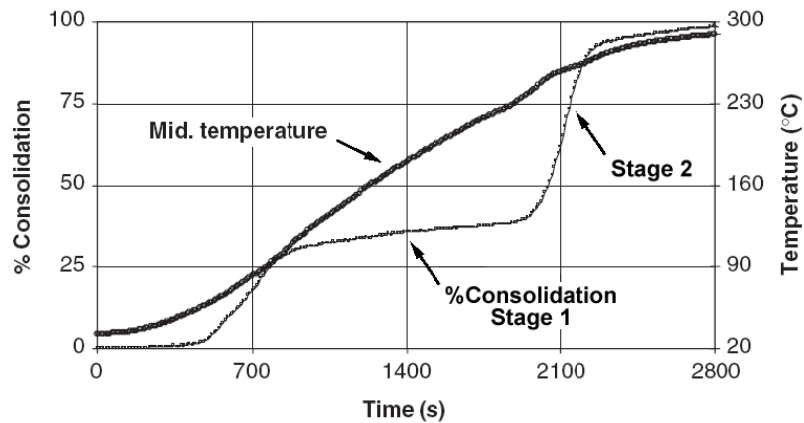


Figure 4.10: Consolidation measured for PET-glass laminates [38], versus temperature at the middle of the laminate

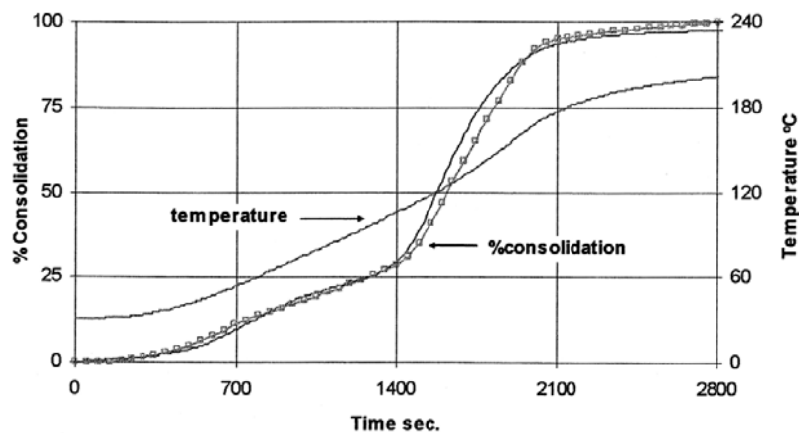


Figure 4.11: Consolidation measured for PP-glass laminates [37], versus temperature at the middle of the laminate

Certain compaction is expected at temperatures between  $T_g$  and  $T_m$  for commingled PP-glass, due to the softening naturally occurring in semi-crystalline thermoplastics beyond  $T_g$  [84]. This compaction occurs while all the material is still solid as  $T_m$  has not yet been reached. Because of the influence of the temperature on the mechanical transitions of TPC resins, a thermally-activated formulation looks appropriate to model the initial de-bulking. Also, this solid-state process must have a limit, as it is unlikely that if we leave the laminate

subjected to a pressure of 1 bar at room temperature, we will find it fully consolidated after some patient wait. It is hence reasonable to expect that the PP fibres will soften and bend between  $T_g$  and  $T_m$ , until a certain limit which probably corresponds to the material modulus at a temperature near  $T_m$ , and the stiffness of the network combining glass and PP fibres. From the data published by Gibson and Ijaz, this limit can be estimated as approximately 40% of the whole consolidation.

This initial de-bulking is more difficult to observe during compression moulding, as the laminate is often heated to its melting temperature and then forced to compact in a hot press. This is one of the reasons why most of other available consolidation models, being focussed on compression moulding, ignore it. However, the results published in 1991 by Van West et al. [31] are remarkably similar, although reasoned in a different way. This model, corresponding to compression-moulded commingled PEEK-carbon, shows a quasi-linear first bit of the consolidation curve, followed by a sharp increase of the consolidation rate that finally slows down in an asymptotic manner towards full consolidation (Figure 4.12).

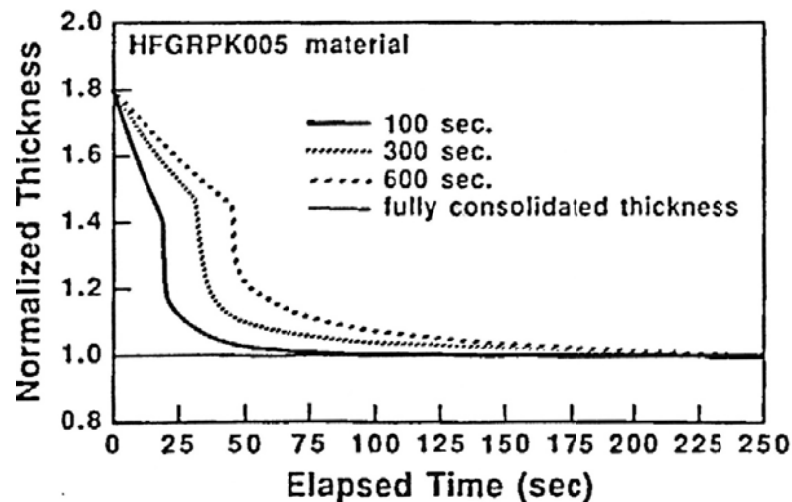


Figure 4.12: Normalised compression-moulding consolidation of PEEK-carbon laminates, as modelled by Van West et al. [31] – A quasi-linear first stage can be observed in all cases reported

This behaviour was explained as liquid-state inter-bundle compaction (quasi-linear bit) followed by intra-bundle impregnation (sharp drop and final slow down). The inter-bundle compaction phase, described as melted resin coalescence in between dry fibre bundles, also covers the first 40% of consolidation remarkably resembling the mentioned initial de-bulking. If the laminates reach the melting temperature while pressure increases, it is



possible that both phenomena may be occurring simultaneously within the first 40% of consolidation: following the mentioned solid-state de-bulking, a short inter-bundle resin coalescence could take place, rapidly followed by the final intra-bundle impregnation.

Gibson and Ijaz modelled with good agreement the entire consolidation of PET and PP-glass shown in Figure 4.10 using a form of the Kamal equation [38]:

$$\frac{dX_i}{dt} = A_i \exp\left(\frac{-B_i}{T}\right) (1 - X_i)^{m_i} \quad (4.2)$$

where  $X$  is the consolidation degree,  $T$  is the absolute temperature and  $A_i$ ,  $B_i$  and  $m_i$  are fitting constants, corresponding to the stage “ $i$ ” (either 1 or 2) of the consolidation. Finally, the overall consolidation rate was expressed as a balance between those two, determined by the factor  $f$ :

$$\frac{dX}{dt} = f \frac{dX_1}{dt} + (1 - f) \frac{dX_2}{dt} \quad (4.3)$$

This equation is an empirical expression first used by Kamal and Sourour to model the curation kinetics of thermosetting resins [45]. It contains the Arrhenius equation  $A \exp\left(\frac{-B}{T}\right)$ , which is a widely accepted model for many temperature-activated processes. Additionally, the term  $(1 - X)^m$  approaches zero as the consolidation degree increases. As we discussed above, the initial de-bulking will stop at around 40% consolidation, hence this term must decrease as  $X$  approaches the limit value of 0.4, having the form  $(\lambda - X)^m$  with  $\lambda = 0.4$ . For simplicity, we will assume  $m = 1$  resulting on the following expression for the initial de-bulking process:

$$\frac{dX_d}{dt} = A \exp\left(\frac{-B}{T}\right) (\lambda - X_d) \quad (4.4)$$

In equation (4.4),  $X_d$  is the consolidation degree corresponding to the de-bulking stage,  $t$  the time,  $T$  the local absolute temperature,  $A$  and  $B$  fitting constants and  $\lambda$  is the de-bulking limit for temperatures below  $T_m$ .

Please note that the variable  $X_d$  cannot be used for the impregnation process. The reason for this is that by the time the impregnation starts, local consolidation would have already reached a value of about 20-40% due to initial de-bulking. However, the impregnation degree  $X$  must start from zero, and then needs to be linearly scaled up by  $X^i = \text{transf}(X)$  before it is added to the de-bulking  $X_d$ , which remains constant as the impregnation has started. Finally, the local consolidation  $\bar{X}$  is equal to an initial de-bulking  $X_d$  plus a subsequent impregnation  $X^i$ :

$$\bar{X} = X_d + \text{transf}(X) = X_d + X^i \quad (4.5)$$

Both phenomena do not occur simultaneously. Therefore local consolidation progresses due to solid-state de-bulking, or liquid-state impregnation. However, the actual algorithm underlying in equation (4.5) computes the local consolidation  $\bar{X}$  as solid-state de-bulking  $X_d$  for  $T < T_m$ ; whereas for  $T \geq T_m$ , the re-normalised liquid-state impregnation  $X^i = \text{transf}(X)$  is added to the value of de-bulking attained when the local layer reaches the melting temperature,  $X_d(T_m)$ .

## **Impregnation**

The resin viscosity drops suddenly as each local layer reaches  $T_m$ , allowing for coalescence and impregnation of bundles of dry reinforcing fibres. It is commonly accepted [30, 32, 34, 35, 43] that prior to impregnation, inter-bundle coalescence takes place. This phenomenon, first measured and reported by Van West et al. [31], consists of the formation of melted resin pools on the outside of dry reinforcing fibre bundles. One reason for this phenomenon is a certain degree of fibre segregation, naturally occurring during the actual commingling process (Figure 4.13).

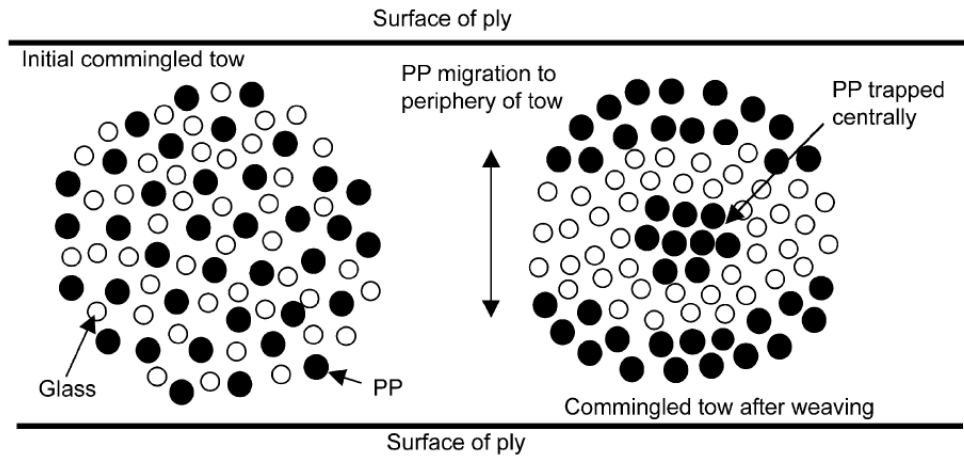


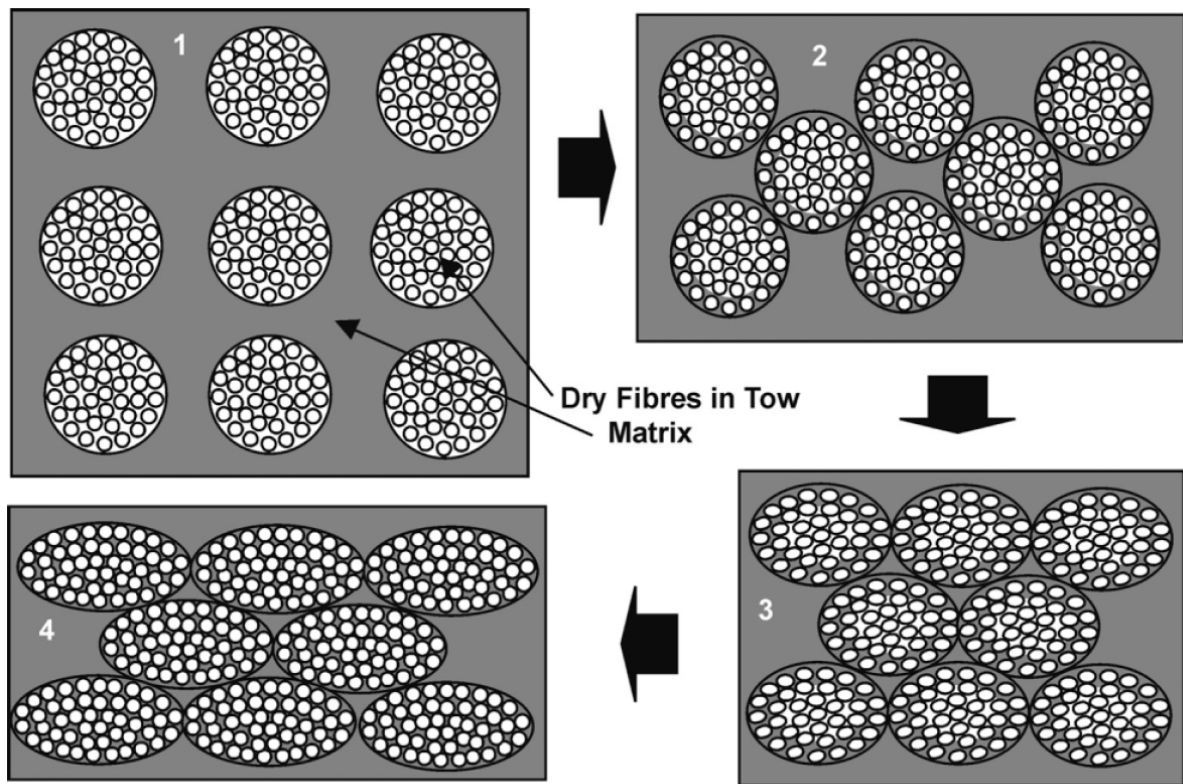
Figure 4.13: Fibre segregation occurring in commingled TPCs [35]

When pressure is applied to commingled yarns, bundles containing resin and reinforcing fibres are subjected to non-uniform forces which lead to further segregation. This phenomenon, typical of weaving, is likely to occur to a degree in other processes such as knitting or stitching. By the time the fabric is rolled and distributed, a number of bundles free from resin fibres have probably formed within each commingled tow. The segregated resin fibres tend to first coalesce and then impregnate the reinforcing fibre bundles. These bundles can be considered the smallest and hence basic geometrical unit of consolidation, since the last occurring consolidation mechanism appears to be the resin melt impregnation of these bundles. Figure 4.14 shows the impregnation sequence after the resin has melted in pools around the dry bundles [35].

Whereas inter-bundle compaction has been assumed to occur before intra-bundle impregnation and therefore modelled separately by Van West [31], other authors [30, 32, 34] ignored initial compaction and only modelled the subsequent intra-bundle impregnation. Because of the lower pressure ( $\sim 0.1$  MPa) used in vacuum forming, longer times at a reasonable processing temperature are usually needed to achieve full consolidation with the desired void content.

The choice of the processing temperature is a trade-off between energy cost and manufacturing cycle duration. Thus, the consolidation of a thin layer of Twintex will take significantly longer by vacuum forming ( $\sim 1500$  sec) [37] than by compression moulding ( $\sim 30$ - $600$  sec) [30]. Over this time, it will be assumed that liquid-state inter- and intra-bundle

compaction have sufficient overlap to be considered simultaneous, and indistinguishable with regard to the evolution of the consolidation rate above  $T_m$ .



**Figure 4.14: Impregnation sequence of a commingled TPC – figures indicate impregnation of dry fibre bundles inside a commingled tow by compression moulding [35]**

As commonly assumed, the resin flow during the impregnation of dry fibre bundles will be described with Darcy's law [20, 28-34, 36, 40, 43]. This approach had been reported not to fit isothermal vacuum consolidation of PP-glass [37], PET-glass [38] and coPET-glass laminates [44]. However, the local non-isothermal application of Darcy's law to the discrete layers of the laminate leads to surprisingly good results as discussed below.

The Darcy equation phenomenologically describes the flow through a porous medium. Considering one-dimensional flow towards the centre of a dry fibre bundle in cylindrical coordinates, assuming constant hydrostatic pressure in the resin pool shown in Figure 4.15, the equation can be expressed as follows (next page):

$$\frac{dr}{dt} = \frac{S \cdot p}{\eta \cdot r} \quad (4.6)$$

where  $r$  is the depth of melt penetration (in the direction of the radius of the circular bundle),  $t$  is the time,  $S$  the permeability,  $p$  the driving pressure and  $\eta$  is the resin viscosity.

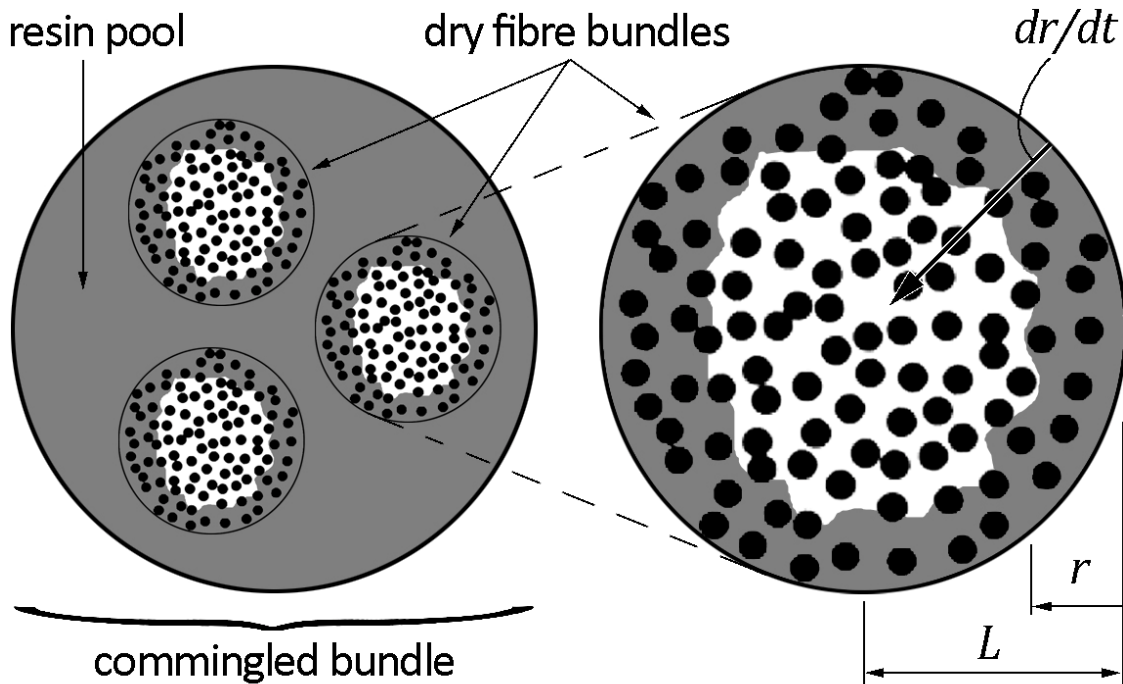


Figure 4.15: Impregnation phenomenon occurring within a bundle of commingled yarns, corresponding to those shown in Figure 4.14, (2)

### Viscosity

The viscosity of thermoplastic resins has been modelled in the past using various approaches. Although some authors occasionally use alternative formulations [36], the Arrhenius-type equation is the most widely used in the available literature [30, 32, 34, 43]. The use of the Arrhenius expression assumes that the PP resin behaves as a Newtonian fluid. This means that the shear stress of the resin depends linearly on its velocity, being its viscosity the constant of proportionality. Some models [28, 33] are based on a non-Newtonian resin sub-model, while most authors assume that thermoplastic resins can be considered Newtonian during impregnation within commingled bundles. Effectively, Long et al. experimentally showed that the Twintex® PP resin can be considered Newtonian below compaction rates of approximately 5 mm/min [35]. This figure may be relatively low for

compression moulding but is actually very high for vacuum forming where resin velocity during impregnation is typically 2-20 times lower. Although the data shown in Figure 4.4 lead to maximum compaction rates of less than 0.1 mm/min due to single-side heating, values for oven-consolidated laminates can be in the region of up to 1 mm/min, as deduced from published results [37].

Taking the Arrhenius-type equation for the viscosity, as fitted to measurements done on the PP contained in Twintex® PP-glass published by Klinkmüller et al. [30]:

$$\eta = \eta_0 \exp\left(\frac{K}{T}\right) \quad (4.7)$$

where  $T$  is the local absolute temperature,  $\eta_0 = 2.6E - 3$ , and  $K = 5600$ . Hence, from (4.6) and (4.7), and defining the impregnation degree as  $X = r/L$  with  $L =$  local impregnation distance (Figure 4.15), we have:

$$\frac{dX}{dt} = \frac{S \cdot p}{\eta_0 \cdot X \cdot L^2} \exp\left(\frac{-K}{T}\right) \quad (4.8)$$

### ***Pressure and permeability***

The actual impregnation of the dry fibre bundles is assumed to occur as follows: after inter-bundle compaction, the bundles are surrounded by melted resin at constant pressure. The pressure is considered constant because in vacuum forming, the applied pressure is constant and equal to atmospheric pressure. Such pressure is transmitted hydrostatically throughout the continuous melted resin, hence the constant pressure on the fibre bundles.

As seen in Figure 4.14, dry fibre bundles which are surrounded by resin at increasing pressure tend to increase their packing state and decrease their permeability. This situation is common in compression moulding but not in vacuum forming, in which the applied pressure is 10-100 times lower and remains constant. Hence, it is expected that the bundle permeability will not vary as much in vacuum forming as in compression moulding. Nevertheless, despite the low and constant pressure on the boundary of fibre bundles, the

flow of polymer resins through fibres always involves certain drag on the fibres [85, 86]. As a result of this drag, the permeability of the bundle is still likely to decrease. Flow drag is always accompanied by pressure drop in viscous flow. This leads to a combined effect of bundle permeability reduction plus resin pressure drop, which drive together the impregnation rate to zero as observed in Figures 4.10, 4.11 and 4.12.

The relative importance of these two effects is in principle unknown. Hence, it will be considered that it is the product  $S \cdot p$  that drives the behaviour of the impregnation rate described in (4.8), instead of the permeability  $S$  or the pressure  $p$  alone. In turn, this product will be assumed to behave as if the pressure in the resin would be constant and equal to the applied pressure, and the fibre bundle permeability would decrease due to resin drag towards the centre of the bundle. Thus,  $p = 100,000$  Pa.

### ***Bundle permeability***

The permeability can be subdivided into axial and transverse, which refer to the flow along or across the fibres, respectively. In most research done on fibre impregnation in composites, the axial permeability of a well-aligned unidirectional fibre bed is assumed to follow the Kozeny-Carman equation [39]:

$$S_{ii} = \frac{r_f^2}{4k_{ii}} \frac{(1 - V_f)^3}{V_f^2} \quad (4.9)$$

where  $r$  is the fibre radius,  $V_f$  the fibre volume fraction and  $k_{ii}$  the Kozeny constant, being  $ii$  the considered orientation x-x, y-y or z-z.

Later on, Gutowski and co-workers discovered that the axial flow of the impregnating resin along the reinforcing fibres did not fully explain a number of experimental results, which were believed to involve resin flow across the fibres. According to their modification of the Kozeny-Carman equation, fibre network permeability decreases as impregnation progresses because the fibre volume fraction rises as the laminate is compacted. Eventually, a limit value of the fibre volume fraction,  $V_a'$  is reached and the resin flow stops. The resulting expression gives the transverse resin flow across the reinforcing fibre bed [39]:

$$S = \frac{r_f^2}{4k_0} \frac{\left( \sqrt{\frac{V'_a}{V'_f}} - 1 \right)^3}{\frac{V'_a}{V'_f} + 1} \quad (4.10)$$

Alternatively to the semi-empirical Kozeny-Carman and its modified version proposed by Gutowski, some authors [34, 43] have used an analytically derived approach to the fibre bed permeability developed by Gebart:

$$S = C \left( \sqrt{\frac{V'_a}{V'_f}} - 1 \right)^{5/2} r_f^2 \quad (4.11)$$

One interesting feature of this formula is that it does not have a fitting constant because the value of C is fixed given the fibre arrangement. However, it has been reported that the Gutowski formulation shows better agreement with experiments than the Gebart expression, regarding the transverse permeability across both glass and carbon fibres [40], which is the reason why it will be adopted henceforth.

A number of published consolidation models applied to unidirectional TPCs assume that the resin flows only across the fibres during impregnation [31, 32]. Axial flow, when considered, is assumed to take place only after full consolidation is attained. The tested Twintex® multi-axial fabrics comprise four layers approximately 0.37 mm thick oriented [+60°, -60°]<sub>s</sub> per ply, providing a slightly more complicated fibre network than a fully unidirectional arrangement, supporting the argument in favour of transverse flow only, which will be considered hereafter, as described by equation (4.10).

On the other hand, one of the lessons learned on TPC vacuum forming [83] also seen during the consolidation experiments described above is that PP effectively tends to flow axially, especially after prolonged processing times and high temperatures. This axial flow leads to resin squeeze-out, local laminate thinning and edge tapering all of which are visible on most consolidated components and laminates. However, it is reasonable to consider that this axial



flow occurs after full consolidation because of continuously applied heat and pressure. Nevertheless, temperatures during and especially after full consolidation must be controlled so that there is no noticeable resin squeeze out due to longitudinal resin flow. Failing to do so may result in heterogeneous glass/PP ratios and thicknesses along the moulded hull.

Therefore, from (4.8) and (4.10), we have:

$$\frac{dX}{dt} = \frac{r_f^2 \cdot p}{4k_0 \cdot \eta_0 \cdot X \cdot L^2} \exp\left(\frac{-K}{T}\right) \frac{\left(\sqrt{\frac{V'_a}{V_f}} - 1\right)^3}{\frac{V'_a}{V_f} + 1} \quad (4.12)$$

### ***The Kozeny constant***

The value of  $k_0$  derives from the Kozeny constant, which has been typically used to fit the modelled permeability to experimental impregnation data, enabling the modelling of a range of fibre alignments and arrangements. Its value was found to be 0.2 for carbon fibres by Gutowski et al. [39], while data on unidirectional glass fibres were fitted with  $k_0 = 0.9$  by Ye et al. [32] and by  $k_0 = 5$  by Klinkmüller et al. [30]. Other authors fitted their data with values as high as 50,000 [32]. Being the transverse permeability expectably higher for unidirectional than for multi-axial fabrics, and inversely proportional to the Kozeny constant, values for this constant higher than 5 may be expected for the latter.

### ***Evolution of the volume fraction***

On the permeability equation (4.10) the local glass volume fraction  $V_f$  tends to increase as the consolidation progresses, until it reaches the limit value of  $V'_a$ . This limit value is often approximated by the theoretical volume fraction provided by hexagonal close fibre packing, which leads to a value of 0.91 as applied to Twintex® by Cain et al. [33].

The glass volume fraction before impregnation starts may vary from layer to layer, because different layers will attain different consolidation degree by the time local temperatures reach  $T_m$ . This degree may potentially vary from virtually 0 to 40% of the total local consolidation, depending on how quickly each layer is heated. Despite that the dependence

of the initial de-bulking on heating times is unknown, the bottom layers may develop less de-bulking than the top layers, since the latter will be subjected to pressure at resin softening temperatures for a longer time.

Also, the observed PP fibre segregation due to partial commingling may lead to a higher local glass volume fraction, as some of the PP fibres inside the bundles would have migrated to their periphery, increasing the local ratio of glass fibres. Nevertheless, as the degree to which this may occur is unknown, it will be assumed that the glass volume fraction of the fibre bundles to be impregnated is equal to the bulk value given by the manufacturer. Hence, the instantaneous glass volume fraction over glass, PP and voids when  $T = T_m$  can be expressed as:

$$V_{f0} = (1 - (1 - X_m) \times V_{f0void}) \times V_{fG} \sim (4.13)$$

$$\sim (1 - (1 - X_m) \times 0.45) \times 0.35 \quad (\text{locally calculated})$$

where  $V_{f0}$  = glass volume fraction at the beginning of the liquid-state impregnation (i.e. after initial solid-state de-bulking);  $X_m$  = local consolidation degree attained by means of solid-state de-bulking at  $T = T_m$  (real time-calculated in each layer);  $V_{fG}$  = nominal glass volume fraction (as in the fully consolidated material), and  $V_{f0void}$  = void content at the beginning of the solid-state de-bulking.

The progression of  $V_f$  towards  $V_a'$  during impregnation is expected to be related to the evolution of the local impregnation degree, thus  $V_f = V_f(X)$ . It is now convenient to remember that equation (4.12), signifying the local impregnation rate, has the form:

$$\frac{dX}{dt} = \frac{C}{X} \exp\left(\frac{-D}{T}\right) g(X) \quad (4.14)$$

In order to approximate the unknown form of the function  $V_f(X)$  it was decided to plot the function  $\frac{\frac{dX}{dt}}{\frac{C}{X} \exp\left(\frac{-D}{T}\right)} = g(X)$  against  $X$ , based on the experimental data  $X$ , the temperature  $T$

of the middle point of the laminate and provisional values of the constants C and D. From equation (4.12):

$$g(X) = \frac{\left( \sqrt{\frac{V'_a}{V_f(X)}} - 1 \right)^3}{\frac{V'_a}{V_f(X)} + 1} \quad (4.15)$$

It must be noted that the use of a single temperature makes this estimation isothermal, as it assumes that the whole laminate is at that temperature. As it can be seen in Figures 4.6 and 4.7, this is not true. However, it was believed to be useful to estimate the *form* of the function  $V_f(X)$ , towards a suitable local expression for the non-isothermal final model.

From the data published by Van West and Ijaz, it can be deduced that the permeability of the reinforcing fibres to the liquid resin remains constant during most of the impregnation process and decays rapidly when approximately 75-90% of the impregnation distance has been covered (Figures 4.16 and 4.17).

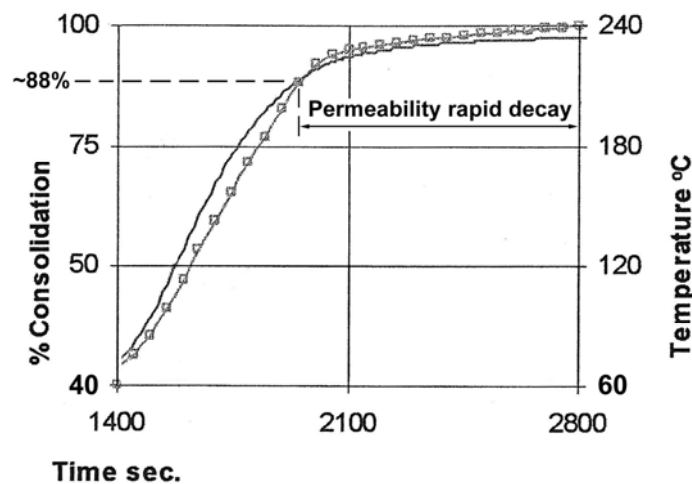


Figure 4.16: Zone of rapid permeability decay during the vacuum consolidation of PP-glass (edited from [38])  
 – Indicated 88% of total consolidation is equivalent to approximately 80% of the impregnation stage

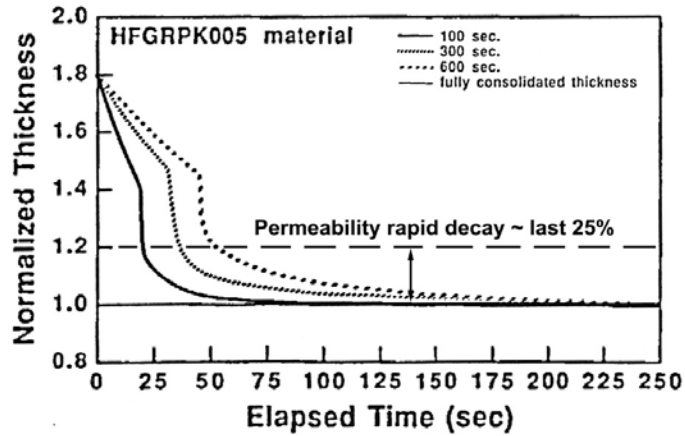


Figure 4.17: Zone of rapid permeability decay during for compression moulded PEEK-carbon (edited from [31])

Therefore, a fit of the last 25% of the plotted expression  $g(X)$  should provide a reasonable form of the function  $V_f(X)$ . This plot can be seen in Figure 4.18. The curve corresponding to the last 25% of the consolidation degree was fitted with the mathematical utility MatLab®, leading to the following relationship between the glass volume fraction  $V_f$  and the degree of impregnation  $X$ :

$$V_f(X) = aX^b + c \quad (4.16)$$

Although it fits well the considered part of the curve, a large discrepancy is observed for  $X$  below 0.75. A quick analysis shows that for  $X < 0.30$ , the plotted curve actually corresponds to solid-state de-bulking, hence makes no sense regarding impregnation. For  $X = 0.30$  to 0.75, isothermal assumptions applied to a non-isothermal process are likely to be the cause of the disagreement.

From equation (4.16), at the beginning of the impregnation stage:

$$V(X = 0) = V_{f0} = 0 + c \rightarrow V_{f0} = c \quad (4.17)$$

Hence, from (4.13) and (4.17),  $c \sim (1 - (1 - X_m) \times 0.45) \times 0.35$ , where  $X_m$  is to be locally calculated for each discrete layer. Also, when the impregnation is complete:

$$V(X = 1) = V'_a = a + c \rightarrow a = V'_a - c \quad (4.18)$$

As stated at the beginning of this section,  $V'_a = 0.91$ . Hence,  $a$  is also calculated for each layer. The value of  $b$  governs the decrease rate of the permeability, in such way that for  $b \sim 25 - 75$ , the permeability is practically constant until the local impregnation degree  $X \sim 0.75 - 0.90$ , respectively (Figure 4.19), rapidly decreasing afterwards.

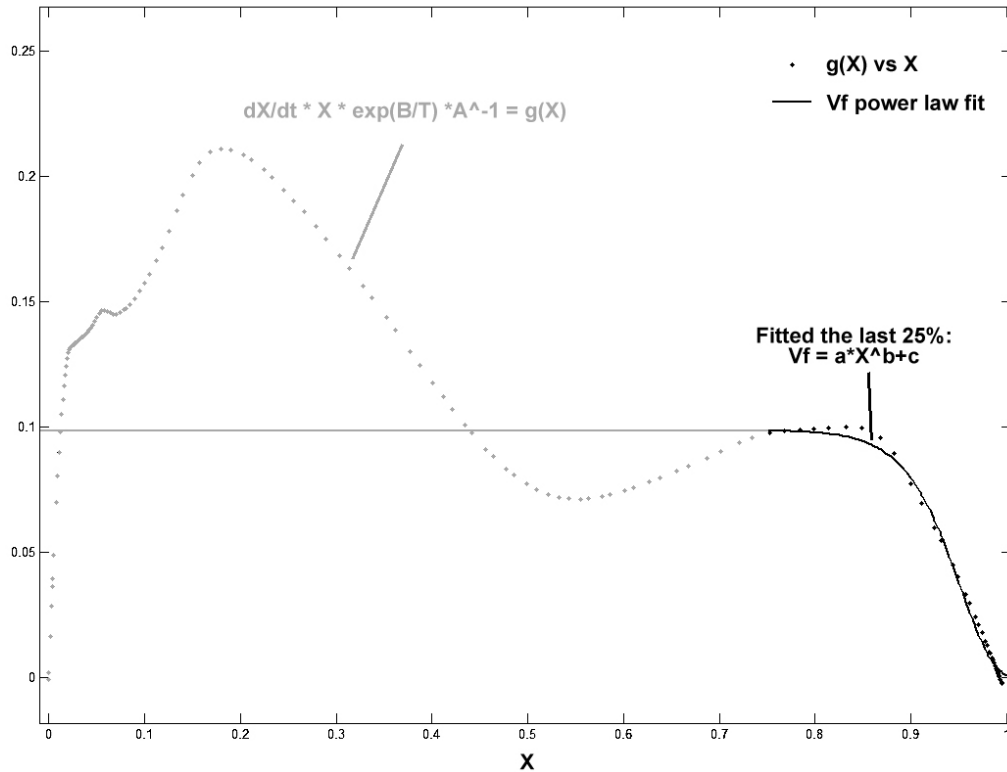


Figure 4.18: Fitting of the evolution of the glass volume fraction  $V_f$  during the final permeability rapid decay

Finally, from (4.12) and (4.16):

$$\frac{dX}{dt} = \frac{r_f^2 \cdot p}{4k_0 \cdot \eta_0 \cdot X \cdot L^2} \exp\left(\frac{-K}{T}\right) \frac{\left(\sqrt{\frac{V'_a}{aX^b + c}} - 1\right)^3}{\frac{V'_a}{aX^b + c} + 1} \quad (4.19)$$

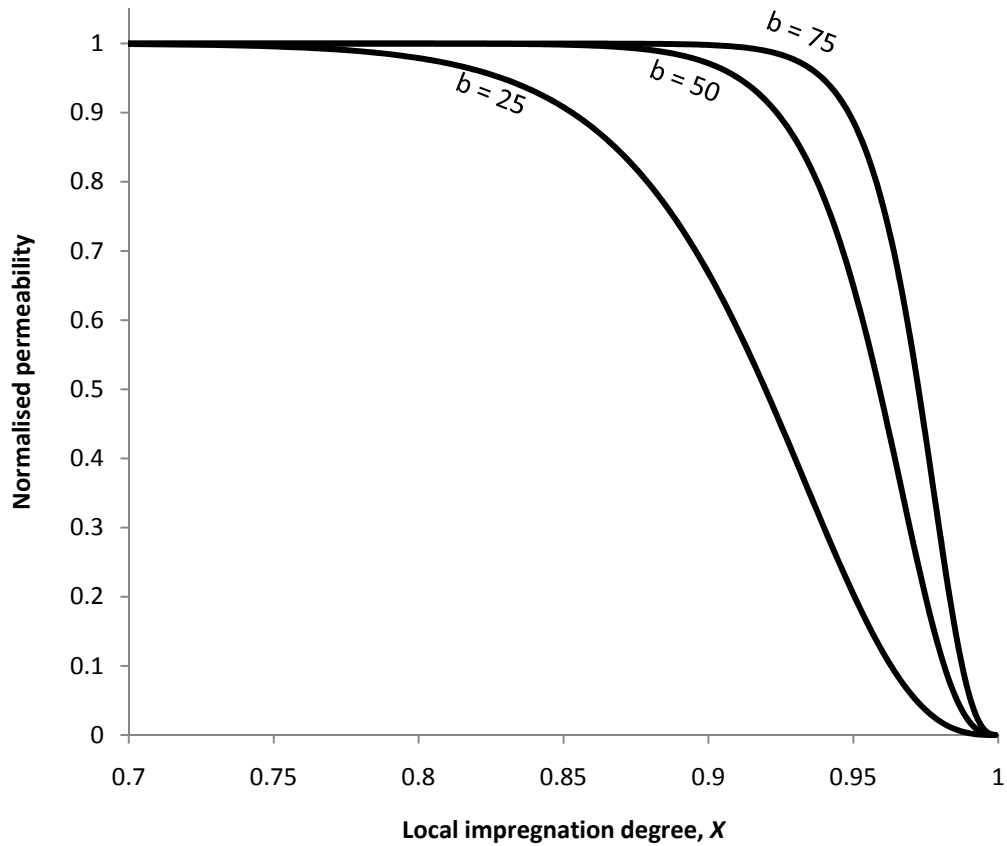


Figure 4.19: Normalised transverse permeability, from equations (4.15) and (4.16)

## Impregnation length

Pressure in the resin pools drives the resin into the dry fibre bundles, until the centre of the bundles is impregnated. Hence, the resin must cover an impregnation length which is equivalent to the average radius of the dry fibre bundles. For Twintex® PP-glass, the size of the dry fibre bundles was experimentally determined by Klinkmüller et al. [30], corresponding to equivalent circular bundles with an average radius of approximately 0.28 mm. Such dry fibre bundle size is coherent with the discretised layer, which varies from 0.41 to 0.22 m as stated above. Therefore,  $L = 0.00028$  m.

## Global consolidation

Following the steps described so far, as the local temperatures increase due to applied heating, each discrete layer undergoes a solid-state compaction  $X_d$ , termed “initial de-bulking” and determined by equation (4.4). When the layer reaches the resin melting temperature  $T_m$ , a simultaneous liquid-state inter-bundle compaction and intra-bundle impregnation  $X$  starts and develops until full consolidation is attained, modelled by equation (4.19). The resulting impregnation degree  $X$  is then scaled as  $X^i = \text{transf}(X)$  before it is added to the initial de-bulking.

This sum determines the final local consolidation  $\bar{X}$ . Finally, the global consolidation  $\bar{\bar{X}}$  is computed as:

$$\begin{aligned}\bar{\bar{X}} &= \sum_1^{41} X \cdot (\text{local layer weight}) = \sum_1^{41} (X_d + X^i) \cdot (\text{local layer weight}) = \\ &= \sum_1^{41} (X_d + \text{transf}(X)) \cdot (\text{local layer weight})\end{aligned}\tag{4.20}$$

This modelling process is shown in the schematic Figure 4.20.

## Summary

As shown by the consolidation experiments carried out, the through-thickness temperature distribution across thick laminates is far from being uniform. To better understand the mechanisms involved in the consolidation, a non-isothermal model has been constructed, which calculates the local consolidation degree within each layer of a discretised laminate. Different consolidation stages have been identified and sub-modelled according to the literature. Also, an empirical relationship has been developed,  $V_f(X) = aX^b + c$ , which relates locally the glass volume fraction with the impregnation degree in each layer.

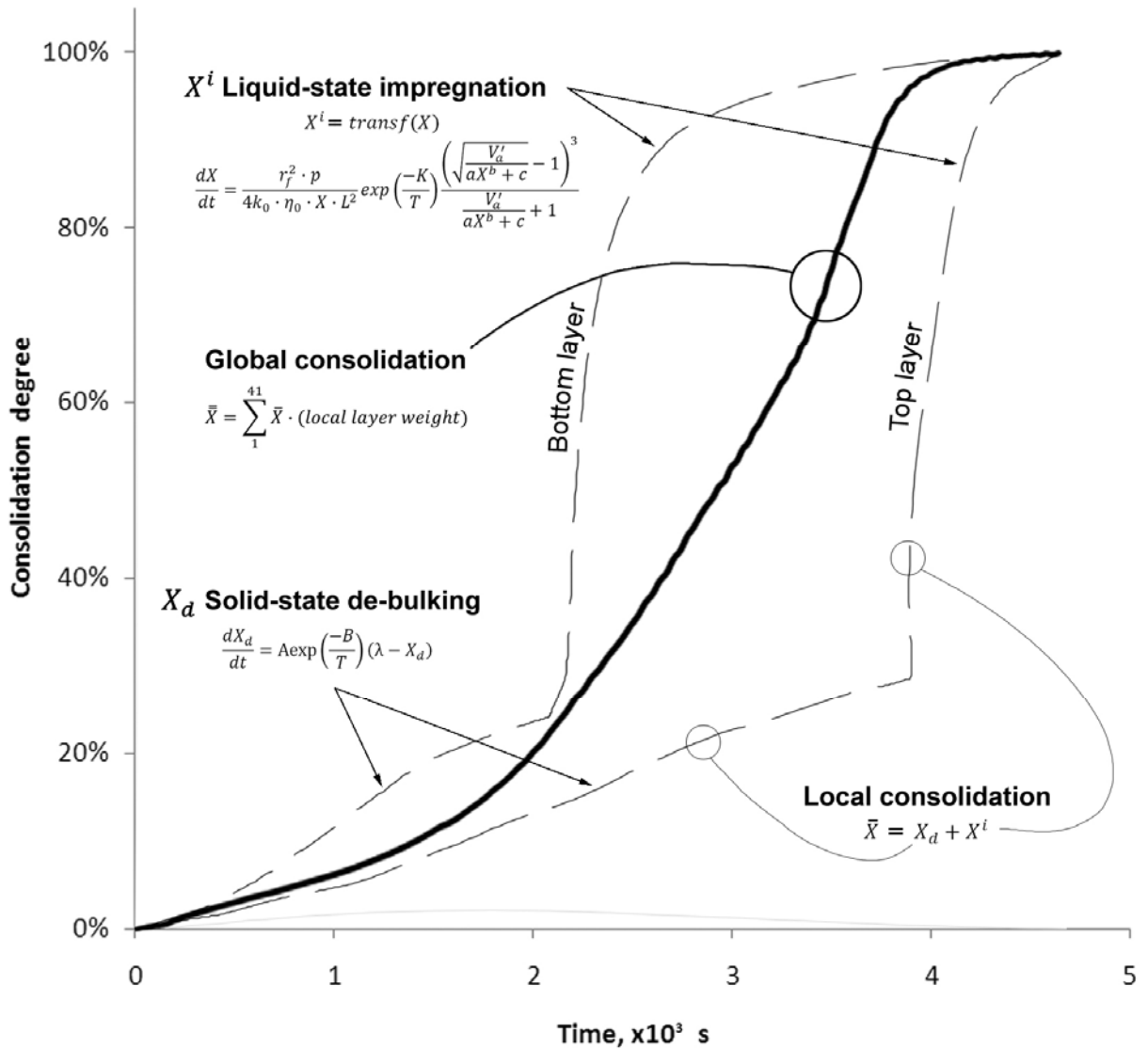


Figure 4.20: Schematic representation of the modelling process

This model implies a number of assumptions, most of which have been discussed above and are listed on the following:

- The initial solid-state de-bulking is considered an Arrhenius-type temperature-activated process with a limit at around 40% of the local consolidation degree with the form:

$$\frac{dX_d}{dt} = A \exp\left(\frac{-B}{T}\right) (\lambda - X_d)$$

where (next page):



Variables	Description	Unit
$X_d$	Local consolidation degree due to de-bulking	[%]
$t$	Time	s
$T$	Local absolute temperature	[K]
Constants		Value
$A, B$	Fitting constants	<i>*Discussed below</i>
$\lambda$	De-bulking compaction limit, set at 0.40 x the overall compaction according to [37]	0.40

- The de-bulking process is assumed to be locally followed by a liquid-state impregnation of circular dry glass fibre bundles, as soon as  $T_m$  is reached. When the local layer reaches the resin melting temperature  $T_m$ , a simultaneous inter-bundle compaction and intra-bundle impregnation occur, which is indistinguishable from a Darcian impregnation of the dry reinforcing glass fibres.
- The pressure in the matrix pools is constant.
- The resin flow during impregnation is Newtonian, and takes place only transversely across the glass fibres up to full local consolidation, whereas axial flow may occur afterwards.
- The matrix pressure is considered constant over all resin fronts, although affected by a reduction of 30% from the pressure applied to the laminate.
- No void nucleation, migration or dissolution in the matrix is assumed to occur.
- No capillary forces are considered, since experiments have shown capillary flow occurs after times in the range of hours [20].
- Gravity is neglected.

- The PP resin viscosity is assumed to be Arrhenius-type, and the Gutowski formulation of the transverse permeability of the glass fibres is adopted, finally resulting in:

$$\frac{dX}{dt} = \frac{r_f^2 \cdot p}{4k_0 \cdot \eta_0 \cdot X \cdot L^2} \exp\left(\frac{-K}{T}\right) \frac{\left(\sqrt{\frac{V'_a}{aX^b + c}} - 1\right)^3}{\frac{V'_a}{aX^b + c} + 1}$$

In the equation above, variables and parameters are as follows:

Variable	Description	Value
$X$	Local impregnation degree	[%]
$t$	Time	[sec]
$T$	Local absolute temperature	[K]

Constants	Description	Value
$k_0$	Kozeny constant (fitting constant)	<i>*Discussed below</i>
$r_f$	Average fibre radius	18 $\mu\text{m}$
$P$	Resin front pressure, with a reduction of 20% from pressure on laminate based on the literature	0.07 MPa
$\eta_0$	Arrhenius constant for the resin viscosity (from [30])	$2.6 \cdot 10^{-3} \text{ Pa}\cdot\text{s}$
$K$	Arrhenius exponent for the resin viscosity (from [30])	5600
$L$	Resin penetration distance to be covered	$1.74 \cdot 10^{-7} \text{ m}^2$
$V'_a$	Maximum glass volume fraction (from[33])	0.91
$a$		Real-time calculated
$b$	Calculated values for $V_f = a \cdot X^b + c$	25 – 75, <i>*Discussed below</i>
$c$		Real-time calculated

## Mathematical solution

The equations governing the initial de-bulking and subsequent liquid-state impregnation of the fibres were numerically solved using the Simulink module of MatLab®. This software allows the construction of a flow circuit containing the elements of the equations and

elemental mathematical operators, which is translated into a code that solves the equivalent ordinary differential equation.

At each discrete point of the laminate, the instantaneous absolute temperature is evaluated and used first with the de-bulking sub-model. Once the melting temperature was reached, the circuit switches into the impregnation degree, applies a scale linear transformation and adds it up to the local consolidation degree. There is one de-bulking and one impregnation circuit per each discrete point in the laminate. Finally, the global consolidation degree is computed as the sum of the local consolidation states divided by the thickness of the corresponding discrete layer, with equation (4.20). A flowchart of this solving process is shown in Figure 4.21, whereas Figures 4.22 and 4.23 show the actual Simulink assembly for one layer and the final complete circuit, respectively. It must be noted that these figures have been included to give only an impression of the appearance of the actual model in the Simulink interface.

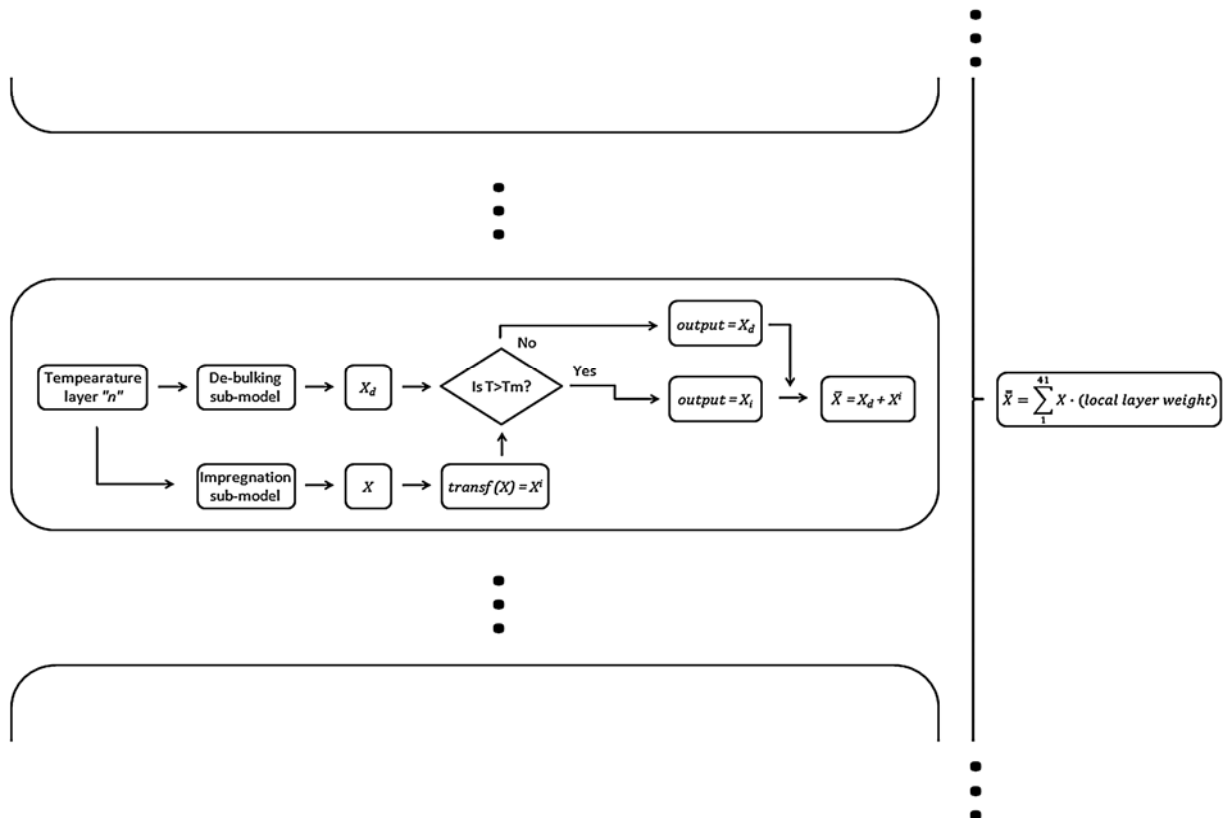


Figure 4.21: Mathematical solver flowchart

A non-isothermal consolidation model for thick laminates

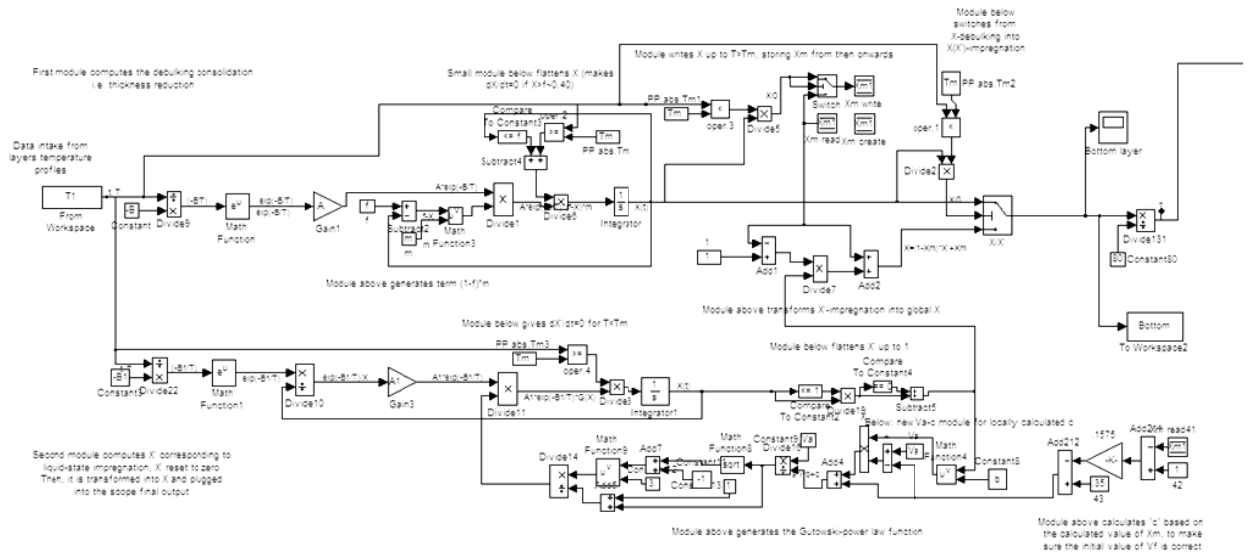


Figure 4.22: Screen print giving an impression of one MatLab Simulink assembly, corresponding to the bottom layer

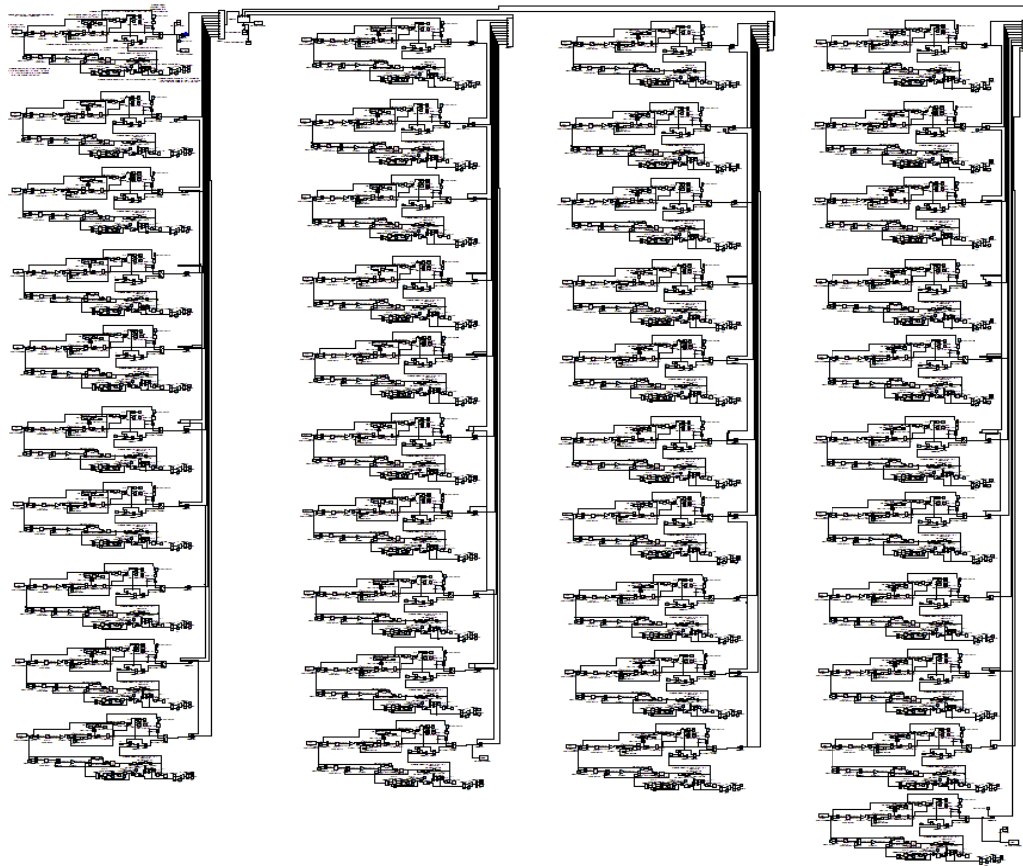


Figure 4.23: Actual parallel connection of the 41 assemblies

The equivalent numerical system was solved by the Dormand-Prince method, and real-time displayed. This allowed the adjustment by hand of the 3 fitting constants ( $A$ ,  $B$ ,  $k_0$ ) and the

fine tuning of the constant  $b$ , which governs the consolidation rate at its very end and is reasoned above to be between 25 and 75.

## Results and discussion

After tuning, the model yielded a very satisfactory prediction of the whole consolidation process, as seen in Figure 4.24.

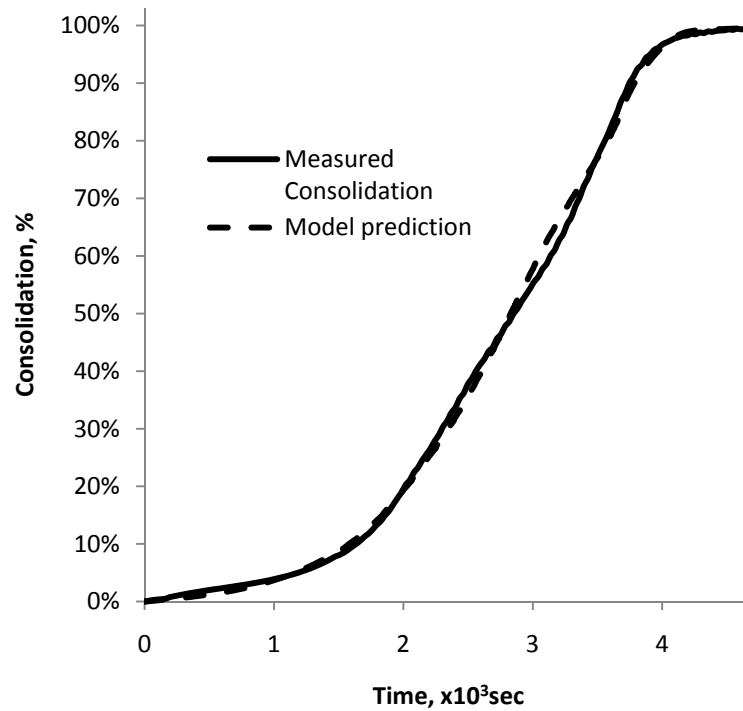
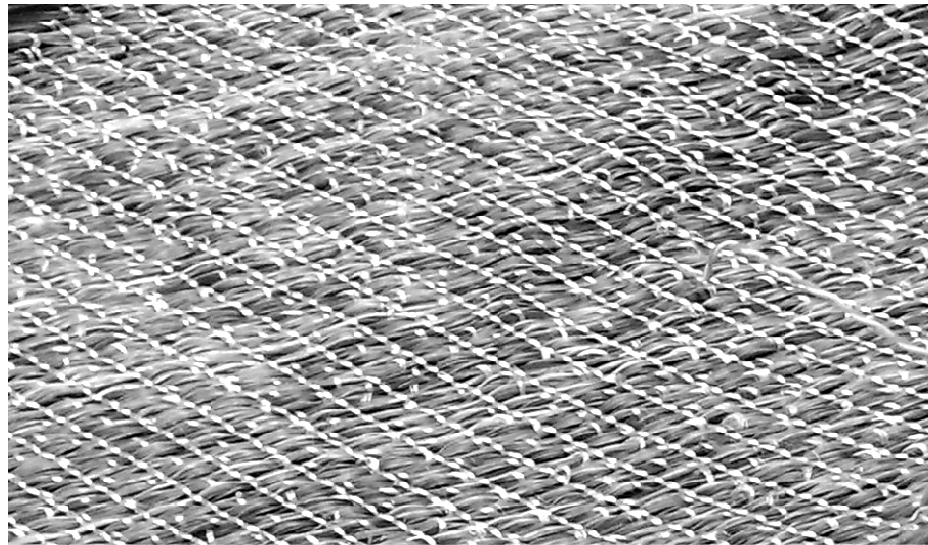


Figure 4.24: Measured and predicted consolidation of a 9 mm thick PP-glass laminate

The final values for the fitting constants are:

Fitting constants	Description	Value
$A$	Constants governing the initial de-bulking rate	2.2
$B$		3100
$k_0$	Kozeny constant (fitting constant)	26.5
$b$	Initiation of the fibre permeability rapid decay	36

The fitting value obtained for the Kozeny constant is 26.5, higher than the values of 0.2 used by Gutowski for well-aligned unidirectional carbon fibres [39], and 5 for equally well-aligned glass fibres reported by Klinkmüller [30]. Hence, the permeability of multi-axial fabrics appears to be approximately 5 times lower than that of the unidirectional Twintex® yarns tested by Klinkmüller. This seems to be a reasonable result, taking into account that multi-axial arrangements are likely to be less permeable and that the fibres, shown in Figure 4.25, were not as well aligned as in the experiments reported by Klinkmüller.



**Figure 4.25: Top ply of the laminate, showing the relatively poor fibre alignment of the multi-axial fabric**

Also, the value of  $b$  found to best fit the data is 36, which leads to a practically constant permeability during all the impregnation, and a final steep decrease starting at around 85% of the impregnation, which is well in line with the related results found in the literature, as discussed above.

The measured consolidation rate (Figure 4.24) increases during the whole process except at the very end, and also between 50-70%. It is a remarkable result that this localised decrease is mirrored by the model prediction, although somehow lagged towards the end of the process, at around 70-80%. The actual connection between the measurements and the model is the temperature profile, which means that this rate decrease is linked with the temperature in the material and is unlikely to be a background effect or a measurement mistake. One possible reason for this discrepancy is that the actual temperature profile

inside the laminate may differ slightly from the interpolated data, leading to the observed lag. The measured decrease itself may be due to local material variability.

As predicted by the model (Figure 4.26), the actual full impregnation of each layer takes about 1500 seconds up to the accepted value of 99.5% thickness reduction. Nevertheless, 99.1% is attained in only 1000 seconds, which can be preferred depending on the application due to environmental and energy cost. The final degree of consolidation reached at the bottom, middle and top layers is respectively 99.7%, 99.5% and 99.1%, which together with the remaining 38 layers deliver the final 99.5% for the whole laminate.

As seen at the beginning of this chapter, the simple 1-parameter model predicted with surprising accuracy the highest consolidation rates observed in the experiments. The comprehensive model developed afterwards predicts very sharp local impregnation rates for the quasi-linear part of the global consolidation, which in fact do not differ much from the concept of “instantaneous consolidation” assumed for the 1-parameter model. The initial de-bulking and final drop of the impregnation rate, account for the large disagreement between measurements and 1-parameter model predictions at the beginning and the end of the process.

One possible way to use the non-isothermal model to optimise boat parts manufacturing is applying the model to an interpolated in-laminate temperature profile. This interpolation can be done by measuring the temperature on both laminate boundaries (top and bottom layers) and assuming an internal temperature distribution as in Figures 4.6 and 4.7. Alternatively, the internal temperature profile could be calculated according with the 1-dimensional heat equation:

$$\frac{\partial T}{\partial t} = \alpha \frac{\partial^2 T}{\partial x^2}$$

where  $T$  is the absolute temperature at distance  $x$ ,  $t$  is the time, and  $\alpha$  is the apparent thermal diffusivity which can be empirically determined. Once the through-thickness temperature profile is determined, the model can predict the consolidation times at any time and any point of the laminate.



If this model is applied to the temperature of a single point on the laminate, a large discrepancy is likely to occur, between the measured and predicted consolidation curves. This can be seen in Figure 4.26, where local and global predicted consolidation curves are shown, and also in Figure 4.18, where the temperature in the middle of the laminate was used to plot and fit the last bit of permeability rapid decrease. If we use for instance the temperature on top of the laminate, we will obtain the curve corresponding to this discrete layer. While this curve may give a reasonable estimation for the total consolidation time, it cannot accurately predict the actual consolidation curve. The reason for this is that the consolidation of thick laminates does not occur in one shot. Instead, it is the additive result of the consecutive compaction of the laminate layers, occurring like a propagating wave from the hot to the cool end, or from both ends to the laminate mid layer if double side heating is used.

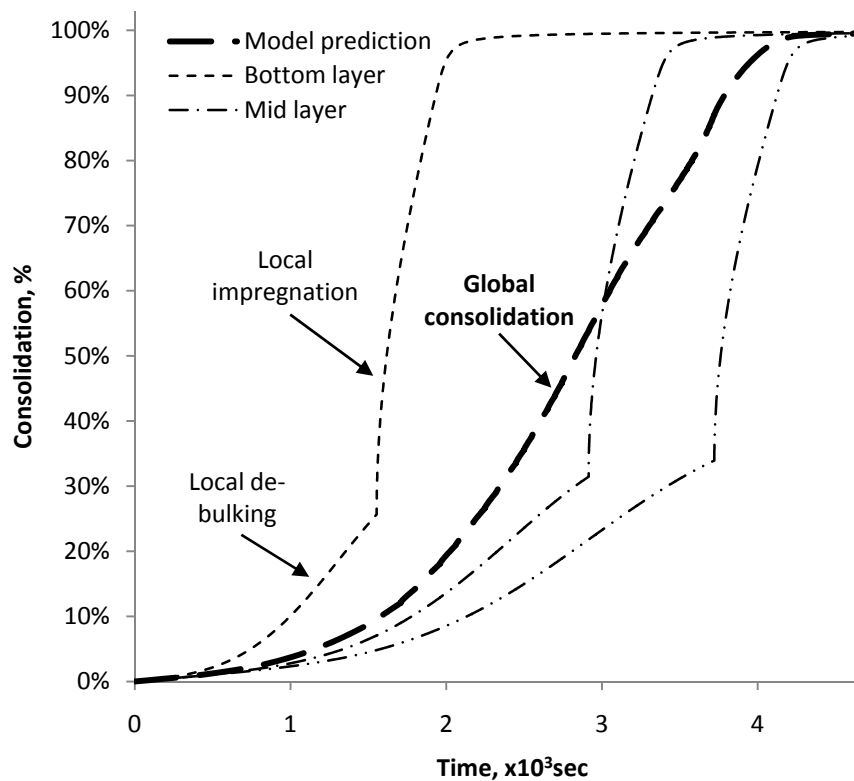


Figure 4.26: Global consolidation predicted by the model and local consolidation curves corresponding to the top, mid and bottom discrete layers of the laminate

Nevertheless, fitting the model using a single temperature measurement may be useful for the practicalities of component-making in the workshop, especially if the temperature is taken on top of the laminate or even top of the bag, where it is very easy to measure.

## **Conclusions**

With the objective to investigate the consolidation under vacuum of PP-glass thick laminates, a representative data set was recorded using a purpose-built, one-side heating testing rig. Data comprised significant temperatures and the thickness evolution of a 9 mm thick Twintex® laminate during consolidation. The laminate was discretised into 41 finite layers, where the temperature distribution was interpolated from 3 measurements (bottom, middle and top) using a cubic polynomial.

A consolidation model was constructed, relating the interpolated temperatures with the local consolidation degree of the laminate in each of the finite layers defined. The model described the consolidation of the laminate as an initial solid-state de-bulking, followed by a rapid liquid resin impregnation when the local temperature reached  $T_m$ . The model achieved excellent agreement with one set of experimental data, suggesting that:

- The consolidation of thick laminates does not occur simultaneously through the thickness, but as a wave that propagates across the laminate from the hot to the cool layers.
- The de-bulking process is responsible of up to 25-35% of the local consolidation, and can be described by a temperature-activated Arrhenius-type formulation
- The impregnation can be considered Darcian, and takes approximately 1500 seconds for an approximately 0.4 mm thick unprocessed material layer.
- The impregnation rate can be described as depending on the product  $S \cdot p$  (permeability x pressure), which remains constant until approximately 85% of the impregnation has occurred.
- This model still requires testing against other materials and process conditions for full validation.

## **Chapter 5 – Tooling materials for TPC vacuum forming**

Full consolidation of TPCs leading to a good quality boat part can only be attained on a mould which complies with a number of requirements [87]. This represents a challenge to the extent that it is one of the reasons why TPC boats are still not wide-spread.

The choice of an appropriate tooling material is one of a very practical nature. Companies often carry out their own research which, if successful, is rarely published because it constitutes a commercial advantage over competitors. To summarise the state of the art, this chapter starts describing and discussing a review on composite, metallic and ceramic materials, containing the industrial expertise from BAE Systems. One of these materials was identified as a cost-effective promising alternative and subjected to laboratory testing, discussed on the second half of the chapter.

### **Mould requirements**

A mould capable of vacuum forming of TPCs requires the ability to stay air-tight, because any air leak into the vacuum bag would reduce the pressure on the laminate and increase the void content. A suitable mould must also be made in virtually any shape as boat hulls usually have complex, double curvature shapes. Traditionally, this has been best achieved with polymer composite moulds, although other composites and materials can potentially offer sufficient shape freedom. Secondly, geometrical stability at the elevated processing temperatures seen in Chapter 4 is required to deliver parts with the desired geometry and dimensions. In particular, the mould must resist its own thermal expansion, and reasonably match that of the material to be moulded. Also, the moulds must survive the loads caused by transportation, handling, material lay up during component manufacturing and especially

component demoulding. Finally, the mould material must have a reasonably long life while satisfying all these requisites within a reasonable cost.

According to the criteria mentioned above, a review was conducted including off-the-shelf and experimental materials. Amongst these, a phosphate based ceramic composite was considered a promising alternative and chosen for laboratory experimentation which delivered interesting results.

## Performance and cost

A range of mould materials including various reinforced composites and metals were reviewed according to the criteria described above. These criteria lead to a number of variables to consider, which are detailed in Table 5.1.

**Table 5.1: Relevant characteristics of tooling materials**

Criterion	Reason
Service temperature	The service temperature determines which range of materials can be processed with a particular tooling material
CTE	There should be an approximate match between the tool coefficient of thermal expansion (CTE) and that of the composites to be laminated
Surface finish	A smooth surface finish is preferred
Tool life	High tool life is desirable
Mould processing temperature	The mould material processing temperature determines the plug material to be used in its manufacturing
Plug material	The plug material influences the overall cost
Cost	A low cost material is desirable

All values of these variables were supplied by the manufacturers, and all cost calculations were related to a Pacific 24 RIB, which mould surface was calculated based on the drawing shown in Figure 5.1. This mould surface was later scaled up to 8.5 m long to best meet the objectives of this research work, according to the industrial partner in this project, BAE Systems. Mould air-tightness was assumed to be satisfactory in all materials. However,

metallic welds usually need an air-tight coating and ceramic materials show an inherent porosity which needs to be sealed, as explained in the sections below.

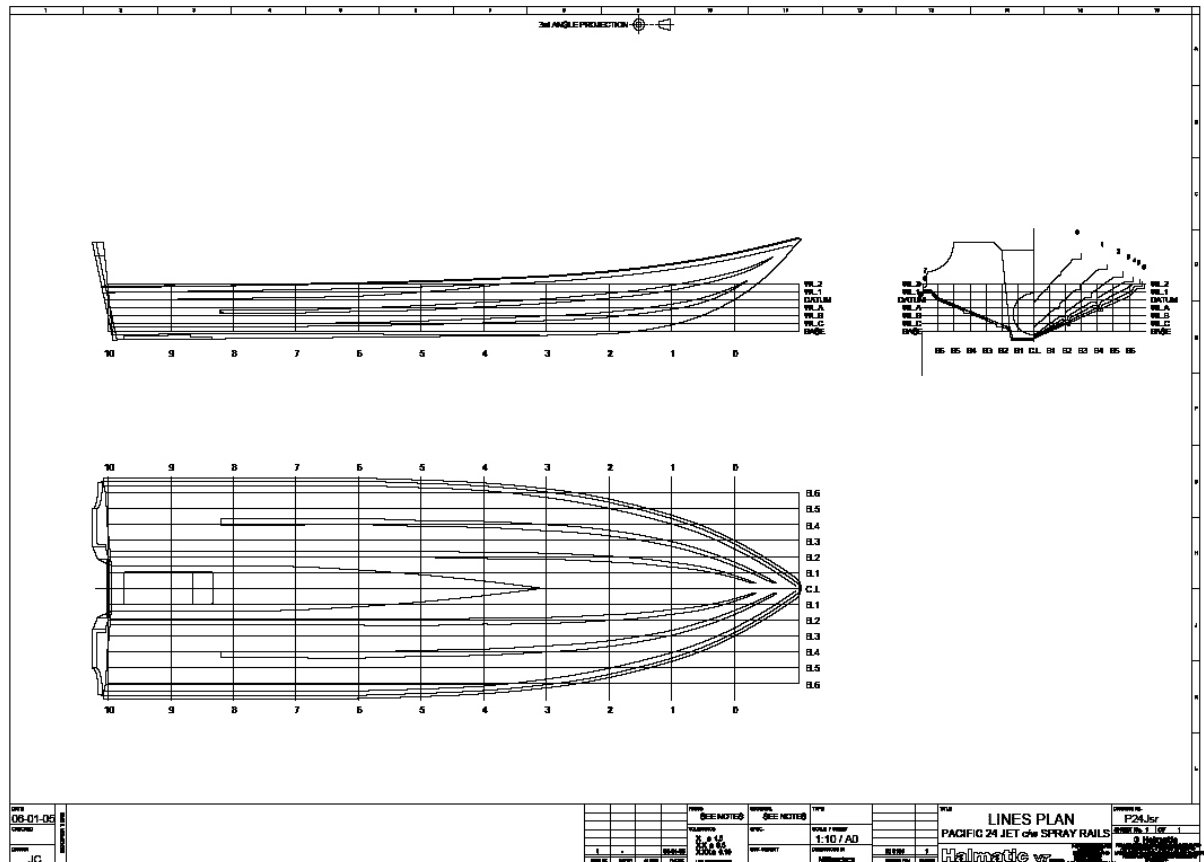


Figure 5.1: Drawing of the Pacific 24 RIB hull

## Polymer composite tools

The polymer composite materials considered include various epoxy-glass, polyurethane-glass and cyanate ester-glass. The use of glass fibre follows the common practice of matching the reinforcing fibre in the mould and the boat, which helps to keep the CTE difference within reasonable limits.

With regard to the mould service temperature, this value for polymer composites is considered equal to the  $T_g$  of the resin. The reason for this value is that polymer resins experience an increasing loss in modulus as the temperature increases beyond their  $T_g$ , as seen in Figure 5.2 [88]. This material softening would make the geometry of the moulded part uncertain. While the  $T_g$  of most of the epoxy resins suitable for glass fibre composites is

usually between 100 and 200°C, only those around 200°C have been included in this review (Table 5.3). Comparing these temperatures with the processing temperatures for TPCs (Chapter 1), it comes that the range of materials we can mould on epoxy-glass moulds is practically restricted to PP-based composites only. In reality, a range of resins can be processed at around 200°C, as PVDF, POM, LPET and PE. However, the suitability of these resins for glass-reinforced composites in boats is rather limited for various reasons including price, availability, degradation in the marine environment, mechanical properties and top service temperature. Epoxy-glass moulds have also a good match with the CTE of PP-glass composites, as seen in Tables 5.2 and 5.3.

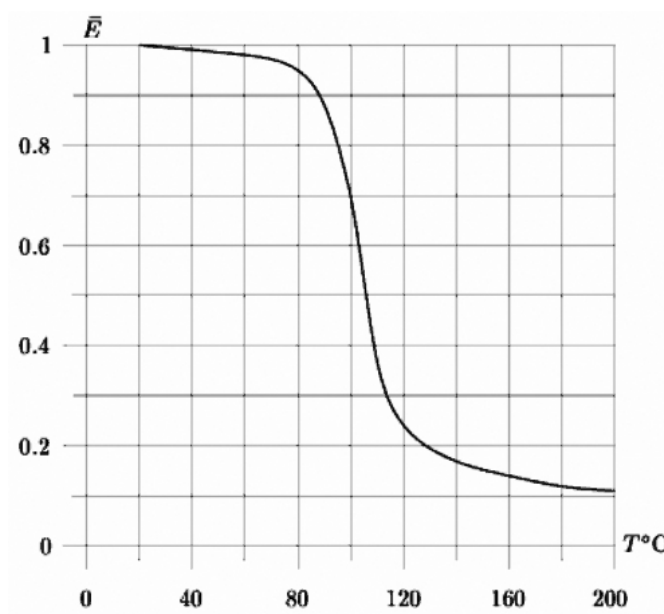


Figure 5.2: Typical mechanical behaviour of a cured epoxy resin near its  $T_g$  (from [88])

Table 5.2: CTE values in  $m/m/^\circ C$  for Twintex® twill woven, 1485  $g/m^2$  fabrics

	Average	STD
Warp	5.44E-06	4.69E-11
Weft	6.28E-06	2.69E-07
Through the Thickness	1.07E-06	7.478E-05

Other mould resins as polyurethane and cyanate ester have a higher temperature service, although their own high processing temperature requires an expensive plug that negatively impacts on the overall cost. The cyanate ester tooling pre-preg, currently marketed for thermosetting moulding, has been experimentally used with TPCs in the past [44] with reservations due to high sensitivity to water during their own curation process, gas emissions at high temperatures, high brittleness and subsequent risk of cracking upon mechanical or thermal loading.

There are other resins exhibiting higher service temperatures as bismaleimides or polyimides but, in addition to their very high prices, they exhibit the drawbacks of cyanate ester to even a higher degree [89]. Hence, moulds made with such resins would be very fragile. In particular, any small crack would damage the necessary air-tightness of the moulds for vacuum forming.

Therefore, high-Tg epoxy-glass attains a reasonable balance between performance and cost for moulds for vacuum-forming of complex shaped TPC parts. Nevertheless, they are restricted to PP based composites, with which they will work at their limits. A bow-shaped composite tool intended for testing can be seen in Figure 5.6.

## **Metallic tools**

As an alternative to polymer composite moulds, metals have a remarkably higher service temperature, a longer tool life and a good moulding surface finish as well. Also, their unmatched thermal conductivity potentially facilitates quick heating and cooling, hence usually desired fast processing cycles. However, their very high thermal expansion may cause problems with parts dimensions, especially in the case of aluminium which has a CTE four times that of PP-glass.

In terms of a reasonable balance between performance and cost, cast or welded aluminium compete with welded steel, the former being used to manufacture one-piece Twintex® catamaran hulls (ÉireComposites, 2008). Cast metal can be manufactured to any shape and then machined if necessary whereas welded plates have a more limited formability. However, steel may be favoured against aluminium under the same conditions because of a lower overall cost, especially when aluminium machining is involved. Machining a mould out

of a metal block demands large quantities of material and energy and may actually be very expensive and very difficult for boat sizes beyond 5 m.

Electroformed nickel provides an excellent shape formability and surface finish, with a tailorable thickness. However, these are delivered at a price per square meter which is approximately 20 times that of epoxy-glass moulds, and 40 times the price of a steel tool.

Thus, welded steel stands out as a feasible and cost-effective mould material for simple shapes as flat or single curvature panels and is being used by BAE Systems to manufacture small PP-glass military boats (Figures 5.3 and 5.4) as the one shown in Figure 2.2, and other experimental structural parts (Figure 5.5).

## **Ceramic tools**

On the experimental end of moulding materials, ceramic composites have a very good formability and very high service temperature, which potentially enables the processing virtually any TPC in any shape and size.

The ceramic matrices suitable for composite moulds are chemically bonded, in contrast to the sintered, or thermally bonded ceramics usually found in other applications. The cost of the raw materials contained in these ceramics is usually low, although the use of expensive fibres and manufacturing methods may increase their final cost. On the negative side, their thermal conductivity is low, although still comparable to that of polymer composites. Another drawback of ceramic composites is their inherent porosity. Both materials considered in this study, namely Pyrotool® and Vubonite®, are naturally porous due to the nature of their manufacturing process. This porosity makes impossible good quality vacuum processing because of air leaks through the tool, preventing adequate levels of vacuum pressure.

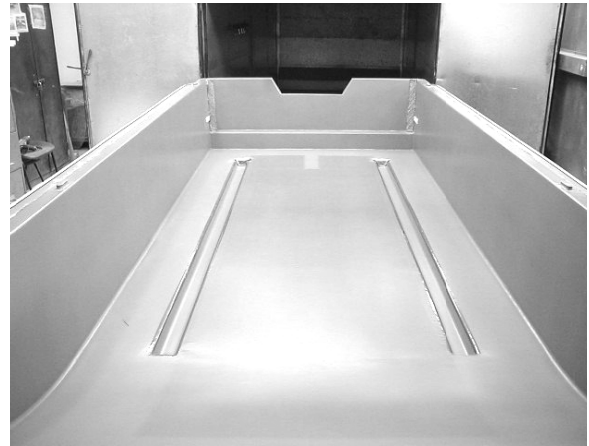
Pyrotool® has been trialled in the past by BAE Systems. The results obtained revealed some porosity and cracking-driven air leaking, to the extent that it was necessary to seal the tool with a bag from both sides (envelope-bagging) to enable satisfactory quality mouldings. Such technique helped to successfully manufacture the Twintex® experimental Atlantic 85 RIB shown in Figures 2.3 and 2.4.



Currently being under development (ÉireComposites, 2010), Pyrotool® has the additional drawback of being remarkably expensive, partly because of the need for carbon fibres. The chemistry of the ceramic matrix is silicate-based in this material; hence it attacks any reinforcing glass fibres, which forces the use of expensive carbon fibres.



**Figure 5.3: PTFE coated 15 mm thick steel tool used in BAE Systems for PP-glass military boats**



**Figure 5.4: Detail of steel tool**



**Figure 5.5: PTFE film coated 6 mm thick steel tool, for an experimental automotive part**



**Figure 5.6: High temperature epoxy-glass test tool, shaped as a RIB bow**

Tooling materials for TPC vacuum forming

Table 5.3: Comparison amongst mould materials for vacuum processing of TPCs

Manufacturer	System	Type	Service Temperature, °C		CTE, e-6/°C	Surface Finish	Tool life tested, cycles
			Manufacturer values	Tested Tg onset			
ACG [90]	LTM 318	Epoxy Prepreg	180 (Tg = 219)	Tg = 189	2.9 - 3.4	Good	10+
Sicomini [91]	SR7900 ABC	Wet Epoxy, Hand Lay Up (visc. = 15000 mPa·s = cP)	160 (Tg = 180-210)	Tg = 193	usual value for glass - epoxy ~ 3-6	Good	3+
Airtech [92]	Toolfusion 2A/2B	Wet Epoxy, Infusion (viscosity = 475 cP)	(Tg = 185)	-	usual value for glass - epoxy ~ 3-6	Good	-
[36]	ToolMaster CEP-G3	Cyanate ester - epoxy Prepreg	230 (Tg = 260)	-	1.9 - 2.7	Good	-
Amber [93]	HX42-00 600gsm Glass	Epoxy Prepreg	190 (Tg = 200 - 220)	-	usual value for glass - epoxy ~ 3-6	Excellent (coupling gel coat)	-
[94]	EL42 Laminating Resin ABC	Wet Epoxy	190	-	usual value for glass - epoxy ~ 3-6	Excellent (coupling gel coat)	100
Axson [95]	Epolam 2090/2026	Wet Epoxy infusion (viscosity = 650 cP)	(Tg = 205)	Tg = 192	usual value for glass - epoxy ~ 3-6	Good	12+
Bayer [96]	Blendur TP.KU 3-4520 + 3-4523	Polyurethane resin (viscosity = 23 cP)	240	-	Resin only ~ 40-65	-	-
<i>Generic steel</i>	6mm Welded steel	Welded metallic tool	Above 400	-	13 [97]	Good	300+
Galvanoform	Autoclave grade Electroformed Nickel	Electroformed tool	Above 400	-	13 [97]	Excellent (galvanic nickel deposition)	300+
<i>Generic aluminium</i>	Aluminium (welded/cast)	Welded/cast metallic tool	Above 400	-	22 [97]	Good	300+
Symbion	Vubonite®	Ceramic - glass, Phosphate-based	Above 400	-	8 [98]	Being tested	-
Pyromeral	Pyrotool®	Ceramic - carbon, Silicate-based	Above 400	-	-	Good (PTFE)	-

Tooling materials for TPC vacuum forming

Manufacturer	System	Thermal conductivity, W/mK	Mould-on-plug processing temperature, °C	Plug material <sup>1</sup>	Costs <sup>2</sup>				8.5 m long RIB 26.4 sqm surface
					Plug Cost, (machined if applicable), £/m <sup>2</sup>	Mould Labour Cost	Mould Material <sup>3</sup> cost, £/m <sup>2</sup>	Total Mould Cost, £/m <sup>2</sup>	
ACG	LTM 318	Typically ~ 1[99, 100]	from 65	Polyurethane toolboard	739	370	232	1341	35392
Sicomini	SR7900 ABC		95	Epoxy resin/toolboard	898	370	170	1438	37956
Airtech	Toolfusion 2A/2B		50	MDF	572	370	173	1115	29425
	ToolMaster CEP-G3		from 120	Epoxy resin/toolboard	898	370	1546	2814	74282
Amber	HX42-00 600gsm Glass		from 65	Polyurethane toolboard	739	370	180	1289	34020
	EL42 Laminating Resin ABC		Room temperature	MDF	572	370	170	1112	29346
Axson	Epolam 2090/2026	40	MDF	572	370	218	1160	30613	
Bayer	Blendur TP.KU 3-4520 + 3-4523	3 (resin only) [97]	160	Hi-Tg Epoxy Tool	1112	370	112	1594	42070
<i>Generic steel</i>	6mm Steel	47 [97]	-	-	-	-	-	800	13200
Galvanoform	Autoclave grade electroformed Nickel	60 [97]	-	-	-	-	-	21000	-
<i>Generic aluminium</i>	Aluminium (welded/cast)	130 [97]	-	-	-	-	-	More expensive than steel	-
Symbion	Vubonite®	1[98]	80	Epoxy resin/toolboard	-	-	-	Affordable (experimental)	-
Pyromeral	Pyrotool®	-	-	-	-	-	-	Very expensive (experimental)	-

<sup>1</sup> Service temperature of MDF: up to 50°C; Polyurethane tool board up to 90°C; and Epoxy toolboard up to 150°C. A High-Tg epoxy composite tool is needed beyond 150°C. Prices according to quotations to BAE Systems in 2008.

<sup>2</sup> Cost calculation was based on indicative man-hours from an established RIB manufacturer required to build a 8.5 m RIB mould, labour prices and material quotations obtained in 2008.

<sup>3</sup> Mould material cost estimation includes resin and reinforcing E-glass fibres

### ***An affordable alternative***

Another, more affordable alternative was found in Vubonite®. This material, also known as inorganic phosphate cement (IPC), was developed in the department of Mechanics of Materials and Constructions (MEMC), Vrije Universiteit Brussel (Belgium), and commercialised by a spin-off company, Symbion NV. It consists of a mixture of wollastonite powder and phosphoric acid plus certain additives. These are mixed and then rolled to impregnate chopped strand glass mats, similarly as done with polymer composites. The resulting textile reinforced cement (TRC) composite has a neutral pH after hardening. Therefore, glass fibres are not chemically attacked by the cementitious matrix, making the use of traditional E-glass fibres possible.

These fibres provide the brittle matrix with sufficient strength and stiffness by means of a mechanism known as “strain hardening behaviour”. If not chemically attacked, fibres appear to arrest the energy which is liberated by running cracks originated in the loaded matrix. If the fibres are long enough not to pull out locally at a crack, and if the minimum amount of fibres is exceeded, a subsequent formation and stabilising of several cracks occurs. After full cracking of the matrix, the fibres can take up additional load, leading to the mentioned strain hardening behaviour (Figure 5.7). The mechanical properties (see Table 5.4) delivered by this series of mechanisms [101-103], whereas lower than those of metals and thermosetting composites, are still sufficient for a boat mould. Its CTE and thermal conductivity are in the region of those of polymer materials used with composite moulds, hence also appropriate for this application. The processing of the ceramic matrix features a relatively high shrinkage (Table 5.4) which is reduced by the addition of Zircon powder to the matrix.

In addition, Vubonite® is water-washable and does not have associated VOCs, both making it an environmentally-friendly option before, during and after manufacturing. Due to these environmental considerations, plus its cost and performance, it was believed that this material had a potential as mould material for thermoplastic composite boatbuilding and other applications [103]. As mentioned, its free shape capability and very high service temperature make it a very interesting mould material for the processing of virtually any thermoplastic composite, especially in a batch production (~10-100 units a year per mould) scheme as usual in boatbuilding. Nevertheless, its porosity and stabilised cracked state do

not favour the use of vacuum-forming with such mould material. The need of a technique that addressed this porosity was the main motivation for the experiments described below.

**Table 5.4: Vubonite properties (from [98])**

		Hardened matrix only	Glass-reinforced matrix
Specific gravity, dry	kg/dm <sup>3</sup>	1.6	1.75
Specific gravity, fresh, wet	kg/dm <sup>3</sup>	1.9	-
pH		7	-
Porosity	%	20 to 30	-
Pores' dimensions	nm	10	-
Chemical shrinkage	%	unmeasurable	-
Shrinkage after drying	%	0.25 to 0.5	-
Gas emission at extreme temperature raise		~ 0	-
Compressive strength	MPa	60	60
Tensile strength	Mpa	10	30
Elasticity (E-modulus)	GPa	18	5-20
CTE	E <sup>-6</sup> /K	8	-
Coeff. heat conduction	W/mK	~ 1	-
Specific warmth	J/kgK	1	-
Areal weight of random glass fabric	g/m <sup>2</sup>	-	300
Thickness of the laminate	mm/layer	-	0.9

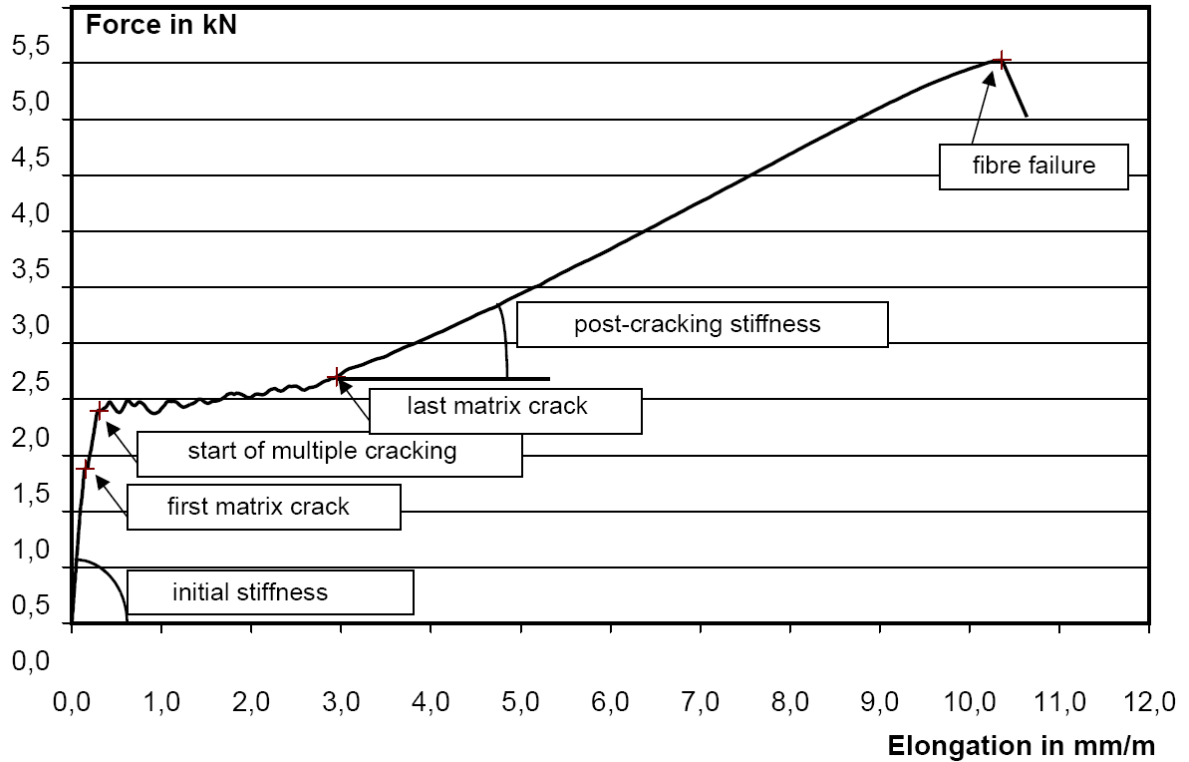


Figure 5.7: Mechanical behaviour of glass-reinforced Vubonite® (from [102])

## Experimental

### Testing rig

With the purpose to test the performance of porosity-sealed ceramic tools, a testing rig was designed and constructed in the Mechanical Manufacturing Laboratory in the School of Mechanical and Systems Engineering, Newcastle University. The design concept for this rig was an insulated heated chamber where TPC laminates of various thicknesses would consolidate under vacuum, with the ability to record the laminate thickness and various temperatures outside and inside the laminates.

The rig was heated by means of a bed of 3 kW electrical heaters and was also thermally insulated to enable sufficiently high temperatures inside. Insulation included 40 mm thick calcium silicate panels wrapping around the heating chamber and an additional layer of panels below the heaters bed, as specified in Table 5.5 and shown in the drawings and figures below. Also, a layer of aluminium-coated mineral fibre blanket was laid up around and above the chamber. A 25 mm thick calcium silicate lid covered the whole arrangement.

The rig was framed in steel, and also prepared to record the variation of the laminate thickness during consolidation with a linear variable displacement transducer (LVDT). The steel frame was designed and fabricated so that thermal deformations would be small enough to be disregarded. In addition, a lateral fan allowed for cooling rate variation by means of circulating air at room temperature underneath the tool, as seen on the drawings on Figure 5.8. For that purpose, air circulation was allowed by removing two sliding calcium silicate boards, next to the fan and on the opposite side.

The data gathered during the consolidation tests described below were post-processed and used to model the consolidation mechanism. The data analysis, post-processing, as well as the results and discussion of its modelling can be found in Chapter 4.

**Table 5.5: Materials and equipment used in the testing rig**

LVDT	Solartron DC50, with 250 mm rod extension
Heaters	Sheathed rod elements, 3 kW, manufactured by Elmatic (Cardiff, UK)
Electronics	IOtech PDAQ data logger connected to a PC, Temperature controller
Structure	Mild steel
Insulation	<ul style="list-style-type: none"> <li>• Calcium silicate boards: <ul style="list-style-type: none"> <li>○ 25 mm thick (lid)</li> <li>○ 40 mm thick (around the heating chamber)</li> </ul> </li> <li>• Mineral fibre blanket Thermal Ceramics Firemaster 607, 50 mm thick, around and above the heating chamber</li> </ul>

## Addressing the porosity

The processing of Vubonite® implies a certain degree of porosity. The pores, with a typical diameter of 10 nm, would allow for air leaking in during vacuum forming, inducing a high level of porosity in the moulded laminates. Therefore, they must be sealed to ensure air-tightness. This can be addressed at least in two different ways: by applying a sealant coating on the back surface or the moulding surface. It was decided to try both techniques.

### *Sealing the moulding surface*

A suitable coating for the moulding surface would need to be completely air-tight and have good adhesion to the substrate at all working temperatures. Good release properties would be desirable. However, this is usually facilitated by applying a release agent on the moulding surface, for all sorts of mould materials ranging from metals to composites. Four candidate proprietary coatings (Table 5.6) were applied to the surface of flat Vubonite® tools by a front line British coating specialist, selected according to their experience in porosity-sealing coatings applied to aircraft technology. The coated tools were intended to be tested with regard to their air-tightness prior to assess their ability to produce good quality laminates.

The Coating No. 1 failed since it had a very high acid concentration that dissolved the ceramic matrix of the tool. The remaining three coatings respected the material surface and were tested against air leaking.

**Table 5.6: Sealant coatings applied to the moulding surface of flat Vubonite® tools**

Coating No.	Type (proprietary formulations)	Service temperature, °C
1	Coating containing concentrated chromic acid	750
2	Polyimide-based	300
3	Boron nitride based dry film lubricant	600
4	Stoving coating	400



# Tooling materials for TPC vacuum forming

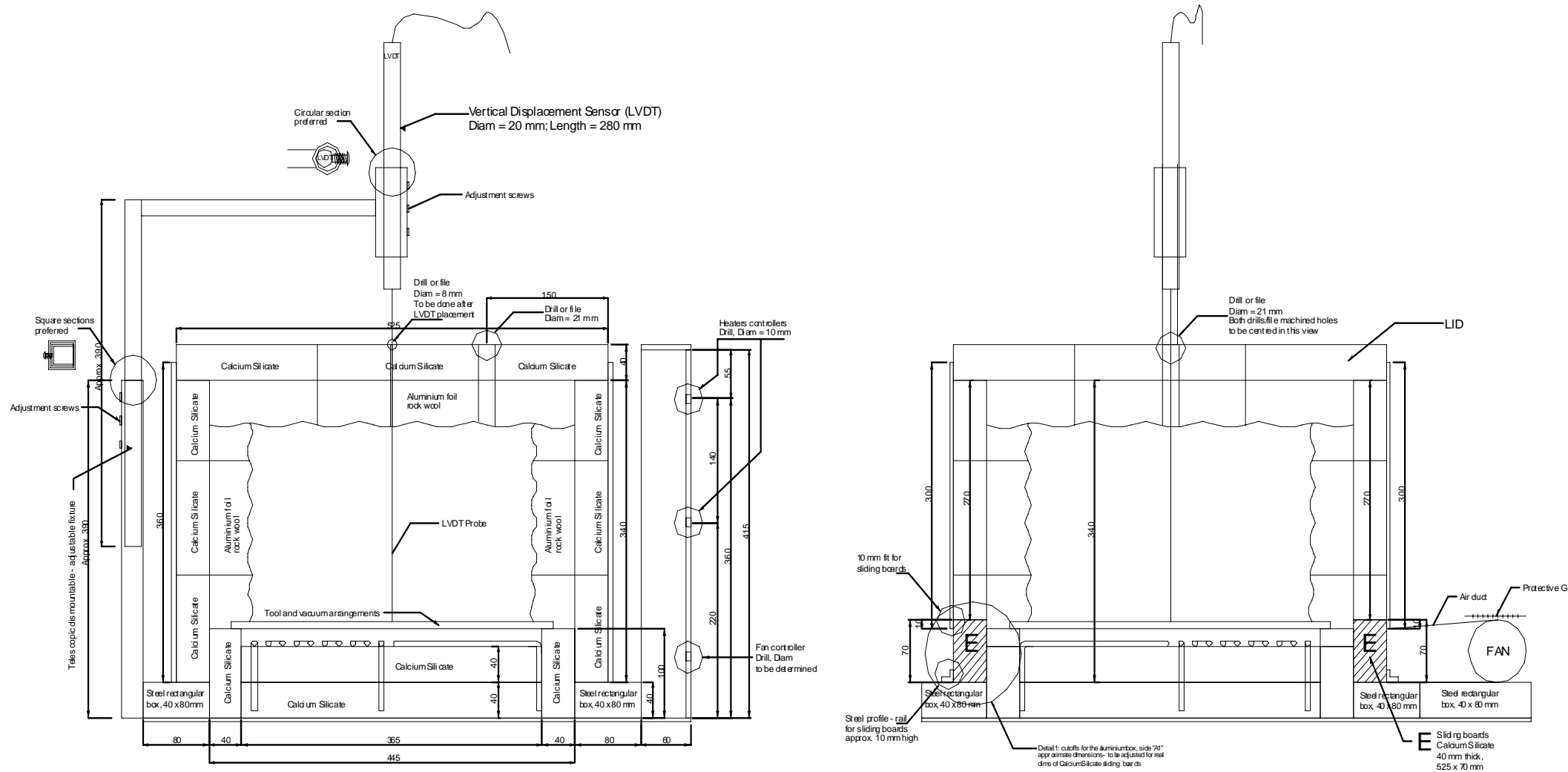


Figure 5.1: Original drawings for the construction of the rig

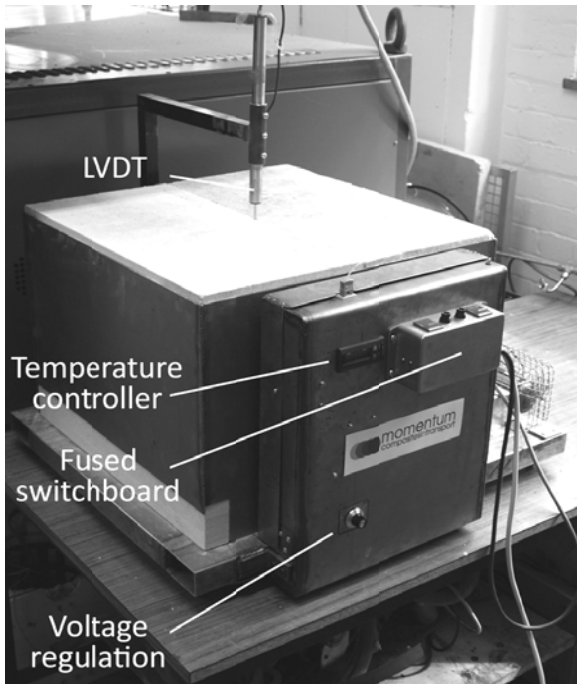


Figure 5.9: Testing rig

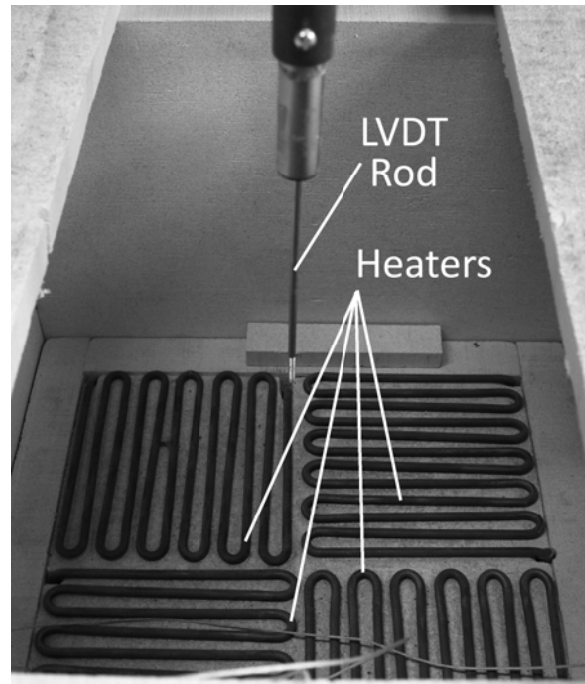


Figure 5.10: Heating chamber view with the lid open, prior to further insulation

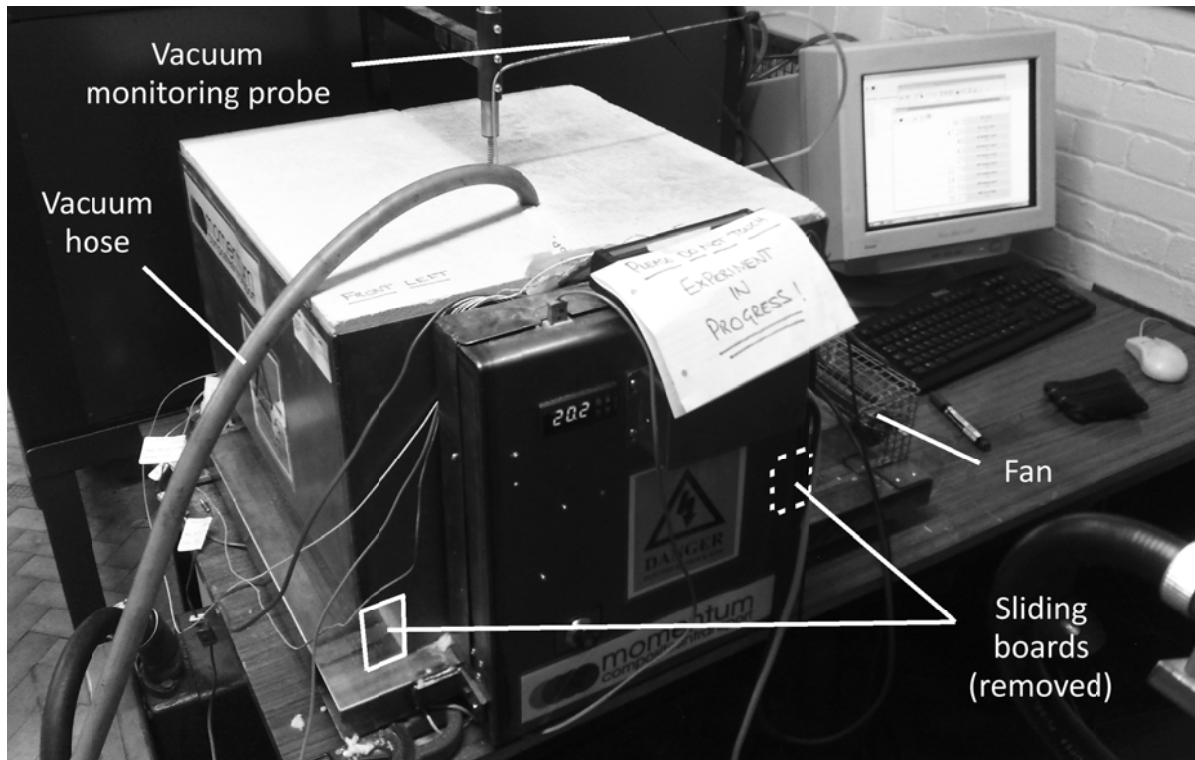
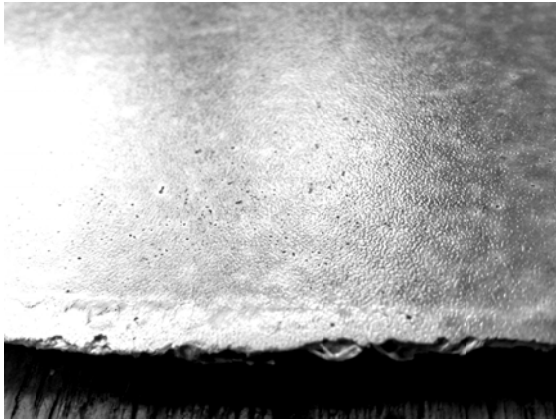


Figure 5.11: Testing rig during one of the consolidation tests (sliding boards removed)

### ***Air-tightness test***

The coated tools exhibited certain visible porosity on the surface (Figures 5.12, 5.13 and 5.14), which suggested that the low viscosity of the coatings led to some absorption through the surface. However, it was decided to perform an air-tightness test to quantify the air leaking under vacuum, if any.



**Figure 5.12: Tool surface coated with Coating 2**



**Figure 5.13: Tool surface coated with Coating 3**

The test consisted in measuring the air pressure within the boundaries of the vacuum bag, the sealant tape and the Vubonite® tool, with the vacuum pump on. Afterwards, monitoring the pressure evolution inside after turning the pump off would reveal any pressure increase due to air leaking in. A breather layer was also included inside the bag to ensure good flow during air evacuation as seen in Figure 5.15. The criterion used to assess the air-tightness performance of the coated tool was a maximum permitted pressure increase with the pump off of 1 mbar/min right after turning the pump off, often used in the industry [63]. A higher leak may lead to a high air pressure with the pump on, which in its turn leads to high porosity in the laminates, as shown in Chapter 7. To ensure that any possible leak measurement corresponded to the tool only and not the vacuum fittings, these were calibrated with a small glass tool to measure any background leak, which was 0.2 mbar/min. Hence, the final maximum allowed leak with this arrangement was 1.2 mbar/min.



Figure 5.14: Tool surface coated with Coating 4

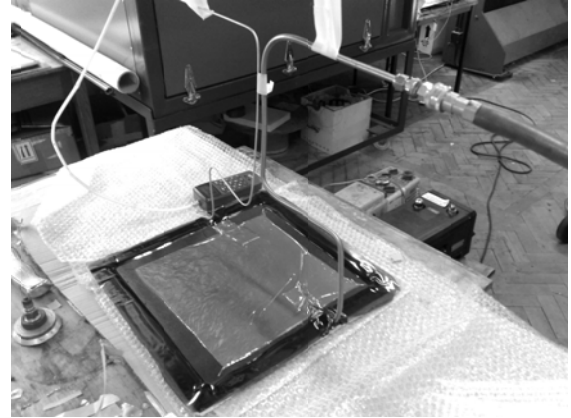


Figure 5.15: Room temperature air-tightness test

### Results

As expected from the surface appearance of the coated tools, their air-tightness was not sufficient for vacuum-forming. It appeared that the very low viscosity of the coatings used allowed for certain absorption through the tool porous surface, finally not sealing the pores. This prevented the vacuum arrangement on the coated tools from attaining sufficient vacuum pressure as seen in Table 5.7 and Figure 5.16. A very severe air leakage was measured on the tools, as shown in Figure 5.17.

Table 5.7: Air-tightness test results

Coating	Pressure pump on, mbar	Leak pump off, mbar/min
Reference value (glass tool)	0	0.2
Uncoated Vubonite tool	120	450.0
1	(the acid coating process dissolved the Vubonite® matrix)	
2	70	415.0
3	383	486.5
4	170	950.0

As reported by the coating industrial collaborator, the viscosity of the coatings No. 2, 3 and 4 was in the region of 12-88 mPa·s (see Table 5.8). This is 10-50 times lower than the viscosity of the usual epoxy resins used for infusion (Table 5.3), which are considered low-viscosity resins. Previous experience with Vubonite® at VUB shows that such low viscosity fluids tend to stay on the surface of the ceramic material for a limited time, after which it is absorbed through the pores. This experience supports the argument that the low viscosity coatings trialled on the moulding surface of the tools suffered from such effect.

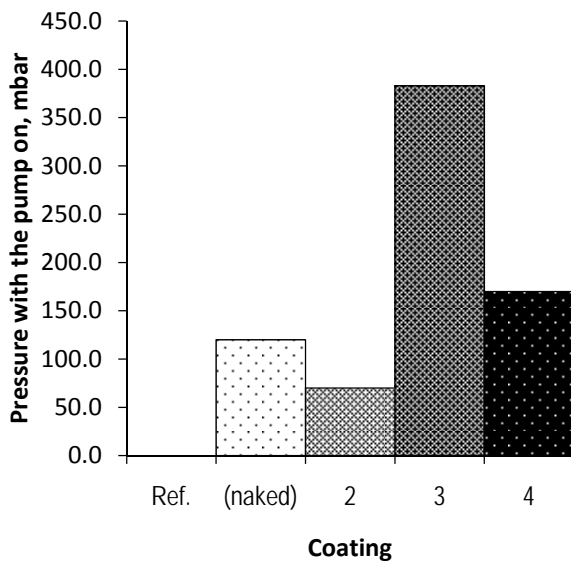


Figure 5.16: Minimum air pressure attained inside vacuum bag sealed to coated tools

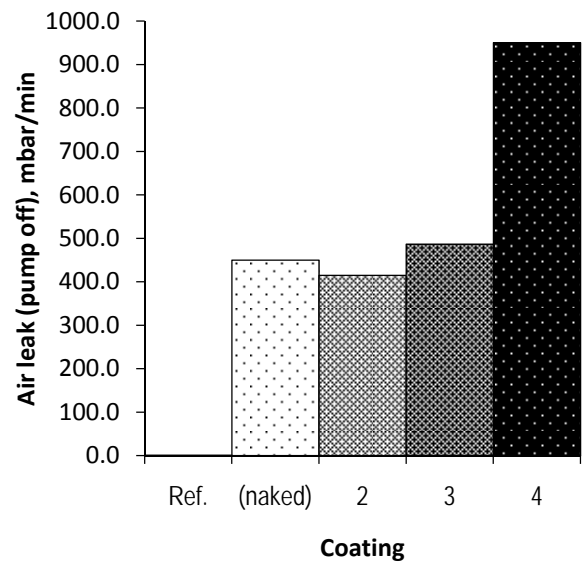


Figure 5.17: Air leak through coated tools

Another effect that has been observed with Vubonite® is related to water content within the porous structure of the material. The manufacturing process of the ceramic matrix involves a certain water content that remains in the pores of the material. This water is evaporated if the material is heated beyond 100°C. For this reason the mould requires a post-process up to the service temperatures to avoid water release. Experience with Vubonite® at VUB revealed that most of the water stays out of the pores, but it cannot be assured that no water will return to the pores after certain exposure to humid air.

The coated tools tested were post-processed at up to 400°C. However, the possibility of water release during the coating process (Table 5.8) cannot be totally disregarded, especially

after only 15 min of room temperature air drying. These conditions could still leave a low viscosity layer through which a small steam bubble could potentially go through, leaving a pore on the coating.

Hence, the unsuitability of the tested coatings for Vubonite® may be related to surface absorption of very thin coatings, or water emission during heating, or perhaps both phenomena. Further work is needed to elucidate the reason of the final high porosity observed in the coatings.

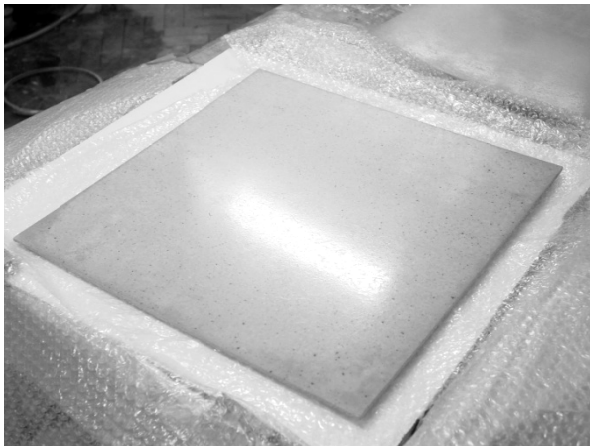
**Table 5.8: Properties and application of moulding surface coatings**

Coating No.	Type (proprietary)	Fluid properties	Application process
2	Clear Polyimide	Coating layers: 3 Viscosity: 27 seconds, ISO 5 flow cup @ 23C ~ 85 mm <sup>2</sup> /s ~ 88·10 <sup>-3</sup> Pa·s Density (as wet paint) 1.04 g/ml Solid content by weight 15% Solid content by volume 14%	Apply coating, air dry for 15 min, bake at 150°C for 30 min. Repeat procedure between coats Final coating, apply coating and air dry for 15 min, bake at 190°C for 2 hrs.
3	Boron Nitride	Coating layers 2 Viscosity: 15 seconds, ISO 4 flow cup @ 23C ~ 10 mm <sup>2</sup> /s ~ 12·10 <sup>-3</sup> Pa·s Density (as wet paint) 1.25 g/ml Solid content by weight 36% Solid content by volume 24%	Apply coating, air dry for 15 min, bake at 150°C for 30 min. Repeat procedure between coats Final coating, apply coating and air dry for 15 min, bake at 150°C for 1 hr.
4	Clear Stoving	Coating layers 3 Viscosity: 15 seconds, ISO 5 flow cup @ 23C ~ 35 mm <sup>2</sup> /s ~ 34·10 <sup>-3</sup> Pa·s Density (as wet paint) 0.97 g/ml Solid content by weight 35% Solid content by volume 27%	Apply coating, air dry for 15 min, bake at 150°C for 30 min Repeat procedure between coats Final coating, apply coating and air dry for 15 min, bake at 190°C for 1 hr.

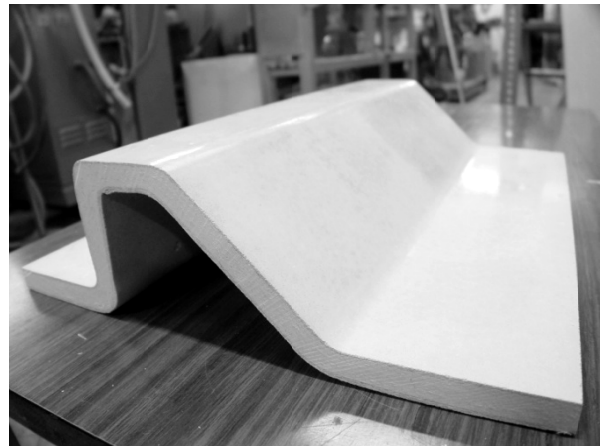
### ***Sealing the back surface***

The back surface can also be sealed to air leaks. One disadvantage of this alternative is that eventual cracks on the coating may be difficult to locate and repair. However, it has the advantage that a strong adhesion to the substrate is not required. Instead, it is only needed that the coating resists the processing temperatures and remains in contact with the mould material so that no void exists in between. Otherwise heat conduction would be remarkably affected on those areas, leading to hot and cold patches on both mould and composite during manufacturing.

A number of flat Vubonite® tools were coated with a 2-component, room temperature vulcanising silicone rubber P50, supplied by Silicones, Inc. The service temperature of 250°C of this silicone rubber enabled processing of composites incorporating PP, PA and possibly some varieties of PET. Images of the tools before, during and after coating can be seen in Figures 5.18 to 5.21.



**Figure 5.18: Flat, 7 mm thick Vubonite® tool**



**Figure 5.19: Top hat, 15 mm thick Vubonite® tool**

Also, a Zyvac Sealer GP was applied to the moulding surface in order to seal very small pores. This sealing agent cannot seal the main macro-porosity which is the objective of the silicone coating, but does improve the surface finish of the moulded composite. Finally, a customary release agent Zyvac Watershield was applied to the resulting surface to facilitate release of the moulded part, as usually done with metallic and composite tools.



Figure 5.20: Flat, 15 mm tool being coated with P50 silicone rubber

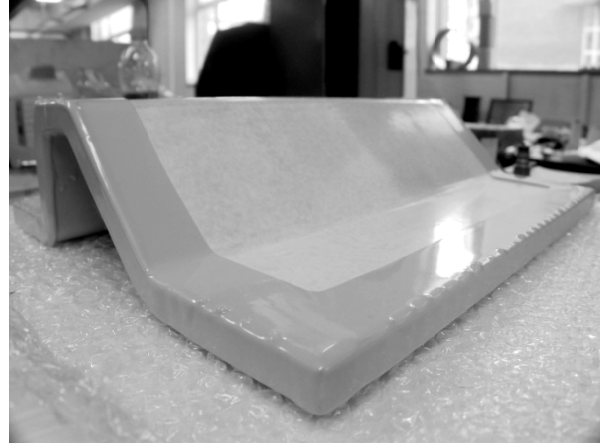


Figure 5.21: Top hat tool coated

The silicone rubber adhesive properties were very low. Nevertheless, it was necessary to have the ability to seal the vacuum bag to the silicone to facilitate vacuum conditions inside. This was achieved with a sealant tape Schnee-Morehead SM 5160, which silicone-based adhesive allowed for a particularly good adherence to both the silicone and the PTFE vacuum bag, Tygavac VB-3. Both consumables actually exceeded the maximum temperature of the silicone rubber. However, they were chosen because of their good adhesive coupling against other combinations which failed to adhere with sufficient tack, not providing the necessary air-tightness. A fluoropolymer release film Aerovac A6000 and the breather layer Airbleed A33N completed the consumables used during consolidation tests, listed in Table 5.9.

### ***Air-tightness tests***

The air-tightness of plain and coated 15 mm thick tools was measured at room temperature. For this purpose, the vacuum arrangement including all consumables was set up and connected to a vacuum pump, similarly as done with the moulding surface-coated tools. After allowing few minutes for all the air to be suctioned, the pump was disconnected and the pressure was measured, recording the pressure increase in the first 5 min. All vacuum fittings were tested beforehand with a small glass tool, where negligible values were measured. This ensured that no air leaks in the fittings would invalidate the results.



**Table 5.9: Top to bottom arrangement for consolidation tests on back sealed Vubonite® tools**

Vacuum bag	Tygavac VB-3 (PTFE)
Breather	Aerovac Airbleed 33N (Nylon/Polyester)
Release film	Aerovac A6000 (FEP)
Laminate	Twintex® multi-axial [+60, -60] <sub>s</sub> – areal weight 2,150 g/m <sup>2</sup>
Release agent	Zyvax Watershield
Mould sealing agents	Zyvax Sealer GP
Tool material	Glass reinforced, Zircon-filled Vubonite®
Back surface air-tight coating	2 component silicone rubber, Silicones Inc. P-50

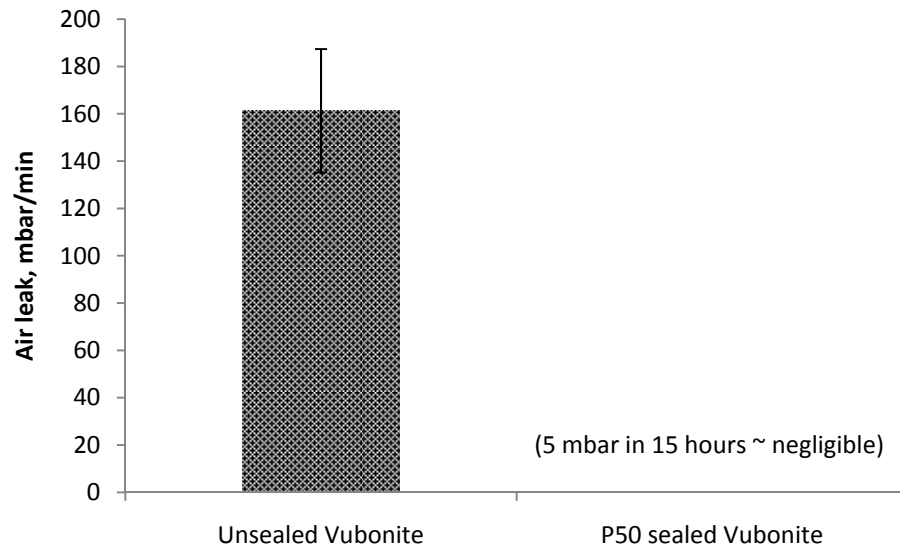
### ***Consolidation tests***

Six layers of multi-axial, non-woven Twintex® with an areal weight of 2,150 g/m<sup>2</sup> were laid up on a 7 mm thick sealed Vubonite® tool, wrapped with the release film, breather and vacuum bag, and tested in the rig. The air pressure inside the bag was monitored during the test with the probe seen on Figure 5.11, and the quality of the resulting laminate examined after consolidation. It was assumed that correct vacuum conditions would lead to good quality laminates of these small dimensions, without the need of void content analysis.

### ***Results and discussion***

The naked Vubonite® 15 mm thick flat tool showed an average vacuum pressure increase of approximately 160 mbar/min at room temperature, as seen on Figure 5.22. It is interesting to note that the 7 mm thick tools showed a higher air leak of approximately 400 mbar/min

(Figure 5.17). This increased leak suggests that most of the air flows through the thickness of the ceramic composite plates, instead of mainly around the sealant tape at superficial level. Otherwise, the leak would be much more similar. In the case of the silicone rubber sealed tool, negligible air leak was measured.



**Figure 5.22: Air-tightness test results on 15 mm thick Vubonite® flat tool, room temperature**

Pressure monitoring showed that during the consolidation tests, the pressure inside the bag maintained similar levels to what seen at room temperature. This was considered enough to ensure good quality laminates with no need for void content tests, especially given the small size of the mouldings. The consolidated laminates released with ease from the tool surface and showed good consolidation and acceptable surface finish. However, after few cycles the tool surface began to show the effect of repeated mouldings (Figure 5.23), and to release small bits of material. This left small cavities that were filled with laminate resin as shown in Figure 5.24. The moulding surface of the tool showed a darkening effect on the heated areas, attributable to the interaction between the ceramic surface, the sealing and release agents and the composite laminate.

The silicone rubber coating appeared to maintain its integrity up to 10 processing cycles, as seen in Figure 5.25.

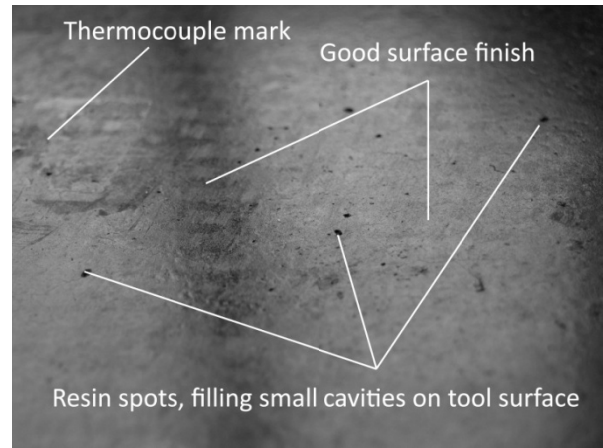
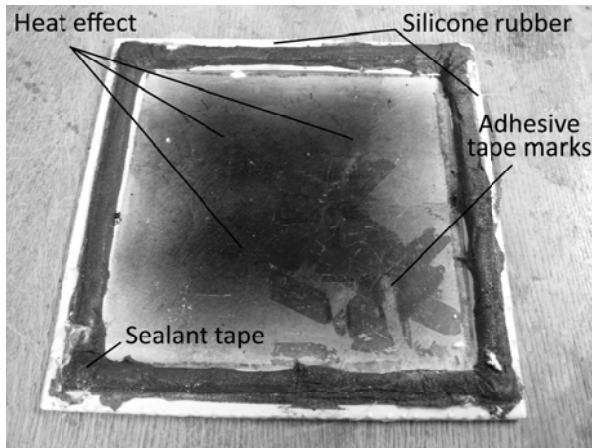


Figure 5.23: Tool state after 10 cycles, moulding surface

Figure 5.24: Consolidated laminate surface at 10<sup>th</sup> tool cycle



Figure 5.25: Tool state after 10 cycles, back surface (marks are remains of consumable adhesive tape used with thermocouples)

## Conclusions

A review on the performance and cost of a number of available and experimental tooling materials has shown that high- $T_g$  epoxy-glass is a low-cost option for vacuum-forming of PP-glass parts with complex shapes. Nevertheless, more knowledge is needed on their tool life and geometrical stability, as the processing conditions are around their  $T_g$ . Welded steel is preferred for simple shapes because of its inherent recyclability, durability, low price, and because any thermoplastic resin can be processed on a steel mould. Cast aluminium has

proven to be useful for up to 5 m long boats, although with a significant price increase over epoxy-glass and welded steel.

Ceramic-carbon composites are under development for TPC hulls, although their cost is still very high. With the aim to explore the possibilities of a low-cost glass-reinforced experimental ceramic composite, a number of experiments have been carried out towards the sealing of their inherent porosity. The air-tightness, releasability and durability of a set of coated ceramic tools have been investigated, with the following results:

- Moulding surface coated with thermosetting proprietary coatings:
  - Coating techniques involving high acidity are not suitable for Vubonite®, which is acid-sensitive.
  - The coatings did not seal the porosity of the ceramic substrate, probably because their very low viscosity, in the range of 12-88 mPa·s, allowed surface absorption leading to air leaks through the cured coatings. Also, the vaporisation of residual water in the pores of Vubonite® could be a reason for the remaining porosity.
- Back surface coated with high-temperature silicone rubber:
  - Air-tightness was satisfactory both at room temperature and during consolidation.
  - Release of consolidated parts was correct.
  - The sealing layer of silicone rubber maintained its integrity up to 10 cycles.
  - The moulding surface showed some damage after 10 cycles:
    - Darkening of the surface.
    - Small material wearing, leaving visible cavities that were filled with resin from the laminates, demoulded with these.

These results show that this ceramic composite has the potential to be an affordable solution for any thermoplastic composite. Its maximum continuous service temperature (limited by the reinforcing glass fibres, at around 400°C), its ability to be formed in any shape and its low price make it an interesting alternative for small boats manufacturing.

Nevertheless, its inherent porosity needs to be addressed if vacuum processing is needed. In the experiments shown above, the back and the moulding side of the tool have been coated to seal the substrate porosity. A high-temperature silicone rubber was used to seal the back surface. The resulting tool was partially successful as it provided with good air-tightness and delivered a number of mouldings with sufficient quality. However, the moulding surface did not attain the required durability, being unusable after less than 10 cycles.

Experiments on moulding surface coating showed that a high acid content may dissolve the Vubonite® surface. Also, a remaining macroscopic porosity was observed, which prevented adequate vacuum levels. It was probably caused by either thin coating absorption through the surface, or vapour release due to residual water in the Vubonite® mould, or a combination of both. Despite these results, the low durability of the plain ceramic surface would benefit from a durable coating of appropriate composition and viscosity. Therefore, a moulding surface coated solution appears to be the best alternative for porosity sealing, good surface finish and enhanced tool durability with this material.

## **Chapter 6 – Fusion bonded T-joints**

The joining of moulded parts is a technology that enables the design and construction of large and complex assemblies, such as boats requiring internal structure. The emerging TPC boatbuilding industry has been using several joining techniques in the currently available boats, comprising mechanical fasteners, adhesive bonding and seamless one-piece manufacturing. However, a technique capable of delivering strong and tough joints of adequate shape and size that connect different sub-structures is still unavailable.

One possibility that makes use of the re-melting ability of TPCs is fusion bonding. This chapter presents an experimental study on the application of bulk heating fusion bonding to PP-glass composite joints in the boatbuilding context. The objective of this study was to assess the feasibility of the construction of T-joints such as those useful in a small boat. With this in mind, fusion bonded lap and T-joints were manufactured and tested, showing a number of interesting results. Firstly, it was revealed that woven precursor materials are preferred for joint manufacturing due to their inherently higher interlaminar strength. The effects of added resin interlayers along the bond line were also assessed, with notable improvement of bond quality for both lap and T-joints. Finally, it was found that the pull-out strength of the T-joints was comparable to that of thermosetting designs, demonstrating that fusion bonding is a suitable joining technique for thermoplastic composite craft.

### **Study on lap and T-joints**

A number of joint samples were manufactured for tensile testing in order to assess the manufacturability and properties of lap and T-shaped joints for TPC boats. The inclusion of resin layers in between composite plies was tested in these joints, because of its potential

advantages in bond quality. Whereas this technique is known as *interleaving* in the literature on thermosetting composites, it is referred as interlayering with regard to TPCs, and so will in the text from now onwards.

Firstly trialled in thermosets, interlayers of thermosetting or thermoplastic resins have proven to increase toughness of typically brittle composites [104, 105]. When applied to TPC joints, interlayering with the same resin contained in the composite led to improvements in bond strength, resilience and repeatability [51] and is also being used to enhance skin-core adhesion in PP-glass sandwich laminates in boatbuilding [106].

Thus, two different interlayers consisting of one and/or two layers of an off-the-shelf PP woven mat were laid up on the interface of selected joints, resulting in 0.15 mm and 0.30 mm thick layers, respectively, after processing. Also, it was considered that a comparison in performance between woven and non-woven PP-glass commingled fabrics would be of interest. The characteristics of both precursor materials can be found in Table 6.1.

**Table 6.1: Materials used for the manufacturing of the lap and T-joints**

Base material	TPP 60 Twintex® (60%wt. glass content)	
Fabric type	Woven	Non-woven
Orientation	[0°, 90°],	[+60°, -60°] <sub>s</sub>
Areal weight	745 g/m <sup>2</sup>	2,150 g/m <sup>2</sup>

The resulting set of samples combining woven and non-woven fabrics with several cases of interlayering were manufactured using local heating under vacuum. Heating was provided by silicone rubber insulated electric heaters, placed inside the vacuum arrangement in order to maximise heat transfer (Figures 6.3 and 6.12). Their high electric power of 15.5 kW/m<sup>2</sup> was chosen in order to restrict the heated area as much as possible to avoid excessive warping. These commercially available flexible heaters can be tailored to any size, facilitating

this process to be scaled up to the desired boat size. The vacuum forming process applied to the joints was in all respects equivalent to the manufacturing process of PP-glass laminates described in the previous chapters. As such, it required a number of consumable materials which are summarised in Table 6.2.

**Table 6.2: Summary of consumables used in the manufacturing of lap and T-joints**

Vacuum bag	Aerovac Capran 526 (Nylon)
Breather	Aerovac Airbleed 33N (Nylon/Polyester)
Release film	Aerovac A5000 (FEP)
Sealant tape	Aerovac low temperature LTS90B
PP interlayer	Woven PP mat, 135 g/m <sup>2</sup>

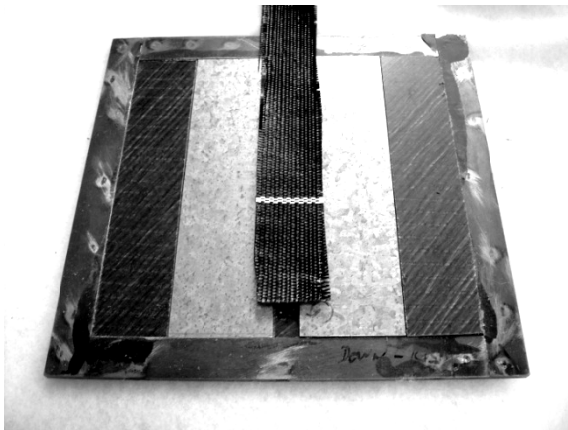
It is interesting to point out that the sealant tape did not require high temperature resistance as it remained at the boundaries of the heated area, not being heated directly.

Bearing in mind the objective of developing a joining process that could be repeatable and scalable to the size of a real boat, one-sided heating was used for T-joints (Figures 6.3 and 6.4). This allows the processing of bulkhead-hull attachments and other on-board T-joints to be carried out from the interior of the hull during construction. However, the first lap shear testing results revealed a need for thick coupons which demanded heating from both sides (Figures 6.12 and 6.13), using two steel plates and two metallic blocks to prevent deformations during melt processing. Although certain differences in the recrystallisation of the matrix can occur due to differences in local cooling rates [107], it was considered that the actual melting, molecular diffusion and cooling process was equivalent regardless whether the heat comes from one or both sides.

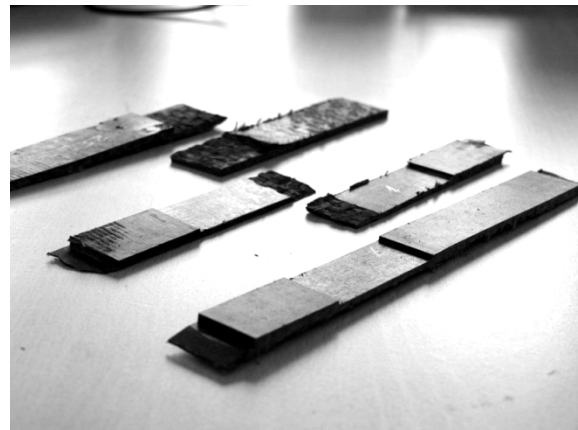


## Lap shear

The first of this series of experiments on lap shear strength were carried out for both woven and non-woven materials in accordance to Standard ISO 4587, manufactured with the aid of a steel jig as seen in Figure 6.1. During the tests, it was observed that the non-interlayered (plain) fusion bonded samples failed without significant bending, whereas PP-interlayered samples showed a remarkably stronger bond and developed notable bending and peel forces around the lap joint, visible during the test in the form of sample bending before failure. It was decided that a higher thickness was needed in order to decrease peel forces and in such a way obtain a more accurate value of the shear strength, especially for woven interlayered specimens.



**Figure 6.1: Pre-consolidated non-woven laminates with one PP interlayer in the fabrication jig for ISO standard samples**



**Figure 6.2: ISO woven samples manufactured and tested**

Thus, a total of 6 non-standard, 250 mm long samples were manufactured with 13 mm thick laminates, following the arrangement shown in Figure 6.3. Each of these samples was sliced into testing coupons for lap shear strength testing. The laminates which formed the joints were previously consolidated and placed between two steel plates with appropriate aluminium blocks to prevent the resin from flowing out of shape. The aluminium blocks were wrapped in release film to prevent the flowing resin from adhering to their surface as seen in Figure 6.5. The steel plates enclosing the laminates were heated with flexible electric heaters and all the arrangement was covered with a breather layer, and placed inside the vacuum bag. The breather layer also provided with thermal insulation, although additional thermal

insulation on the exterior of the bag was needed to prevent excessive heat losses and thus provide shorter processing times. The samples were processed at the approximate conditions of 200°C, heating ramp of 60 minutes, dwell time of 60 minutes, and cooling ramp of 60 minutes. Such process ensured the full melt and consolidation of the joint through the thick laminates, finally delivering the finished samples shown in Figures 6.4 and 6.6.

After processing, the samples were cut into coupons with a typical width of 30 mm, and tested under tension in a Dartec machine. Each sample delivered a minimum of 6 coupons which were considered to deliver results with sufficient statistical significance, given the microscopic nature of material variability and the coupon size. During tests, the samples failed as required, with unnoticeable joint deformation near failure and therefore minimum peel forces developed.

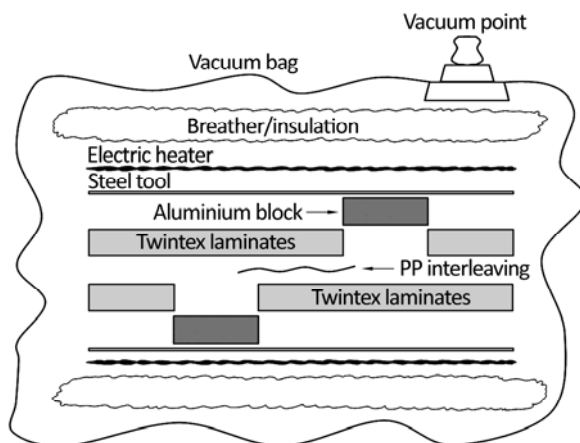


Figure 6.3: Typical arrangement for thick lap joints manufacturing



Figure 6.4: Finished lap shear thick coupon, typically 30 mm wide

### Results and discussion

A comparison between tensile tests results (Figure 6.7) shows that the non-woven samples yield much lower lap shear strength than their woven counterparts, as illustrated in Figure 6.5. The resulting fracture surfaces were examined, showing that non-woven joints failed cohesively in the substrate with remarkably low strength values, regardless of the PP interlayering (Table 6.3). In contrast, the woven joints tended to fail along the bond line, occasionally including fibre breaking and substrate delamination.

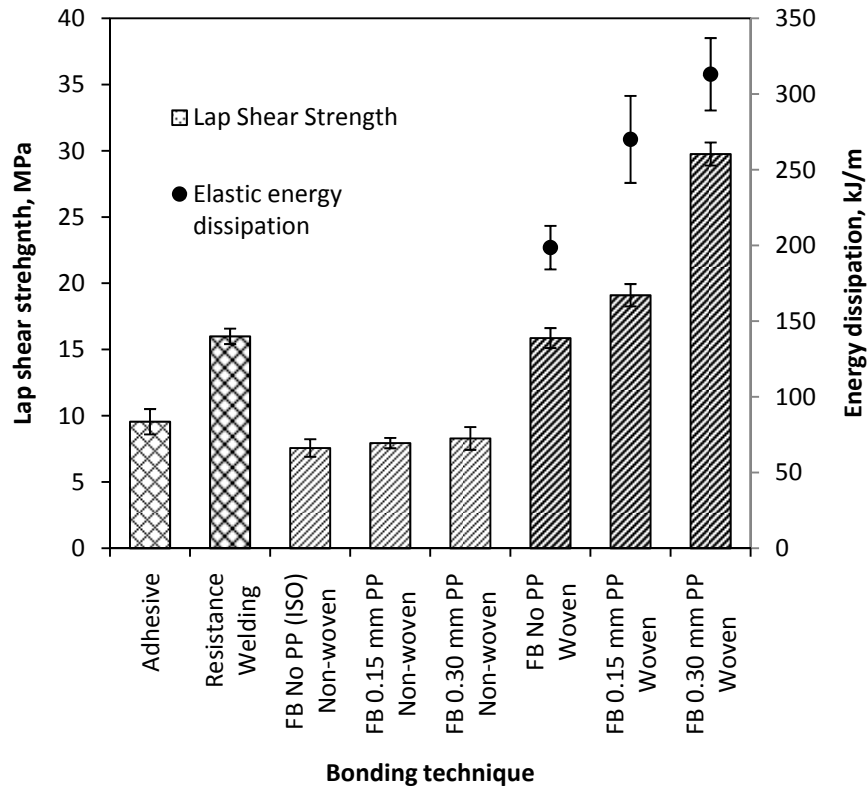


Figure 6.5: Lap shear strength values for adhesive [108], resistance welded [109] and fusion bonded (FB) Twintex® – bars indicate 95% confidence

It must be noted here that the non-woven samples suffer from high shear due to their continuous fibre orientation [+60°, -60°]. This orientation makes impossible to completely avoid the shear effect under lap shear strength testing. However, this shear effect is not present in the woven samples, because their orientation is [0°, 90°]. Hence, the comparison between the shear strength of non-woven and woven samples cannot be like to like, because in-lamina shear is an important failure mechanism for the non-woven material, whereas it is not in the case of the woven samples. The relative importance of in-lamina shear and interlaminar strength is not shown in these tests. Nevertheless, from the results of pull-out tests of T-joints shown in the next section of this chapter it can be deduced that the peel strength of both woven and non-woven is remarkably similar. Therefore, it is reasonable to expect that the mentioned in-lamina is, in fact, to a great extent responsible of the low final lap shear strength of the non-woven samples.

This different behaviour shows that the woven material is suitable substrate for lap joints, whereas non-woven materials tend to fail prematurely in the laminate. This is why the PP interlayers do not have any effect on the shear strength of non-woven lap joints, while an interlayer of 0.30 mm PP practically doubled the strength of woven joints. Additionally, plain woven samples exhibited notable fibre glare on the failure surface, which noticeably diminished with the addition of PP interlayers. Thus, it appears that PP interlayering displaces fibre-resin debonding in favour of a different failure mechanism.

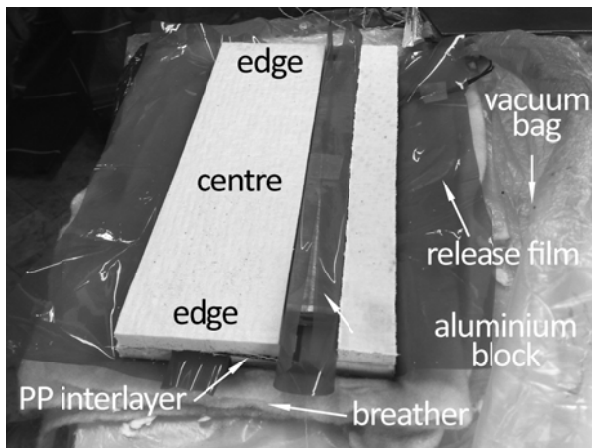


Figure 6.6: Thick lap joints manufacturing

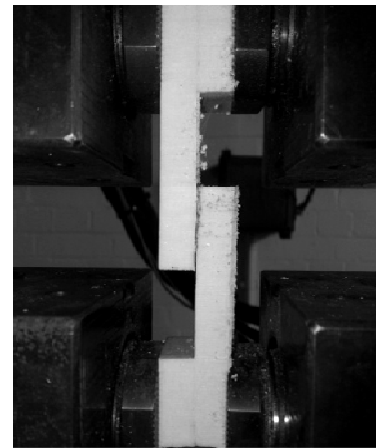


Figure 6.7: Thick lap joints testing

Table 6.3: Failure modes recorded for lap-joints

	Non-woven lap joints	Woven lap joints
No PP interlayer (plain)	Cohesive in the substrate	Cohesive in the resin plus fibre-resin debonding along the bond line
0.15 mm thick PP interlayer	Cohesive in the substrate	Cohesive in the resin plus reduced fibre-resin debonding along the bond line, with occasional delamination and fibre breaking
0.30 mm thick PP interlayer	Cohesive in the substrate	As 0.15 mm thick PP interlayer, with less fibre-resin debonding and more delamination and fibre breaking

It can also be seen that the strength values attained by woven interlayered lap joints are superior to those of Twintex® joints bonded with adhesives [108] and resistance-welding [109] found in the literature, even taking into account that these values were obtained from thinner laminates (Figure 6.5).

With the purpose to further examine the nature of the PP interlayering reinforcing effect, the elastic dissipated energy was estimated from tensile tests data and plotted against the PP layer content (Figure 6.5). This energy was found to increase by 36% with the first 0.15 mm of added PP, while a further 0.15 mm PP layer increases energy dissipation by only 21% more. However, despite this apparently lower contribution to resilience, this second layer of PP leads to a threefold shear strength increase compared to the first layer. Therefore, mechanisms other than elastic strain in the resin-rich bond interface must be considered to explain the increase in shear strength. With respect to this, a higher PP content on the joint line is likely to facilitate the movement of glass fibres around the joint interface during processing, thus enhancing fibre wetting and mechanical interlocking. Fibres dispersed within the resin-rich interface in such a way would improve the properties of the structural composite network, improving stress distribution and energy dissipation. This mechanism would also explain the observed change in failure mode from fibre-resin debonding (decreasing glass fibre glare) into resin cohesive failure plus fibre breaking and occasional delamination (Table 6.3).

The test data on lap shear strength exhibited a low scatter, which nevertheless appeared to follow a temperature-dependant trend, as seen in Figure 6.8. The validation of the repair method developed, tested and discussed in Chapter 7 involved the heating of a thick scarfed joint from one side only, shown in Figure 6.9. This joint did not consolidate completely due to inevitable heat losses, displaying a clearly visible cross-section recrystallisation line. This line was fitted with very good agreement by a parabolic distribution through the laminate thickness (Figure 6.10).

Fusion bonded T-joints

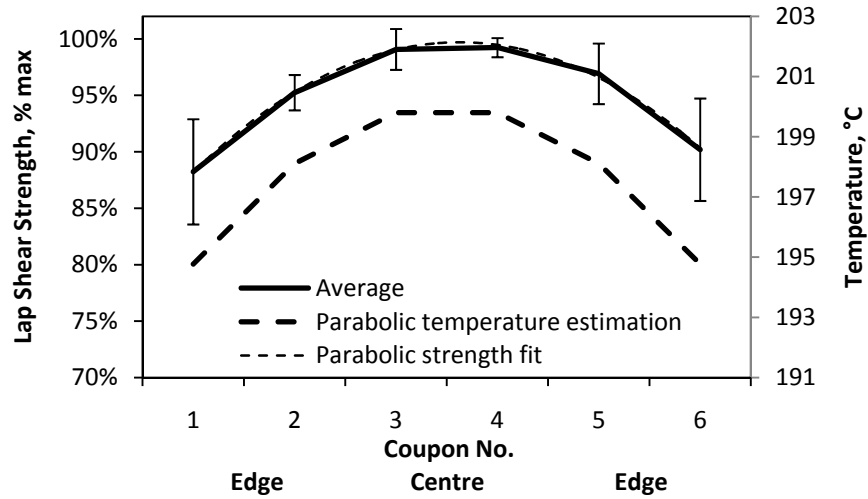


Figure 6.8: Lap shear strength and processing temperature variation along samples – “edge, centre, edge” correspond to Figure 6.6

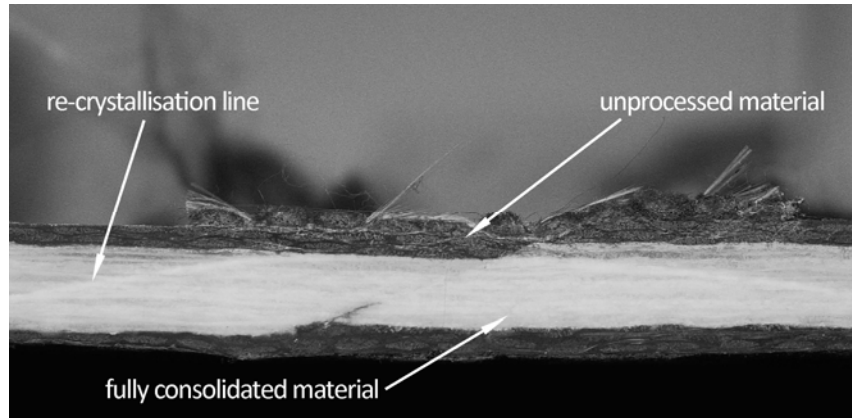


Figure 6.9: Re-crystallisation line observed during repair validation tests (see Chapter 7)

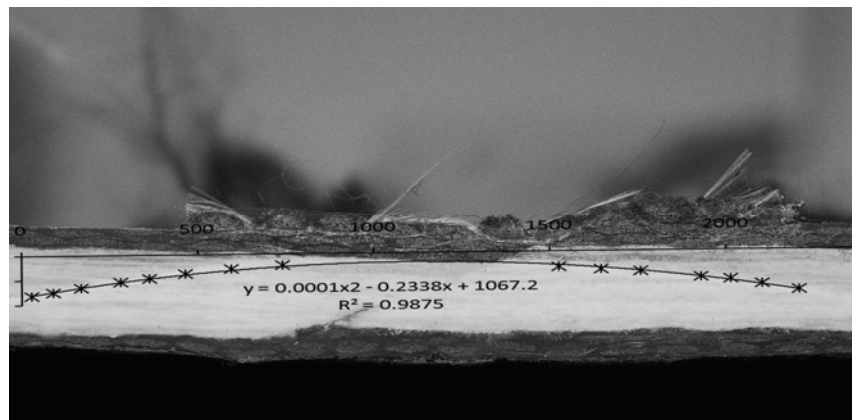


Figure 6.10: Parabolic fit of the re-crystallisation line

As the matrix re-crystallises at the same temperature throughout the whole laminate, this re-crystallisation line can be identified with an isothermal line, indicating that the temperatures inside laminates heated in this way can be fitted by parabolic curves, with its maximum in the centre and its minimum on the edges due to inevitable heat losses.

The temperatures along the manufactured lap joint samples were estimated from measurements at the edges and centre of the samples.

Figure 6.8 shows that both strength and temperature distributions are remarkably similar, being the variation in shear strength in the range of 13%, corresponding to approximately 5°C processing temperature difference, even in the region of 30°C above the resin melting point. This unexpected difference may be attributable to a strengthening of the interlocking and fibre-resin debonding reduction phenomena mentioned above, influenced by the remarkable sensitivity of polypropylene viscosity upon temperature [110]. Effectively, the viscosity of the PP contained in Twintex® would lower its viscosity by 12% between 195°C and 200°C, according to the formulation proposed by Klinkmüller [30] (see Chapter 4).

Also, the cooling rates are probably lower at the joint centre than at the edge due to the mentioned heat losses (Figure 6.11). As reported for other thermoplastic resins [107], a difference in cooling rates will affect the local crystallinity of the PP at the joint, which in turn will impact on its mechanical properties. Therefore, the observed joint strength difference is probably due to a combination of lower viscosity at high temperatures and higher crystallinity after cooling at the centre compared to the edges, as signified in Figure 6.11.

Published research on resistance welded lap joints has reported that increasing temperature for a given pressure leads to a maximum in shear strength beyond which processing conditions may lead to a resin squeeze out, affecting negatively the joint strength [111, 112]. It is certainly expected that the benefits of added PP to the bond line will have a limit. However, no decline has been recorded in these tests, thus the obtained results seem to leave room for potential process optimisation with regard to PP interlayer thickness and processing temperature on lap joints.

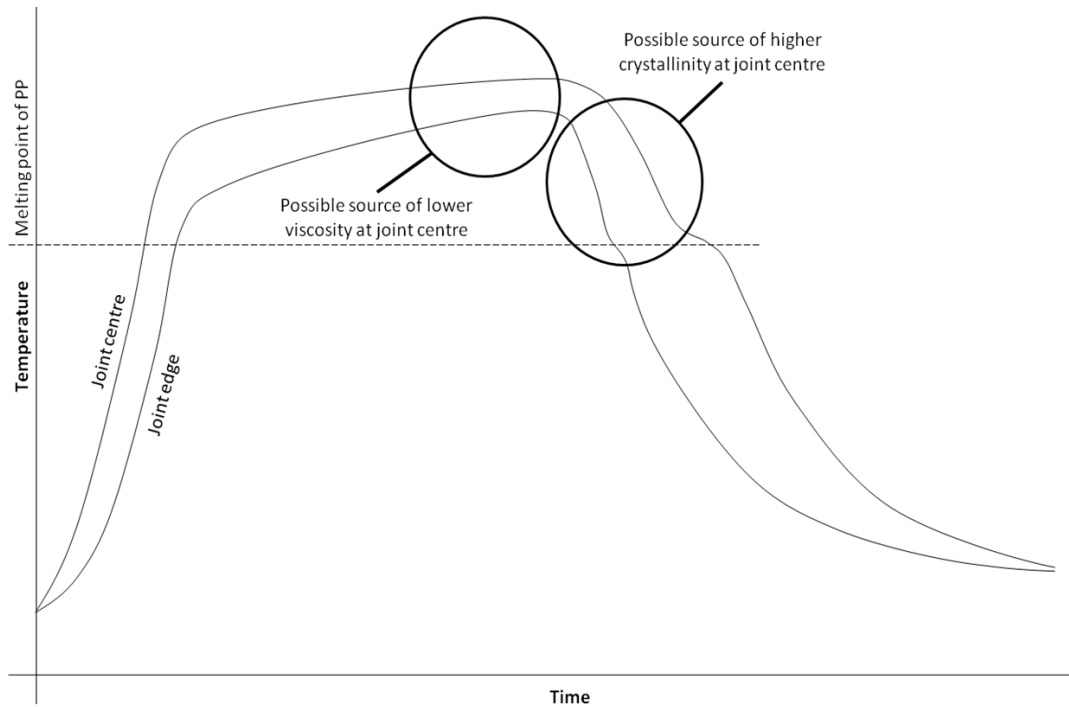


Figure 6.11: Approximate heating and cooling curves for centre and edge of LSS joints samples

## T-joints

### Design

To date, the few existing thermoplastic composite boats make use of no-joints one-piece manufacturing, mechanical fasteners, and/or adhesive bonding [106, 113]. With the purpose to manufacture and test T-joints in PP-glass which may be of use in the hull of a real boat, their design was addressed first. It is worth mentioning that the purpose of this research work was not to produce an optimised T-joint design, but to assess the feasibility of its construction. Hence, the design approach taken aimed at producing a T-joint relevant to small boats in general terms, although scantlings and dimensions could change, depending on the particular loading conditions on the joint.

Unlike for other hull elements for which load-related scantlings are available, the literature provides only general design principles and minimum requirements related to thermosetting designs of joints and attachments.

Classification societies establish minimum requirements for marine composite T-joints. These are mostly qualitative recommendations with occasional useful quantities. Lloyd's



Register specifies overlapping thicknesses over 2 mm and areal weights of at least 50% of the lightest member connected to the joint [114]. American Bureau of Shipping stands out with quantitative requirements for adhesives, setting a minimum shear strength in adhesive bonded joints of 6.9 MPa, at up to 49°C [115]. In turn, Det Norske Veritas states a conservative safety factor of 5 in dimensioning T-joints [116]. Greene and Gibbs & Cox both recommend 50 mm minimum overlapping in bulkhead-hull attachments, as well as avoiding close-to-90° sharp corners lamination [7, 117], which would easily lead to high void content and lower properties because of the limited flexibility of commercial fabrics for composites. When the fabrics are laid up and impregnated with resin at very sharp corners as on the joint shown in Figures 6.12 and 6.13, the flat areas tend to stick to each other, preventing the plies at the corners from stacking neatly and attaining close fibre packing. This leads to higher resin and void contents, which in turn provide higher laminate thicknesses.

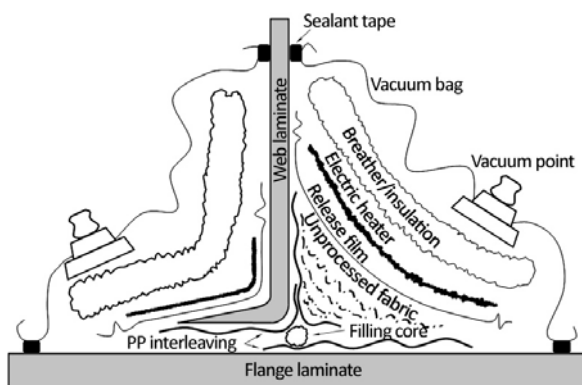


Figure 6.12: Typical arrangement for T-joint manufacturing

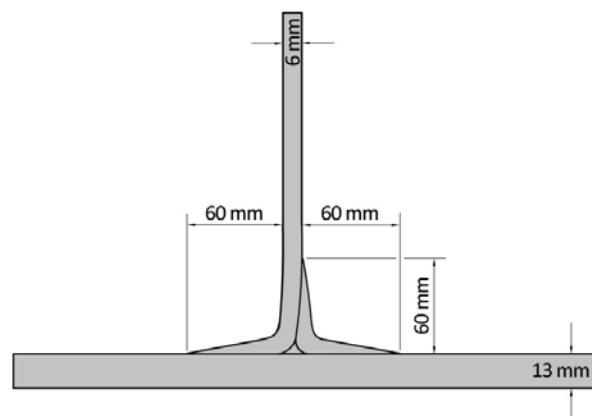


Figure 6.13: Finished T-joint sample, typically 20 mm wide

This phenomenon is known in the industry as “bridging”, because of its resemblance with the way suspension bridges stay in place.

The scantlings of the T-joints were chosen in accordance with these recommendations, as shown in Figure 6.13. This way, it was ensured that the scantlings and shape of the joint related in general terms to small boats in the region of 8 m long. However, it was necessary to fully process the joint core. Therefore the distance between the heaters and the joint core

needed to be as small as possible in order to reach processing temperatures in a reasonable time. This led to notably sharp corners, with curvature radii of approximately 6.5 mm, despite the risk of bridging-driven void formation.

### ***Manufacturing***

Six T-joints with a length of 250 mm were manufactured, one joint per type, so that valuable comparisons amongst woven, non-woven, plain and interlayered could be done. One of the samples featured sandwich substrate, with 5 mm thick skins and 18 mm thick balsa core, to investigate its manufacturability and structural behaviour. All of them were cut into slices approximately 20 mm wide, which were subjected to a 90° pull-out test in a Dartec tensile machine. It was considered that this number of samples would produce testing results of adequate statistical significance.

The T-joints comprised a pre-consolidated web and flange, corresponding to the bulkhead and the hull of a small composite boat respectively, and a number of unprocessed fabric plies, to be co-consolidated to the web and flange during joint process. The web incorporated a small flange itself, temporarily fixable to the hull in order to keep the bulkhead in place during the fusion-bonding process. A flexible heater was placed on this side of the joint, covering the small flange and also a small area of the vertical web to avoid heat losses by conduction inside the laminates and ensure heat flow towards the joint core. During the processing the pre-consolidated material and the substrate laying close to the heaters were melted again and fusion-bonded together (Figure 6.12). The additional unprocessed plies were laid up to form a smaller L-beam, opposite to the small flange mentioned above. Another flexible heater was positioned covering all the added fabrics to facilitate their full processing. These were co-consolidated during the bonding process, facilitating molecular interdiffusion with both the substrate and the existing web. The heater arrangement prevented the web from reaching very high temperatures during processing by avoiding excessive overlapping of the heaters on both sides of the web. Extreme temperatures in the web laminate between the heaters would have squeezed out the matrix, reducing its thickness and lowering its mechanical properties. Moreover, it would puncture the vacuum bag if temperatures would surpass its melting point, or that of any materials in touch with it as the breather layer.

The resulting asymmetrical design of the T-joint offers the additional advantage that on one of its sides, the joint features enhanced fibre continuity, with potential benefits in case of asymmetrical loading cases, e.g. for tank bulkheads. This geometry serves TPCs better than their thermosetting counterparts, because the resin reflow during joint processing would compensate almost any occurring dimensional inaccuracy, making the process less sensitive to surface mating. Given the reduced size of the joints, processing conditions were approximately those of lap shear coupons. Nevertheless, preliminary tests demonstrated that a dwell time of 30 min is sufficient to realise a joint of adequate strength, although with approximately 10 cm sacrificial ends because of unavoidable edge heat losses leading to insufficient consolidation degree at certain areas of the joint. This would not make sense in the case of small samples but could be useful to save energy and time with real full size joints such as a bulkhead-hull connection, typically several meters long.

The T-joints processed with this technique typically suffered from small deformations due to matrix flow and the absence of any tooling to keep the shape. Typically, the pre-consolidated web laminate tended to move about 3 mm towards the joint centre, providing a quasi-symmetrical final joint, as seen when comparing Figures 6.12 with 6.13 and also the final result in Figures 6.18 and 6.20. Also, laminate deformations due to the release of residual stresses combined with asymmetrical heating were observed (Figure 6.14). This noticeable deformation, a well known drawback of bulk heating fusion-bonding [48, 49], was measured for the single-skin flanged T-joints, being in the region of up to 5 mm vertical deflection over 300 mm base laminate length. However, a T-joint sample comprising sandwich substrate with balsa core (Figures 6.15 and 6.17) overcame this problem. The sandwich core appeared to provide sufficient thermal insulation and a non-melting supporting structure. These facilitated full melt of the hot side skin, which tended to be unaffected by stress release because being thinner facilitated a more uniform through-thickness stress distribution, and maintained low temperatures in the other skin, eventually showing no noticeable deformation after processing.



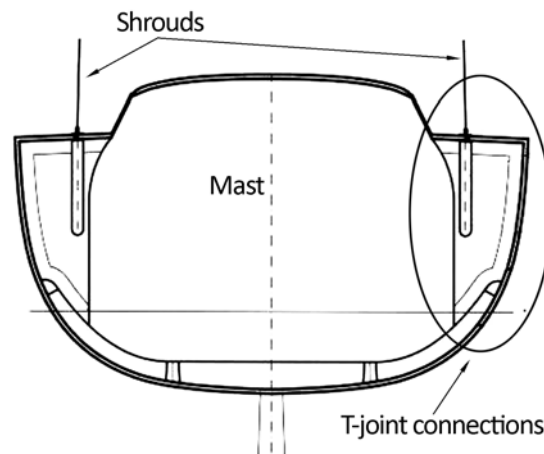
Figure 6.14: Warping in the substrate caused by asymmetrical bulk heating on thick laminates

Figure 6.15: The skins of the sandwich substrate of a T-joint sample remained flat after processing

### *Testing*

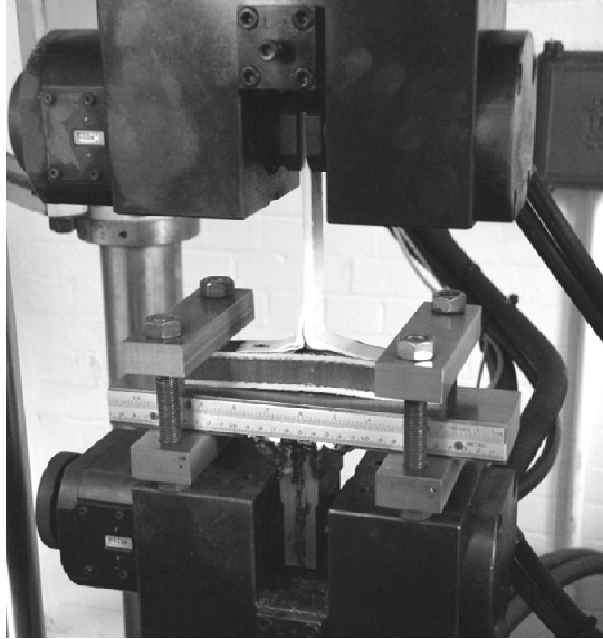
The attachment of a bulkhead to a boat hull forms a complex structure which interacts with the surrounding water. For this reason, its behaviour cannot be simulated with a single laboratory test. However, a range of characterisation measurements have been used for composite T-joints to investigate some aspects of it:

- 90° compression tests [118, 119] have been used to simulate slamming-like forces pressing the hull shell towards the interior of the boat; web bending tests [120, 121] produce pure bending forces on the joint web which, although rare on real T-joints in boats, relate to attachments between the bulkheads at the boundary of fluid tanks and the hull, as the difference in pressure at both sides of such bulkheads create a load asymmetry.
- 45° pull-out tests [122] simulate arguably better the previous joint case, by taking bulkhead continuity vertical forces into consideration, and finally 90° pull-out tests [121, 123-125] simulate joint cases occurring for instance in naval ships super structures under blast or underwater explosions, or sailing boats as shown in Figure 6.16.
- 90° pull out testing, occasionally complemented with pure bending tests, constitute a simple and easily comparable technique to analyse T-joint behaviour, and thus was chosen for this study of thermoplastic T-joints.



**Figure 6.16: T-joints on board a sailing yacht, transverse section (edited from [126])**

Once manufactured and sliced into coupons, the joints were placed on a steel testing jig (Figure 6.17), which was adjusted to a gripping span of 185 mm from centre to centre of the gripping blocks. The use of adhesive bonding between the joint substrate and the jig base has been reported in the literature [121]. This can arguably facilitate the assessment of the mechanical behaviour of the joint itself because it prevents the flange bending, in such way that the joint receives all the deformation energy. However, as mentioned above, it is difficult to adhere PP substrates because of their inherent low-energy surface, and most important the surface of a real boat hull shell is rarely fixed anywhere but moves freely as a whole structure. This free-moving characteristic may lead to crack initiation and failure cases that could be neglected if the substrate would be adhesively fixed to the jig. Therefore, the samples were simply held in the jig by the blocks, avoiding any further bonding between the joint and the jig. Certain vertical movement was allowed at the gripping points, making the gripping conditions approximately equivalent to pinned-pinned, as reported in published works [124, 127]. It is necessary to note that different gripping conditions such as fixed on both ends, adopted by other authors [125, 128], may deliver different strength values, due to the different flange deformations and energy dissipation mechanisms of the whole joint.



**Figure 6.17: T-joint with non-woven PP-glass-balsa sandwich substrate under pull-out testing**

### ***Results and discussion***

As observed in the case of lap joints, the test results revealed that the pull-out strength of T-joints manufactured with woven materials exceeded that of those made with non-woven fabrics. The failure of the joints during the tests was monitored, and the final fracture surfaces examined to study the failure modes. All the observed failure modes (Table 6.4) consistently matched the observed superior strength values attained by the woven joints, and within these, the interlayered joints.

It is notable that the strength of the plain woven lap joints nearly doubled that of their non-woven counterparts, whereas pull-out strength was virtually the same in both cases (Figure 6.22). However, this virtual equality was undone by the addition of PP interlayers, which virtually doubled the strength of woven joints with a 0.30 mm thick PP interlayer but had no noticeable effect on non-woven samples, similarly to what was observed with the lap joints.

**Table 6.4: Failure modes in T-joints**

	Non-woven T-joints	Woven T-joints
No PP interlayer (plain)	Crack along the bond line above joint core, followed by cohesive failure in the resin and fibre-resin debonding	Crack along the bond line above joint core, followed by cohesive failure in the resin, fibre-resin debonding and fibre breaking
0.15 mm thick PP interlayer	Crack along the bond line above joint core, followed by cohesive failure in the substrate with some fibre-resin debonding	–
0.30 mm thick PP interlayer	As 0.15 mm thick PP interlayer although with less fibre-resin debonding	Internal delaminations in the web, at the sides of the joint core, followed by cohesive failure in the resin and the substrate, plus reduced fibre-resin debonding and occasional fibre breaking

The plain non-woven samples developed a visible crack along the bond line above the joint core, followed by a cohesive failure in the resin along the bond line. The addition of PP interlayers displaced the cohesive failure to the laminate, but achieved similar failure loads, signifying that the inherent low peel interlaminar strength of the non-woven Twintex® is driving the behaviour of the joints, regardless of whether the failure occurs in the laminate or the joint line.

With regard to woven joints, plain samples also showed an initial crack above the filling core (Figure 6.18), and followed the same clean snap-off along the bond line (Figure 6.19) at similar failure loads. This notable result suggests that the interlaminar peel strength of woven and non-woven Twintex® laminates is notably similar, despite the fact that the interlaminar shear strength of the former is much higher than that of the latter as seen with lap joints. The addition of PP on woven joints led to a twofold increase in failure load and a different failure mode, characterised by delamination on the sides of the filling core (Figure

6.20) followed by progressive cracks propagation and finally substrate delamination (Figure 6.21).

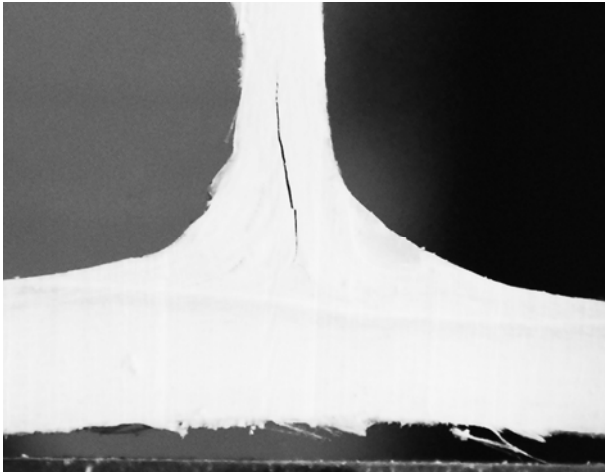


Figure 6.18: Initial major failure in a plain woven T-joint, initial crack above filling core

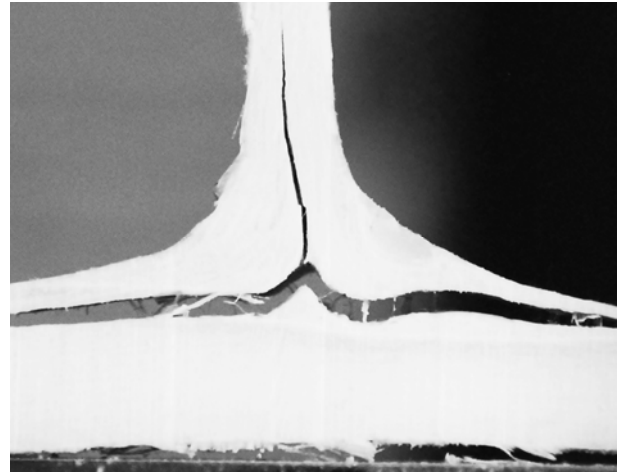


Figure 6.19: Plain woven T-joint final snap-off

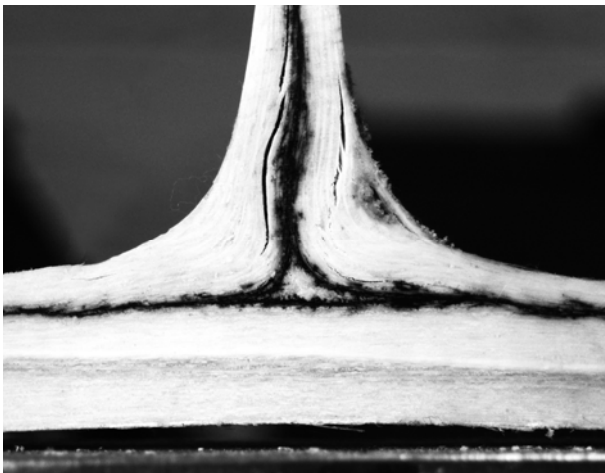


Figure 6.20: 0.30 mm thick PP-interlayered T-joint, initial side-delaminations

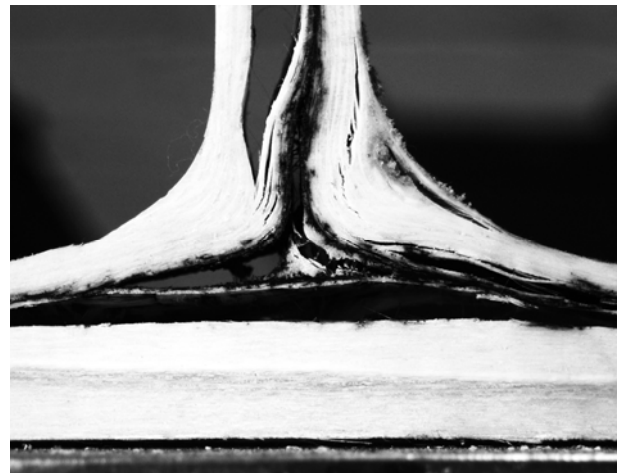


Figure 6.21: Final collapse of the joint pictured in Figure 6.20

The values of ultimate pull-out strength per unit length shown in Figure 6.22 let us see a significant scatter for plain T-joints, attributable to local variation in joint quality due to material heterogeneity, bridging-driven porosity and other local defects. This suggests that there is significant room for optimisation in these T-joints. Local defects and porosity can be addressed by reducing the angle to which the L-beams need to adapt while consolidating, and/or including more interlayers in between plies in order to increase the void-filling ability



of resin-rich regions. The significant scatter observed also suggests that a higher number of samples would be beneficial towards the reliability of the results and the repeatability of the manufacturing process, especially in the case of plain samples where additional PP does not reduce scatter as seen in Figure 6.23.

The improvement in pull-out strength and scatter reduction provided by the added PP (Figure 6.23) may follow the same interlocking mechanism that improved the lap shear strength. The resin-rich bond line would have a filling effect, reducing local porosity (Figures 6.24 and 6.25). It would also allow for certain through-thickness fibre dispersion during processing which in turn would even out stress distribution and energy dissipation during pull-out loading. In such way, the interfacial failure could shift into cohesive delamination in the substrate (Figure 6.21) as observed. These beneficial effects are believed to ultimately lead to the observed 80% increase in ultimate pull-out strength per unit length and an improved repeatability as well. The influence of re-crystallisation on these results could not be proved, as no trend was found in strength differences along the joints.

The strength of the non-woven sandwich T-joint (Figure 6.17) was comparable to that of single-skin non-woven samples. Its failure comprised approximately simultaneous core shear, skin-core debonding and joint core crack initiation. Being a usual validation principle to verify joint failure after core failure, this result qualitatively validates the joint sandwich arrangement for pull-out loads. This is a remarkable result, since the sandwich core constituted a sufficient thermal insulation to prevent any noticeable post-processing deformation on the outer hull surface. Therefore, it demonstrates that bulk fusion bonding is a structurally and cosmetically viable technique if appropriate insulation protects the outer surface from thermal deformations due to asymmetrical bulk heating.

As mentioned above, one design recommendation which was not followed related to the avoidance of sharp corners, because the need for full processing of the joint core required proximity to the heaters. Micrography analysis showed that the expected high porosity around the joint core amounted for up to 10% (Figures 6.24 and 6.25). Despite this source of local defects, the ultimate pull-out strength of woven interlayered T-joints is in the region of that of thermosetting examples tested under comparable conditions found in the literature (Figure 6.22).

Fusion bonded T-joints

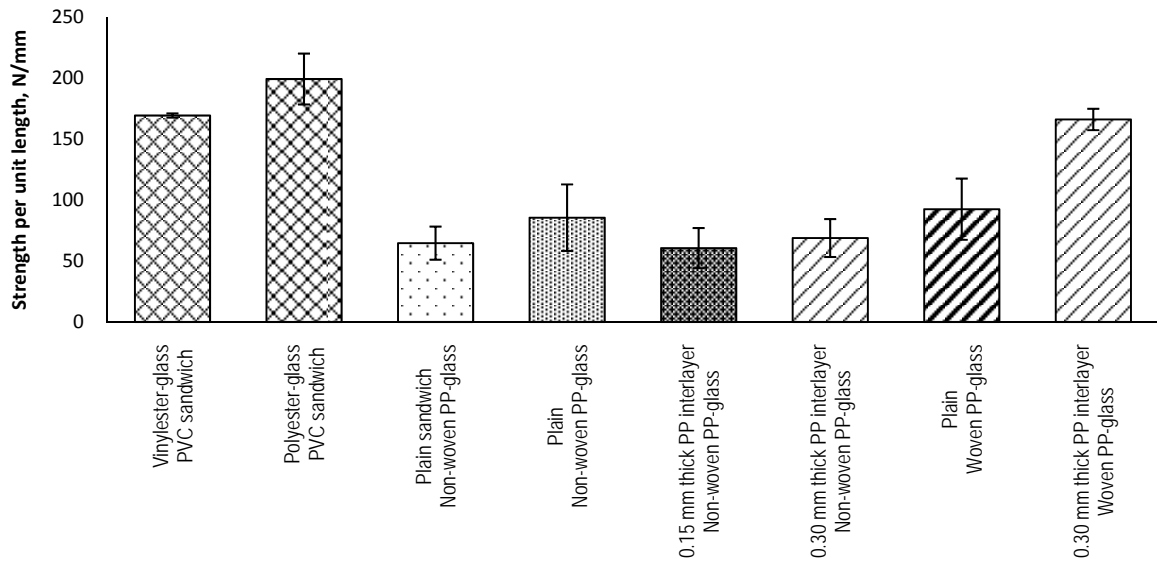


Figure 6.22: Pull-out strength per unit length of various T-joints, including vinylester [124] and polyester [128] systems

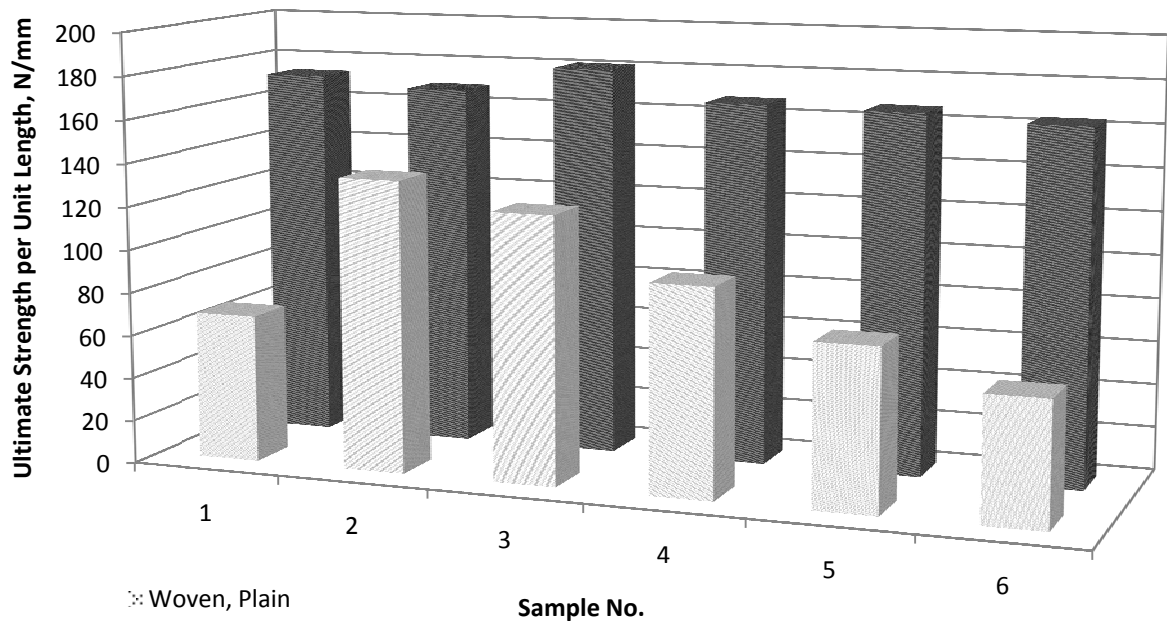
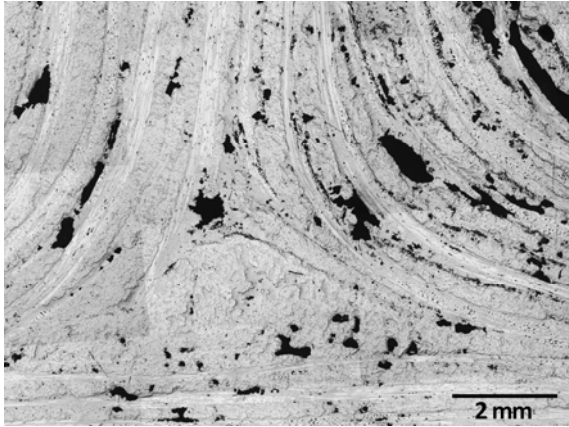


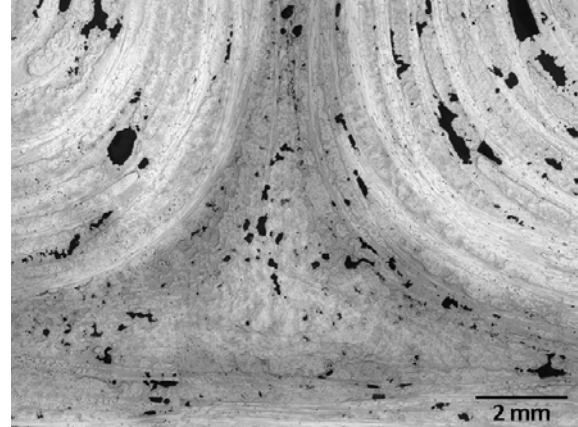
Figure 6.23: Comparison sample-to-sample between woven plain and interlayered T-joint samples

It is necessary to remark that the thermosetting T-joints included in the graph were significantly larger in many respects, particularly in bond surface size, which was 27% larger for vinylester joints [124] and 67% larger for polyester joints [128]. Despite these differences

in joint geometry, materials and size, it becomes clear that the design and construction of the assessed joints, although largely improvable, provide a pull-out strength that is comparable to that of existing and even optimised thermosetting T-joints.



**Figure 6.24: Optical micrograph showing high void content around the joint core in the case of plain woven T-joint**



**Figure 6.25: Reduced void content due to added PP interlayer (dark areas in the micrograph)**

## **Conclusions**

This experimental study on PP-glass lap and T-joints in the context of small boat manufacturing yields the following conclusions:

- A joining method intended for thermoplastic composite boats manufacturing has been developed, based on fusion bonding achieved by vacuum-assisted local bulk heating.
- Non-woven precursor materials are not recommended for lap or T-shaped joints, because their sensitivity to in-lamina shear when loaded in a direction different to that of the fibres. This effect, possibly in combination with a lower interlaminar strength than that of woven precursors, led to lower failure load values, regardless of PP interlayering.
- Results show that a 0.30 mm thick PP interlayer improves lap shear strength on samples made with woven materials by approximately 80%, mainly by enhanced fibre wetting and mechanical interlocking, and secondly by elastic energy dissipation along the resin-rich joint line.

- Lap joints manufactured with this technique, yet allowing for optimisation, notably outperform known lap shear strength values for adhesives and resistance welding applied to the same substrate materials.
- Measurements show that asymmetrical bulk heating in T-joints is likely to induce noticeable warping on thick, single-skin substrate laminates. However, sandwich constructions can also provide sufficient strength while maintaining their shape after processing due to the reduced thickness of the skins and the insulating effect of the core.
- The inclusion of a 0.30 mm thick PP interlayer improves the ultimate pull-out strength per unit length of T-joints made with woven fabrics by approximately 80%. It also adds significant resilience and reduces scatter, improving their repeatability.
- Despite bridging-driven porosity of up to 10%, the strength of these novel TPC T-joints is comparable to that of thermosetting known values.

The results on T-joints also showed that their significance, hence the repeatability of the process would to some extent benefit from a higher number of samples manufactured and tested, given the complexity of the construction. However, the relevance of the results obtained demonstrate that bulk heating fusion bonding can be used as a joining method in the construction of small thermoplastic composite boats and that it provides sufficient strength compared to existing thermosetting joints.

## **Chapter 7 – Repair technology for thermoplastic composite boats**

The viability of TPC boatbuilding depends on the availability of an effective manufacturing technique, in which scientific understanding, suitable tooling materials and joining techniques are of high importance. However, it also depends on a simple repair method, because through-life support for repairs and maintenance is a feature without which a product cannot last long in the marketplace.

The repair of the existing TPC boats is available only for very simple geometries and sometimes requires the use of the boat mould. An industrial interest was acknowledged regarding the ability to quickly repair a complex TPC boat in the absence of a mould. In response to this interest it was decided to develop an emergency repair technique and assess its feasibility from the manufacturing point of view. With this purpose, an experimental TPC RIB, built by BAE Systems, was subjected to a controlled impact and subsequent repair. The damaged area was inspected by ultrasonic non-destructive testing to identify delaminations, and enable the removal of the damaged material. A pre-consolidated composite patch was cut to the opening dimensions, and the scarf joints were covered with extra unprocessed precursor fabrics. Local bulk heating was applied inside a vacuum arrangement, achieving the fusion bonding of the joints. This procedure, intended for in-situ repairs which do not require a repair yard or any large facility, involved simple and easily portable equipment, and avoided the use of a mould. A micrography study, accompanied by tensile tests, demonstrated that this technique provided a watertight repair with sufficient structural integrity.

## Controlled impact

With the objective to develop and characterise an emergency repair technique for a large hull damage typically corresponding to a grounding event, the hull of the thermoplastic Atlantic 85 introduced in Chapter 2 was subjected to a controlled impact at the facilities of BAE Systems. The controlled impact was aimed at simulating a grounding incident. For the purpose of this simulation, the energy exchanged in the impact of the RIB hull on a hypothetical rock on its way was delivered by allowing a 500 kg steel striker to fall 6.5 m onto a hull panel near the port bow, as shown in Figure 7.1.

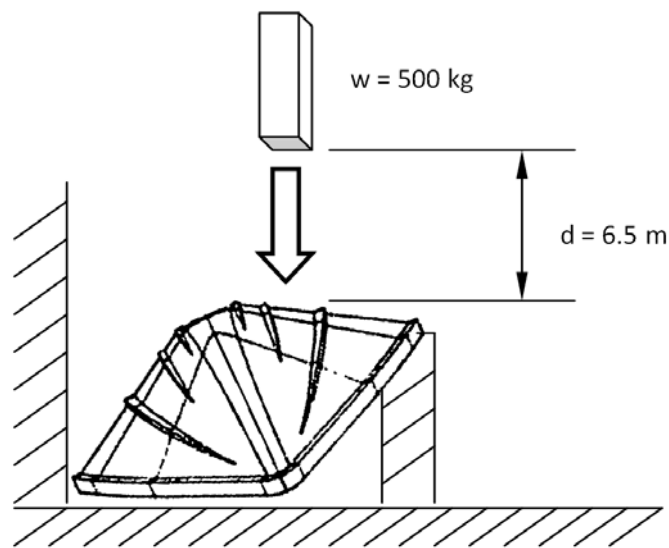


Figure 7.1: Controlled damage arrangement at BAE Systems – Portchester Shipyard

The hull was secured on the heavy-load proof concrete ground by means of standard steel pillars and a fully loaded steel container. The 250 x 250 x 1100 mm steel striker was lifted and released on the hull with a truck-mounted crane. Under these conditions, the impact of the steel block provided with a kinetic energy dissipation of approximately 32 kJ. According to classic physics calculations, this energy is equivalent to an impact mass and velocity of 2,300 kg and 10.25 knots ( $5.27 \text{ m}\cdot\text{s}^{-1}$ ), respectively. Such loading and velocity conditions approximately correspond to a typical grounding event of a fully loaded RIB. However, the difference in impacting mass led to a difference in impact velocity, being the test velocity  $11.25 \text{ m}\cdot\text{s}^{-1}$ , approximately twice the envisaged speed of the craft.

At the recorded ambient temperature of 5°C, pure PP is just above its glass transition temperature and shows a tough-brittle transition in this region [129]. In this case, this means that high velocity impacts produce a brittle response on the PP resin, whereas low velocities are associated with a tougher response. Nevertheless, this does not occur in the same way in long glass fibre-based PP composites, since many other toughening mechanisms, involving interactions between the glass and the polymer, are present.

With PP-glass, as with most other types of composite, the energy absorption in impact increases with testing velocity [130], meaning that for a high velocity impact, the material allows for higher loads before failure. Although for a factor of two speed increase this effect would have been small, it is conceded that the damage might have been slightly less extensive than for an impact at normal speed.

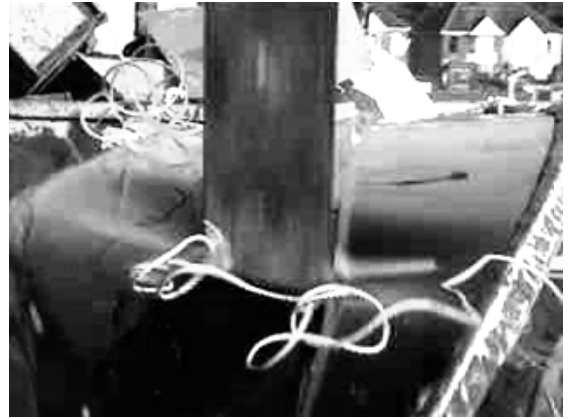
As seen in the video key frames of Figure 7.2, and especially in frames 7.2.2, 7.2.3 and 7.2.6, the hull structure absorbed part of the impact energy but also returned a notable share of it, bouncing off the striker onto the ground. This controlled impact dramatically demonstrated the toughness of PP-glass structures, which is remarkably advantageous in relation with the dynamic impact loading which is typical of the marine environment. Notably, the impacted panel significantly bends down forced by the impact and back up again. The sharp edges of the striker pierced the hull shell along the contact lines, as seen in Figure 7.4.

However, apart from this perforated region itself, the remainder of the hull appears to largely recover its original shape, with little chipping and no cracking. This tough recovery is characteristic of thermoplastic composites, and differs greatly from that of thermosetting composites, which are usually much more brittle.

While potentially advantageous from the repair viewpoint, the observed behaviour may leave an intact look from the outside despite severe internal damage. Similarly to what observed with other composites, this implies that it is not possible to assess the true extent of damage following an impact solely from the appearance of the structure. This underlines the importance of using non-destructive evaluation (NDE) methods to determine the true extent of damage.



7.2.1



7.2.2



7.2.3



7.2.4



7.2.5



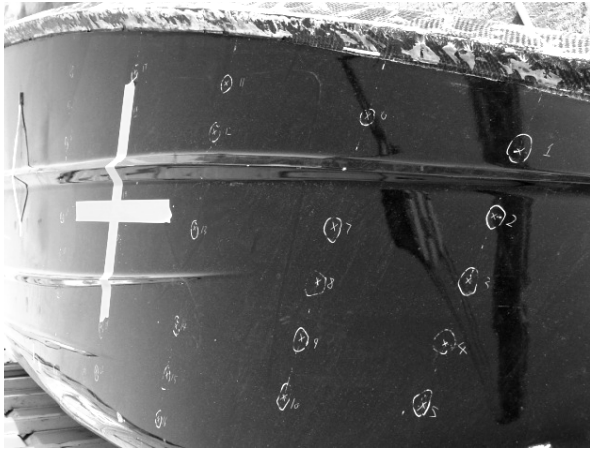
7.2.6

Figure 7.2: Key frames from the video recording of the impact event.

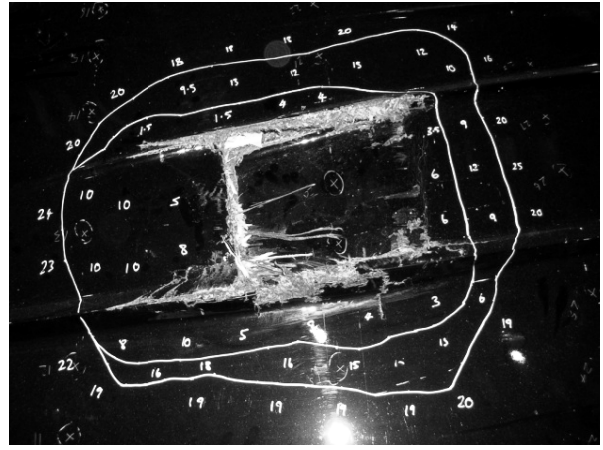


## NDE inspection

Ultrasonic NDE was performed before and after the damage test, as shown in Figures 7.3 and 7.4, respectively.



**Figure 7.3:** RIB hull ready for the impact – the marks indicate recorded NDE signal to compare with after-impact values



**Figure 7.4:** Extent of the damage region, as assessed by NDE

As it is found with other composites, PP-glass may be affected by delamination under certain loading conditions. This phenomenon comprises layers separation inside the material and significant loss of mechanical continuity and properties, not always followed by obvious visible signs on the outside of the structure as mentioned above. This way, a sudden reduction in thickness measured by NDE would mean a discontinuity inside the laminate, most likely an internal delamination in this case.

The device used, an Epoch-4B (Pulse-echo A-scan) with a 500 kHz transducer, was calibrated with sample Twintex® panels to allow accurate thickness measurement with the thermoplastic composite. Preliminary thickness measurements were performed and recorded on selected points on the hull (Figure 7.3) prior to the impact event. These recorded values allowed for comparison with the data to be obtained after the impact, in order to assess the extent of the damage. Finally, further measurements were needed to finely determine the extent and shape of this damage. The final contour of the delaminated region determined with this method is shown in Figure 7.4.

Despite the mentioned calibration, significant differences between NDE- and physically-measured hull thicknesses were observed after the material removal, being the marked 18 mm approximately corresponding to 12 mm as confirmed with a vernier caliper. However, thicknesses were measured up to where their values stabilised, which was indicated by a line containing the damaged region as seen in Figure 5. Therefore, despite the disagreement in absolute terms, the overall comparative aspect of the NDE analysis was considered reliable with regard to the identification of internal delaminations.

## **Fusion bonded patch repair**

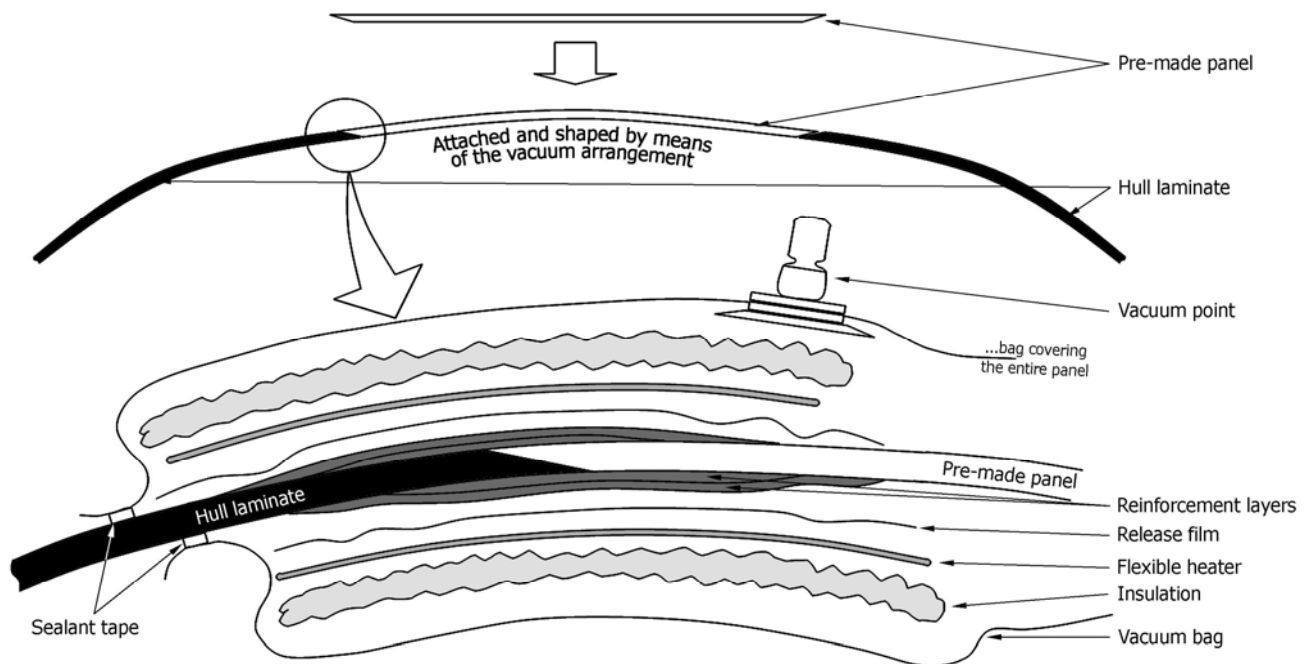
As discussed in the introduction, the repair of thermosetting boats is a well-established technology. Regarding the repair of TPC boats, craft with simple geometry as the BAE Systems PP-glass assault boat shown in Figure 2.2 are currently repaired with small flat repair patches and also by reprocessing the entire structure after disassembling. This “relief” process is very cost-effective but requires a mould and an oven. BAE Systems reported the need of an in-the-field repair technique which does not involve the use of any mould and can be carried out with small, portable elements and equipment wherever remotely the repair needs to be done. The technique also needed to deliver the boat back to the water in 24 hours with restored water-tightness and structural integrity. This repair, not requiring a cosmetic finish nor “as new” mechanical properties, would represent a strategic advantage especially in military and rescue craft.

In order to achieve such emergency repair, a number of solutions were considered. As the co-consolidation of unprocessed material requires a mould to keep the soft material in shape during processing, the use of a pre-consolidated patch was preferred. Thus, a mould-free technique was developed involving a pre-manufactured flat panel, to be cut to the opening dimensions and joined to the hull solely by fusion bonding of the edge joints. The panel and hull opening edges would require appropriate scarf preparation. Once this is done, vacuum-assisted local heating would be applied to the scarf joints only, leaving the rest of the panel in its previous consolidated state, as seen in Figure 7.5.

The need for easy storage and portability restricted the equipment that could be used to simple heating blankets, a portable vacuum pump and some conventional vacuum processing disposables. The latter are listed in Table 7.1 and shown in Figure 7.5.

**Table 7.1: Disposable layers used in the repair**

Vacuum bag	Aerovac Capran 526 (Nylon)
Breather	Aerovac Airbleed 33N (Nylon/Polyester)
Release film	Aerovac A5000 (FEP)
Sealant tape	Aerovac SM5127
PP interlayer	Woven PP mat, 135 g/m <sup>2</sup>



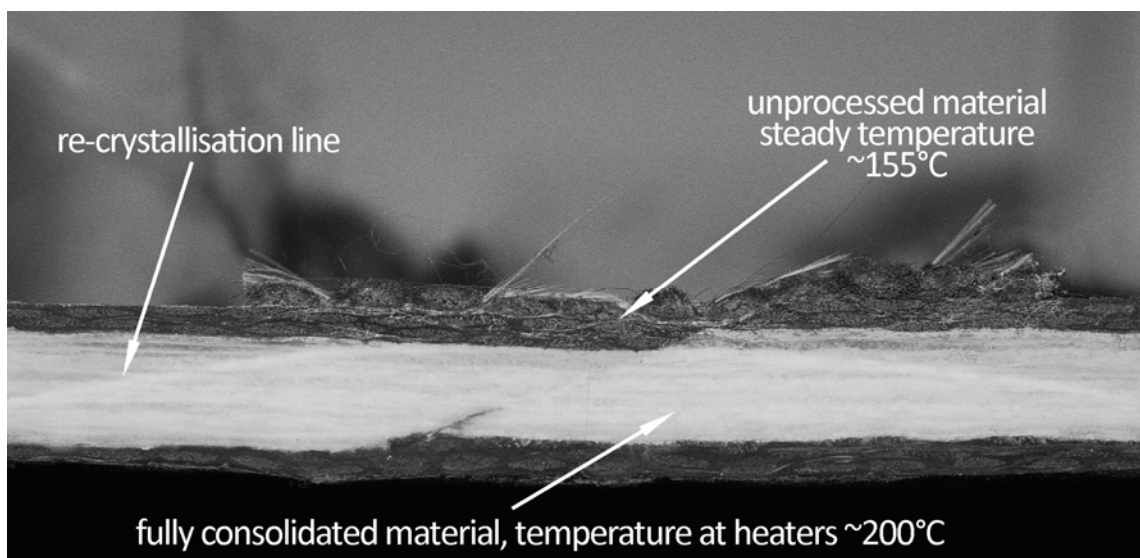
**Figure 7.5: Repair layout diagram. Further insulation was laid up on top of the vacuum bags on both sides to prevent heat flowing outwards.**

The flat PP-glass patch was manufactured from Twintex® T PP 60, matching the measured average hull thickness along the joint line: 11 mm. This thickness was attained with white non-woven plies and a reduced number of black woven layers. This configuration was similar

to the original hull construction, but featured a larger content of white Twintex®, which conveniently helped with find the bond line in the later microscopic examination of the repair joints. Finally, they provided an exterior look similar to the hull finish, which was convenient to evaluate the cosmetics of the final repair.

The repair joints were heated with silicone rubber coated electric heating blankets. This choice was made because of their flexibility, which would allow them to adapt to the shape of the hull, and relatively high power density of  $7.75 \text{ kW}\cdot\text{m}^{-2}$ . Firstly, these heaters were used in a series of trials which were conducted to determine whether a good quality repair could be achieved with single-sided heating or whether it would be necessary to heat the repair with blankets on both sides.

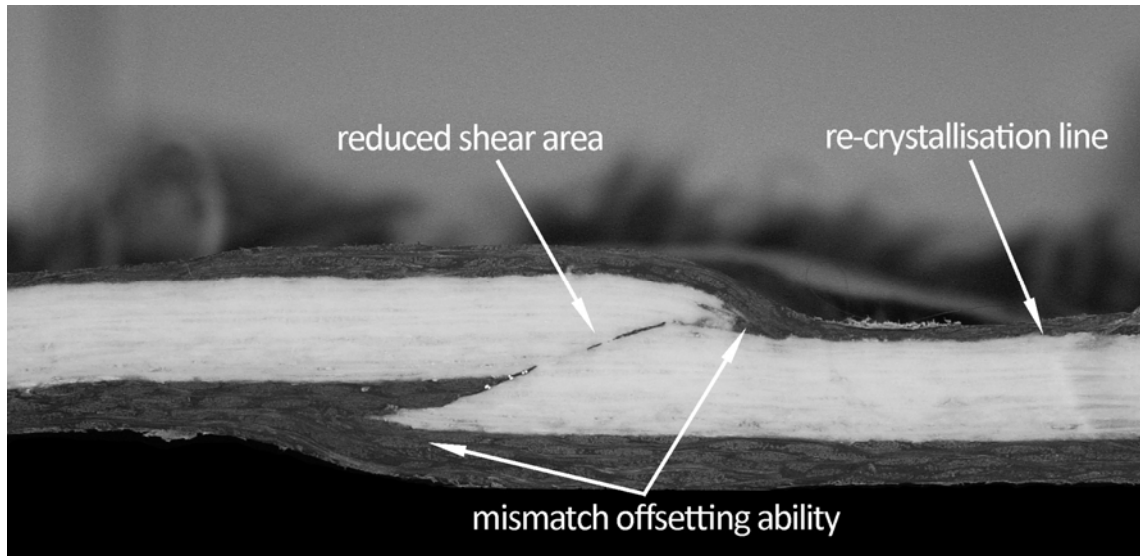
As seen in Figures 7.6 and 7.7, single-side heating could not lead to full processing of the scarf joint due to inevitable heat losses. Regardless of how good is the insulation, some heat is transferred in-plane through the whole laminate towards the cool exterior; hence a certain heat power is needed in order to compensate this heat loss and bring the bond region up to the processing temperatures of  $180\text{-}200^\circ\text{C}$ . In this respect, a single heater on one side appeared to provide with insufficient power for the thickness assessed.



**Figure 7.6: Unsuccessful repair test featuring single-side heating – scarf joint is visible in the centre (low brightness of images allow to see re-crystallisation line)**

A re-crystallisation line is observed in both figures, indicating that on one side of the line, all resin has re-melted, whereas on the other side remained below melting point. The form of

this re-crystallisation line is approximately parabolic as shown in Chapter 6, enabling the interpolation of temperatures inside the laminate if needed.



**Figure 7.7: Successful repair test with heating on both sides – remarkable mismatch offsetting ability due to resin reflow**

In contrast, it was found that both sides-heating led to full through-thickness consolidation, which demonstrated the feasibility of the repair method. This second repair test suffered from an accidental scarf joint mismatch, which occurred because the laminates were not clamped in place and moved while the vacuum was applied to the arrangement. This reduced the contact area along the scarf line in approximately 40%, but had the benefit of showing the offsetting ability of TPC materials due to resin reflow. It was decided to force this effect in the real repair to evaluate its influence on the final properties.

## **Repair procedure**

Prior to carrying out the fusion bonding process, damaged and delaminated material was removed from the hull, using the results of the NDE study as a guide (Figures 7.9 and 7.10). The material removal included some damaged and apparently intact internal structure because of the space needed for disposables and vacuum arrangement on both sides of the panel. The reason for this is that the vacuum bag coverage must include both sides of the whole area to be repaired, plus the space required for the sealant tape, to provide the necessary pressure and air-removal from the repair joint. Inside the boat, the area to be

covered is likely to intersect internal structure elements, as occurred in this work (Figure 7.10). Paint and dirt were sanded away and the edges were prepared with 35 mm long scarfs, giving a scarf angle of roughly  $17^\circ$  (Figures 7.11 and 7.12). Scarf lengths in composite boat repairs are usually 4 times larger [131], but the space restrictions inside the small hull of the RIB made them unpractical for this damage size.

Additional reinforcing material in the form of 2 unprocessed woven plies fabrics, 1 mm thick each, was lied up on the panel edges (Figures 7.13 and 7.14). Then it was manually fitted to the scarfed hull and subjected to pressure in the vacuum arrangement (Figure 7.15). On both sides of it, the heaters and layers of disposables were applied and kept in place with temporary spray adhesive. Heavy insulation was added on the exterior of the vacuum bag (Figure 7.16), to avoid excessive heat losses that could prevent the joint from reaching full melting. Although a one-stage process is achievable, in this work the fusion bonding of the panel joints was performed in four stages, corresponding to the four sides of the panel. In each processing stage, two heater blankets of the same size were used, one on the outside surface of the hull and the other on the inside. As a result, the intersections of the heated areas were processed twice. The heaters were controlled individually, providing with heating and cooling ramps of 30 minutes each and a processing time of 30 minutes once the centre of the joint had reached  $185^\circ\text{C}$ . These conditions, shown in Figure 7.8, were considered appropriate following the results obtained in the validation tests described above. The resulting process cycle of about 100 minutes is extremely quick in comparison with the cure times needed for the adhesive bonding normally used in thermosetting composite repairs, in the order of 3-6 hours. It is estimated that this technique would allow an emergency repair in less than 24 hours, especially if the joints are processed in one stage only.

The final repair is shown in Figures 7.17 and 7.18. As the four sides of the panel were fusion bonded to the hull, the former matched the double curvature of the latter solely by means of the ambient pressure on the vacuum bag. This curvature, shown in Figures 7.19 and 7.20, was measured, approximately corresponding to a 20 mm deflection over 500 mm of panel length.

Small craft as the Atlantic 85 RIB includes spray rails to increase lift force and reduce hydrodynamic resistance. These comprise three longitudinal V-shaped thin, step-like

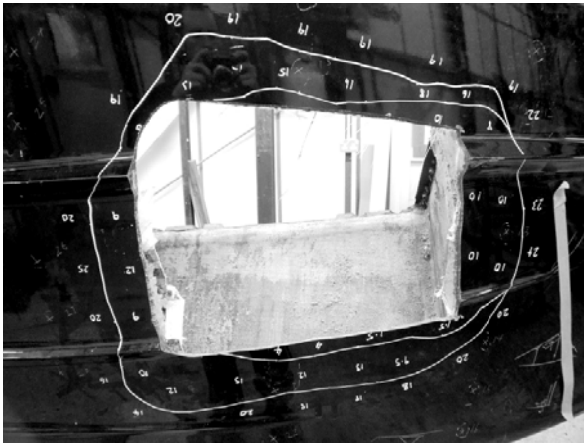


Figure 7.9: Damaged material removed from the hull

Figure 7.10: Inside view of hull opening after material removal

members along the hull (Figure 7.21). Spray rail repair was not included in this work, because it would require the use of a mould, an option discarded from the beginning.

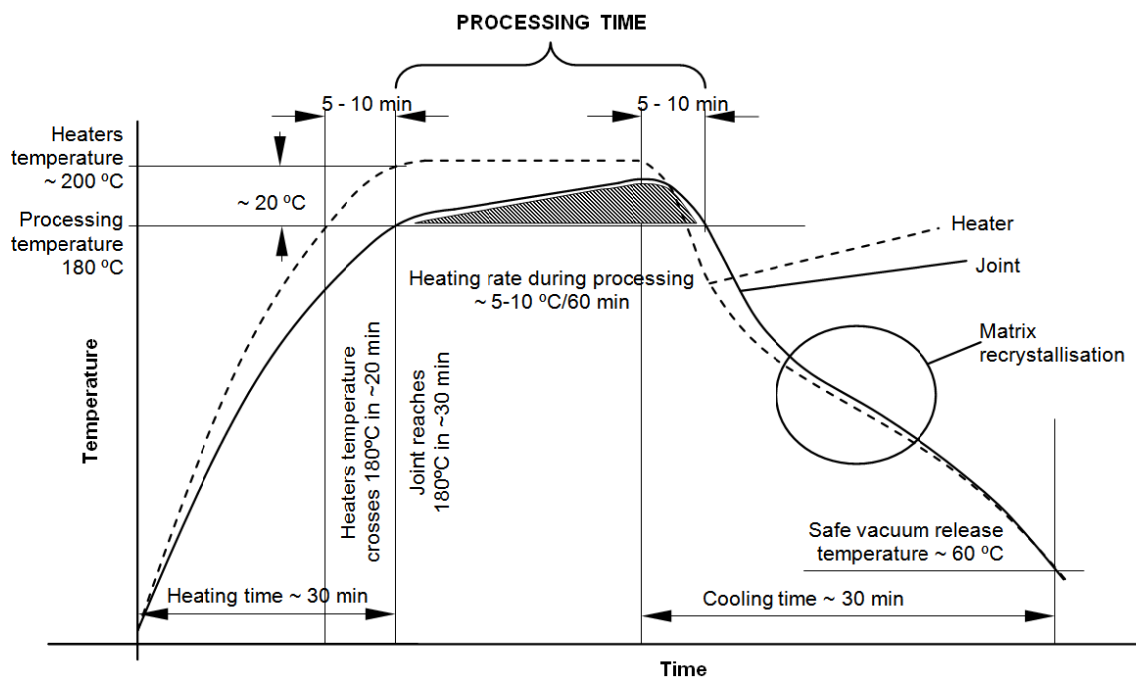


Figure 7.8: Typical processing cycle for the repair panel joints

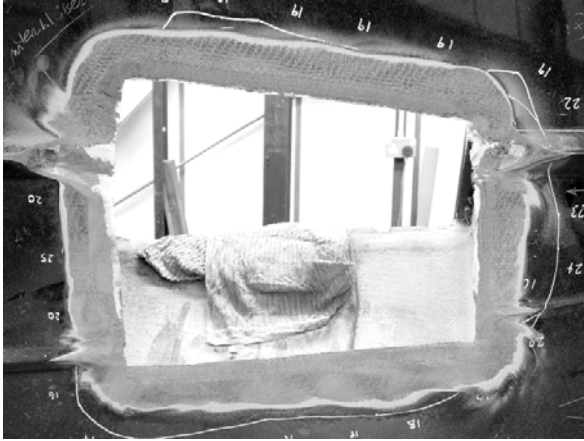


Figure 7.11: Paint sanded away and hull edges scarfed



Figure 7.12: Panel edge preparation



Figure 7.13: Additional unprocessed fabrics on panel

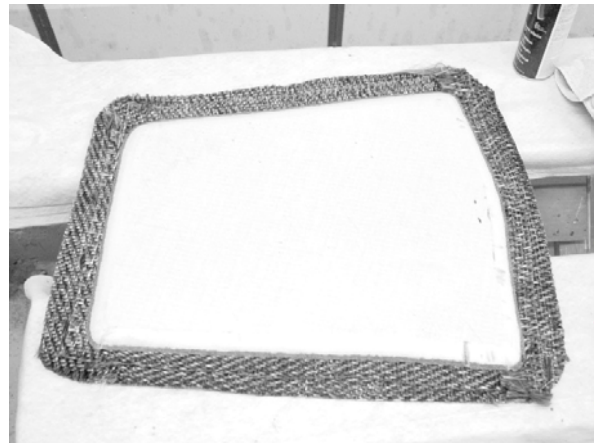


Figure 7.14: Inner side of the panel



Figure 7.15: Fore repair joint prior to be insulated



Figure 7.16: Insulation during processing



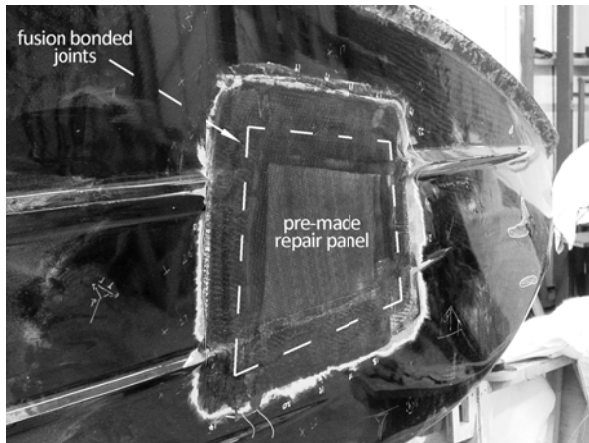


Figure 7.17: Repair done

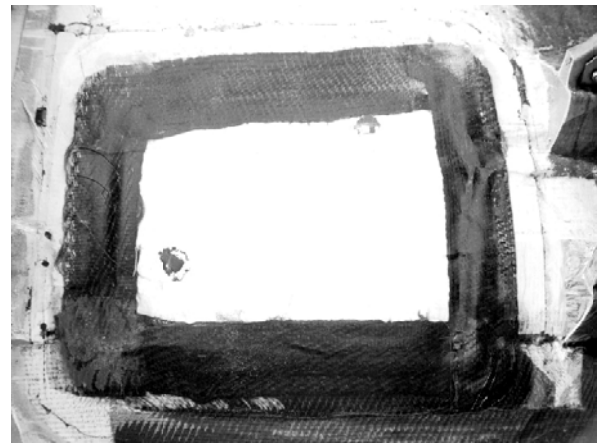


Figure 7.18: Interior of the repaired hull



Figure 7.19: Aft view of the final panel curvature



Figure 7.20: Fore view of the panel curvature



Figure 7.21: Fore view of the repaired hull

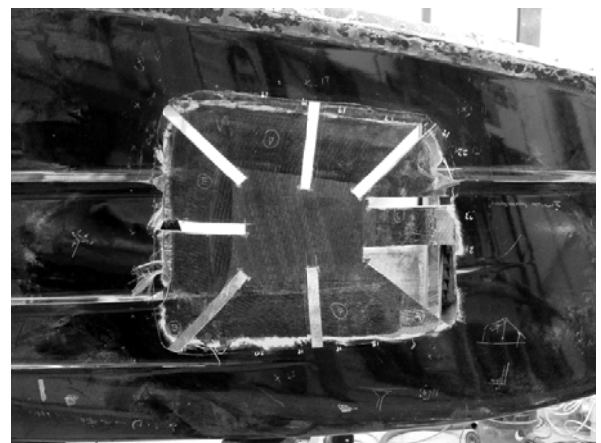


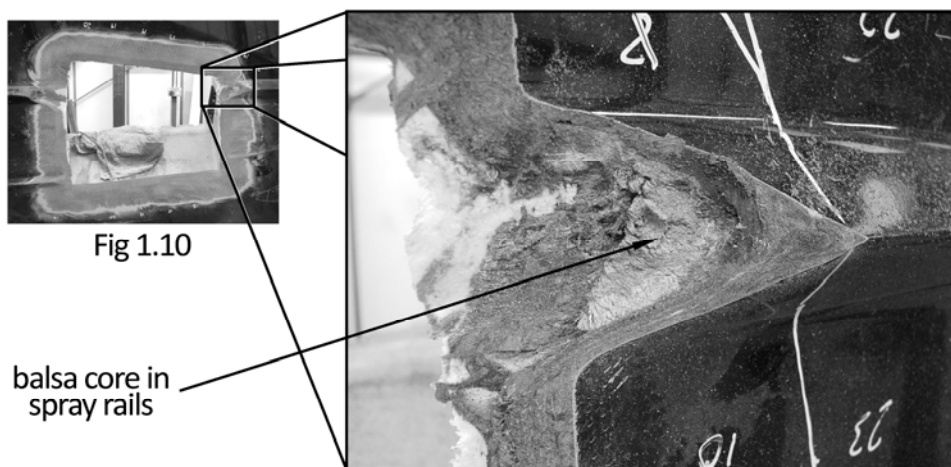
Figure 7.22: Repair joints sliced for characterisation

The repair method described above has the additional ability to heal any internal damage by the application of heat and pressure. As mentioned above, the NDE might have left some delaminations undetected. However, this healing ability would have been likely to heal these delaminations by re-melting of the PP resin matrix up to approximately 50 mm beyond the damaged material removal line, as seen from Figures 7.9, 7.17 and 7.22.

## Repair characterisation

### Micrography

Samples were cut from the repaired hull for characterisation as shown in Figure 7.22. Optical micrography of polished samples showed that good consolidation had occurred along the length of the joint (Figures 7.24 to 7.26). The air pressure inside the vacuum bag was monitored, reaching values of around 0.3 bar (70% vacuum), most probably due to some air leakage through the balsa core in the spray rails, which can be seen in Figure 7.23. This pressure is notably high, especially in comparison with the recommended pressure of virtually 0.0 bar (100% vacuum).



**Figure 7.23: Vacuum level was 70% due to air leaks through the balsa wood core inside the spray rails**

The resulting vacuum level was lower than would have been desirable, as low vacuum levels are usually related to high void content in TPC laminates. This applies both to consolidating material and re-processing of pre-consolidated laminates as is the case of this repair. As seen

in Chapter 4, the former require high pressure to allow resin impregnation of the reinforcing fibre bundles and coalescence of the high viscosity resin pools, whereas the latter need to overcome the residual stresses created in their manufacture [132], which tend to de-consolidate the material as it is heated under insufficient pressure [36]. Figures 7.24 to 7.27 show that, in addition to well-consolidated regions there are occasional voids, apparently evenly distributed over the original laminate, the repair panel and the joint line, supporting the argument of low vacuum-driven increased porosity.

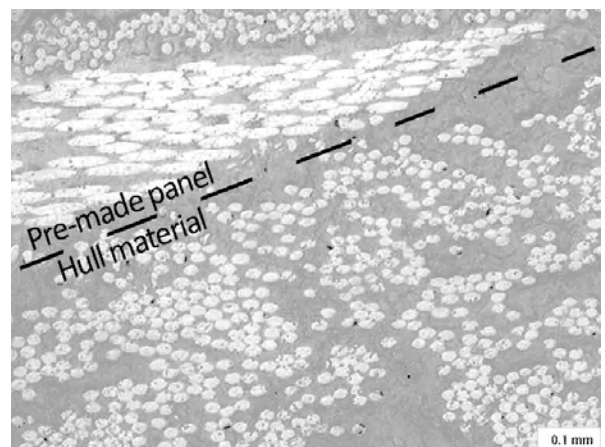
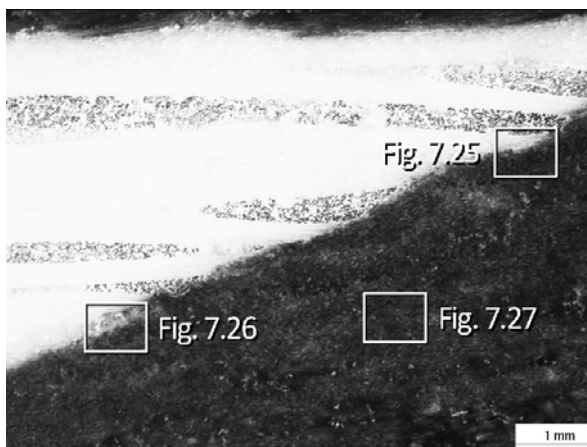


Figure 7.24: Bonded joint section, corresponding to the middle of the sample in Figure 7.29 (pre-made panel in white, left – existing hull in black, right)

Figure 7.25: Well consolidated region along the joint line

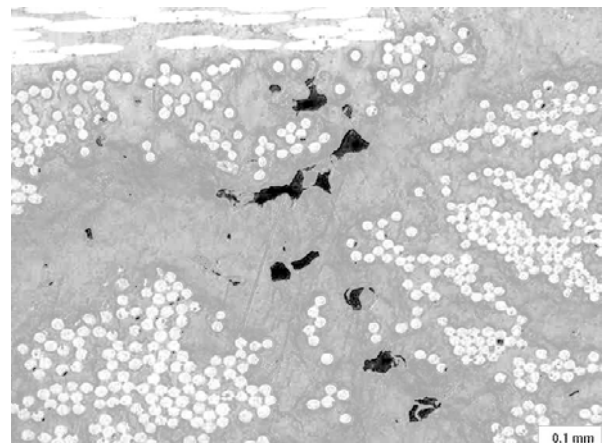
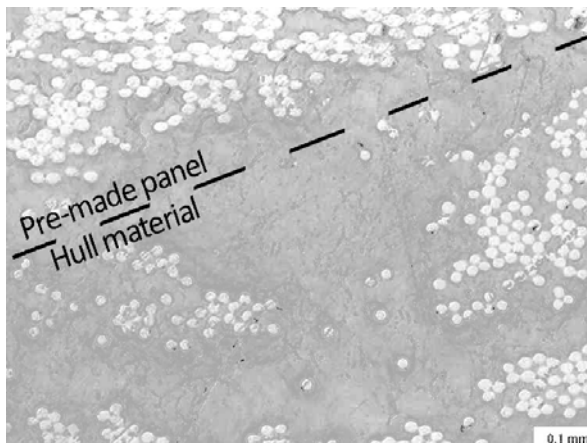


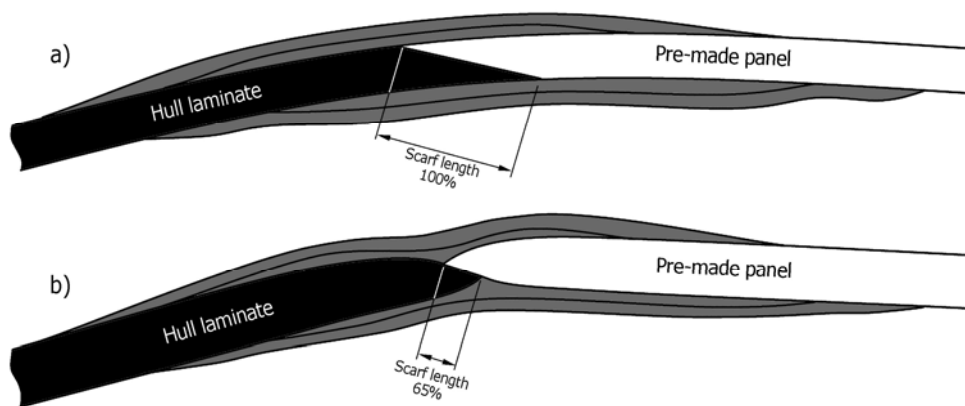
Figure 7.26: Well consolidated, resin rich region

Figure 7.27: Voids due to insufficient vacuum

The overall repair void content was 5-10%, compared to the lower value of 0.5-1.0%, characteristic of good quality vacuum formed PP-glass laminates [42].

### **Tensile tests**

In addition to the qualitative micrography analysis, a study was made on the tensile strength of the fusion bonded repair joints. As mentioned above, the preliminary validation tests revealed a remarkable gap-offsetting ability because of the re-melting resin, which makes the fusion bonded joints particularly insensitive to small geometrical mismatches between the parts to be joined. With the purpose to assess the properties of an offset joint, the panel was cut and the edges prepared so that different scarf lengths were available for testing, ranging from 65% to 100%, as shown in Figures 7.28 to 7.30. This was achieved by fitting the panel in such way that it would not exactly match the opening on certain places, providing reduced contact with the hull edges. In these points, a reduced scarf length occurred, where the melted resin allowed plies re-shaping and resin gap-filling. Due to this effect, noticeable deformation was induced in the joints as shown in Figures 7.28 b) and 7.30. For convenience, samples with full scarf length will be referred as type “a” and samples with approximately 65% scarf length as type “b”.



**Figure 7.28: Different scarf lengths available from the repair joints**

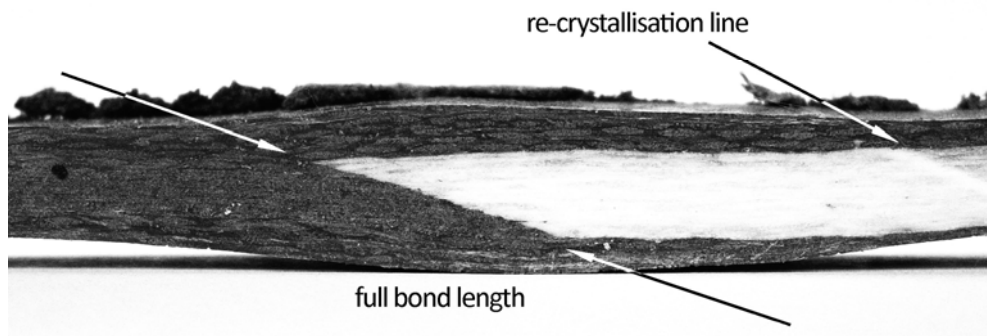


Figure 7.29: Repair joint sample with full scarf bond length

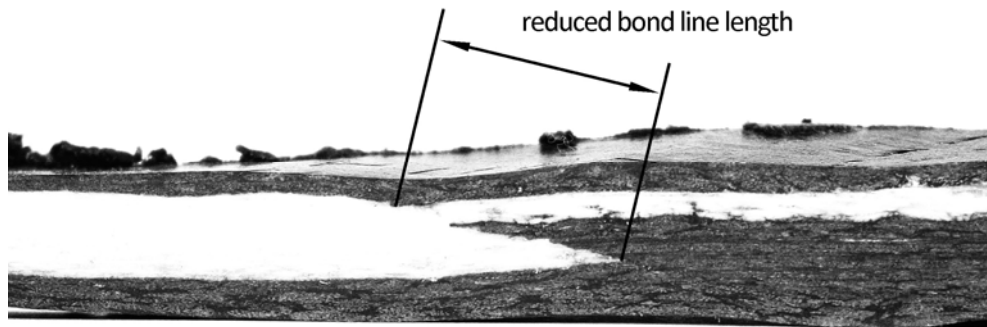


Figure 7.30: Sample with reduced bond length

Five samples approximately 18 mm wide were cut for testing from selected areas of the fusion bonded joints, corresponding to 100% and 65% scarf length, and another set of four 14 mm wide samples from the pre-made panel. Since the joint samples followed the hull curvature (Figures 7.28 and 7.33), certain bending forces surely affected them during tensile tests. This curvature was measured, being within 2.4% of vertical deviation. Thus, this effect was considered small and consequently disregarded, especially considering the comparative evaluation of the results. It must also be noted that most of the hull material is usually subjected to simultaneous and/or alternating tensile, compressive and bending forces during its service. However, it was considered that a simple tensile test would provide a reliable first indication of the performance of the repair, especially as a comparative tool.

Results of the tensile tests, shown in Figures 7.31 and 7.32, revealed that type “a” joints were stronger than the hull laminate, which failed first.

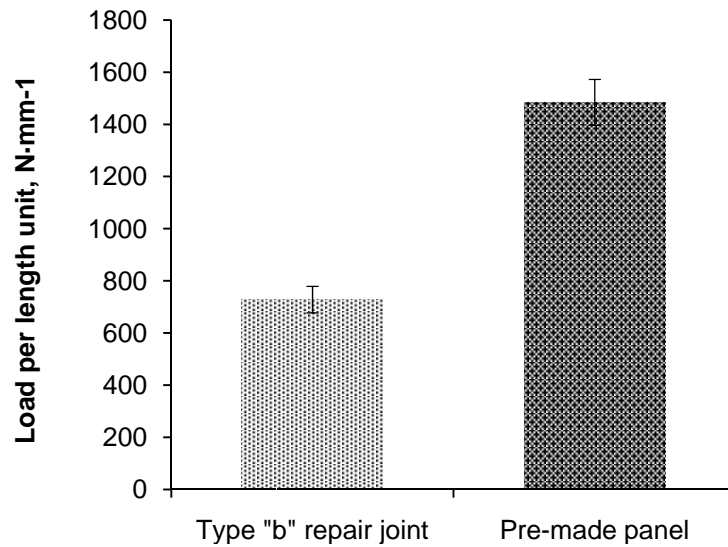


Figure 7.31: Tensile tests results for the type “b” repair joint and the pre-made panel – type “a” repair joints (not included) were stronger than the hull, which failed first

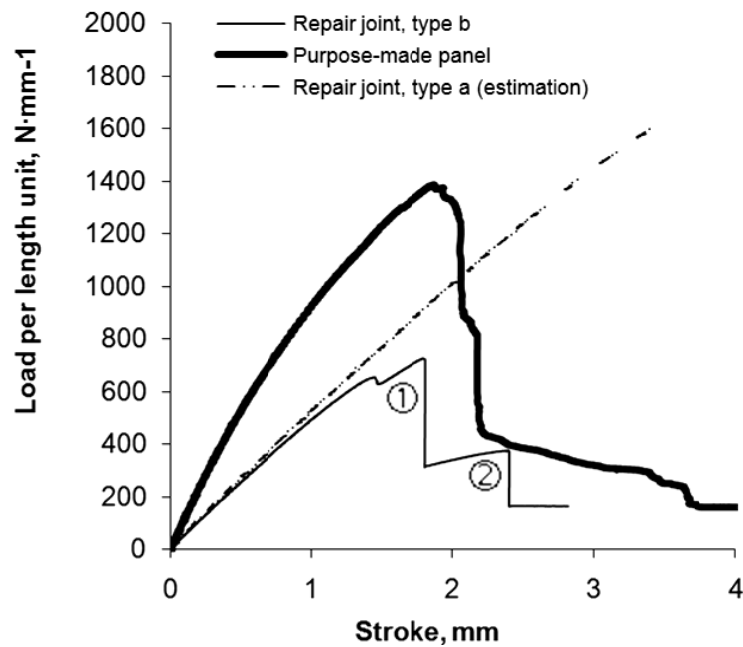
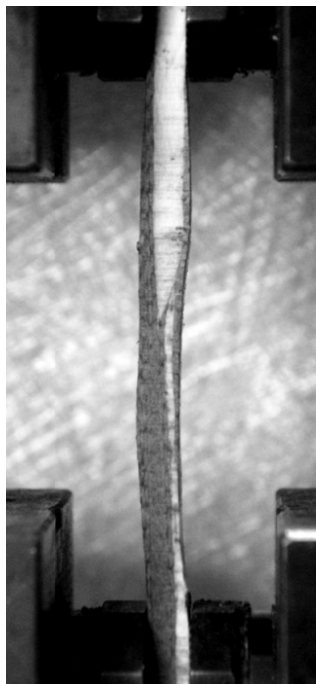


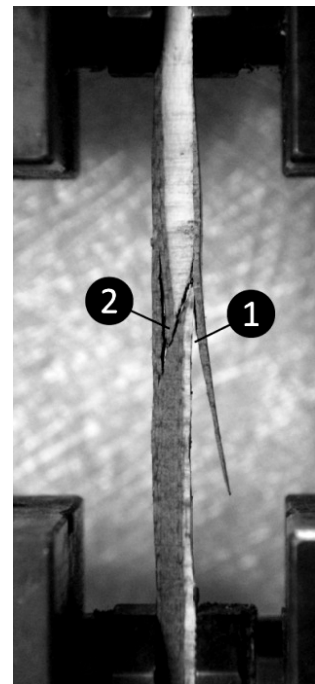
Figure 7.32: Typical tensile test curves for pre-made panel and joint type “b” and estimation curve for type “a” joint – numbers correspond to those in Figure 7.34

Because the failure load of the hull laminate was higher than that of the repair, its strength value is not included in Figure 7.31, and only an estimation of the test curve is available (Figure 7.32). For type “b” joints (65% scarf length), the failure load per divided by the joint length in mm was approximately 50% of that of the pre-made panel for the same fibre orientation.

The repair technique formed fibre discontinuity lines, rich in resin, along the boundaries of the reinforcing extra material and the scarfed joints. As a result, the fusion bonded joint failed sequentially, as expected, along these fibre discontinuity lines (Figure 7.34, numbers correspond to load drops in Figure 7.32). It is notable that the slope of the tensile test curves, signifying the stiffness of the material, is higher for the panel than for the joint. This is also an expected result, because the failure mechanism of the panel involves fibre breaking and fibre-resin debonding, leading to a higher stiffness than that of the sequential failure of the joints, mainly due to resin shear and peel forces.



**Figure 7.33: Type “b” joint being tested**



**Figure 7.34: Failure of type “b” joint – numbers correspond to those in Figure 7.32**

The offsetting and gap filling ability of this technique provides certain dimensional flexibility in the repair. However, it also highlights the possibility that under some circumstances, the strength of the repair may be somewhat limited due to misalignments between the panel and the hull. These limitations must be considered in the eventual design of a repair kit, crewmen training and the spectrum of repair qualities expected from a real in-situ repair, in terms of what can be expected from a hull repaired using this technique.

## **Conclusions**

An experimental TPC RIB was subjected to controlled damage, dramatically demonstrating the high toughness of PP-glass structures. Ultrasonic NDE helped to identify the cracked and delaminated material, which was removed from the hull. A novel repair technique, aimed at emergency situations where the boat needs to be repaired in the field and be back to service in no more than 24 hours, was developed and tested. It involved the use of a pre-manufactured flat panel which edges were reinforced and fusion bonded to those of the resulting opening in the hull, by local heating from both sides of the joints. The panel adapted to the hull shape by means of the applied vacuum.

Optical micrography and tensile tests show that despite the reduced achievable vacuum level led to high void content, the quality and the strength of the repair provide adequate water-tightness and structural integrity, demonstrating that this technique can be used to repair TPC boats. The bulk heating fusion bonding method provides with certain gap filling and offsetting ability, which however does not prevent a significant strength reduction should a panel misalignment occur. Such effect must be considered towards the design of a real repair kit, crewmen training and post-repair hull condition.



## **Chapter 8 – Recycling of end-of-life TPC boats**

The inherent recyclability of thermoplastic resins is one of the reasons why they and their composites are interesting materials for the construction of boats and other structures. However, the recycling of real end-of-life TPC boats is far from being an established industry. The reasons behind this fact are many and complex, ranging from the present lack of a stable flow of end-of-life materials ready for recycling, to the actual profitability of such activity. One research question that was found equally or more important is the technical feasibility of the recycling process. Real boats often combine several materials such as core and paint which may be difficult and expensive to separate prior to mechanically recycle the composite skins.

With the objective to assess this feasibility, this chapter discusses a set of experiments carried out on the mechanical recycling of an Atlantic 85 RIB, originally built by BAE Systems and tested in service by the RNLI. This TPC boat was returned to BAE Systems for further testing. As described in Chapter 7, it was subjected to a damage and repair experiment. After that, it was decided to test its mechanical recyclability. Selected pieces of its hull were cut, ground and mixed with additional PP resin. This mixture was melt-extruded, reground and injection moulded into test samples. It was found that the properties of the resulting material were well within the range of those of virgin materials for injection moulding, demonstrating that structural TPCs are recyclable in practice as well as in principle, hence confirming that they are a sustainable alternative to thermosets.

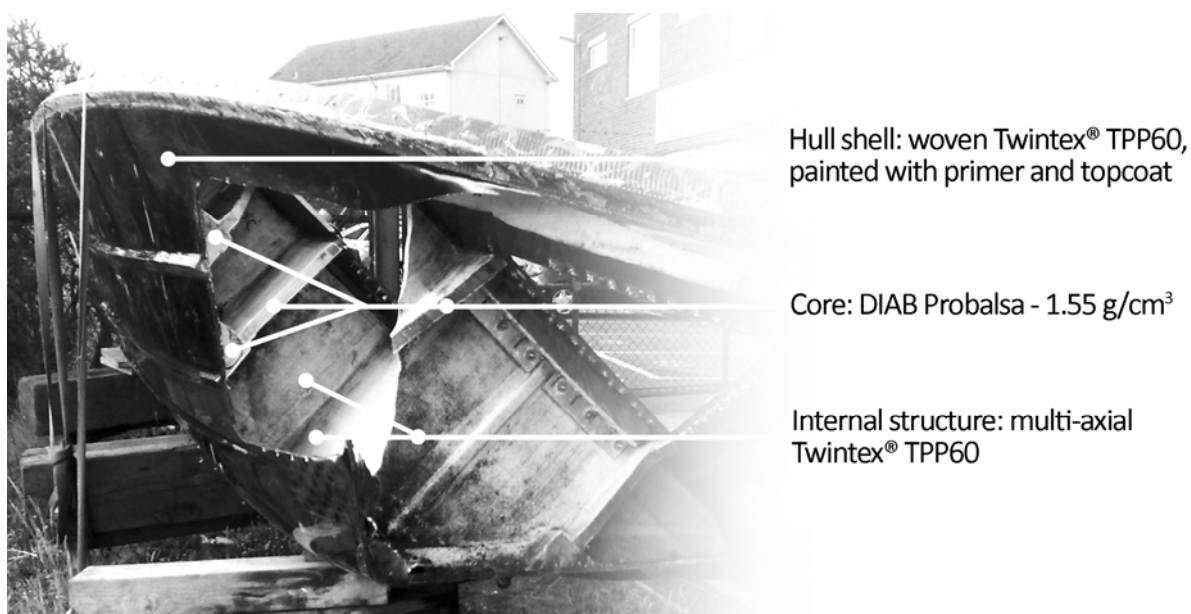
## **Mechanical recycling**

### **Materials**

The materials employed in this recycling study were laminates taken from the Twintex® Atlantic 85 RIB (Figures 2.3 and 2.4), and an additional set of purpose-made glass/PP laminates. The main structural material used in the boat hull was Twintex T PP 60 commingled fabric, containing 60 wt.% glass. The hull was coated with an epoxy-based primer (PPG Industries NEXA Autocolor P572-212), followed by an acetate-based standard marine topcoat (Awlgrip G-line). This system, necessary due to the non-polar nature of PP resin (see Chapter 1), was chosen due to its success in the automotive industry.

The internal structure of the boat was a sandwich construction of the Twintex fabric and a DIAB Pro-balsa Standard core material. The hull core and skins often feature varying thicknesses which are designed to meet its structural requirements, but which also makes it difficult to compute material fractions towards characterisation. For this reason, a number of sandwich laminates were manufactured using exactly the same materials as the hull. Also, a set of plain Twintex laminates were manufactured for benchmarking and to investigate the influence of the balsa and the paint on the properties of recycled PP-glass. The study of this influence was the main interest and challenge of this research work, hence the possibility of separating these materials from the PP-impregnated glass fibres was initially disregarded.

It was desirable to decrease the fibre fraction to facilitate processing into injection moulding material, as manufacturers would not normally employ material containing more than about 40wt.% glass [133]. Also, a high melt flow index PP homopolymer would normally be chosen for impregnated wood and glass fibre products. In the present case, the material used was Sasol HTV145, which had a melt flow rate (MFR) value of 45g/10min, similar to that of the PP present in Twintex®. It should be noted that, although virgin PP was used here, appropriate PP recyclate is available.



**Figure 8.1: Materials in the thermoplastic RIB, Twintex® Atlantic 85 – figure in g/cm<sup>3</sup> indicates core density**

Finally, the adhesion of the PP matrix to wood and glass fibres, thus the final mechanical properties, are known to improve with the addition of a coupling agent to the thermoplastic melt [134]. Therefore, 2wt.% of Polybond 3200 maleic anhydride modified PP was added to the recycle.

The complete set of materials to be recycled comprised three different material batches containing different fractions of balsa, glass and PP. These were intended for comparison with each other and with two additional batches with painted PP-glass and PP-glass only, all of them referred as Batches 1-5 on the following for convenience (Table 8.1).

## **Recycling route and equipment**

Panels were removed from the boat with a pneumatic saw and subsequently cut into approximately 15 mm squares, which were fed to a Homa moulding Granulator Type 01, 4.1 kW (Figures 8.4 and 8.5). The resulting granulate was dry blended with the virgin PP pellets and the coupling agent and fed into a single screw extruder (Figure 8.2) for compounding. The temperatures of the extruder were set at (from feed to die): 200°C, 225°C, 250°C, 235°C and 220°C. The resulting solidified extrudate was again passed through a granulator, to produce injection-mouldable granules. These were processed into tensile bars, using a Sandretto HP 40 (40 ton) injection moulding machine at the facilities of the research

collaborator, E.U.I.T. Industriales, Madrid (Figure 8.3). The injection conditions were optimised for the resin, resulting in: injection pressure: 300 bar; barrel temperatures: 220°C, 230°C, 240°C and mould temperature: 65°C. The resulting dog-bone samples complied with ISO 527-1:1993 and ISO 180:2001 to enable comparison with the results of other experiments.



Figure 8.2: Single screw extruder



Figure 8.3: Injection moulding machine at E.U.I.T. Industriales (Polytechnic University of Madrid)

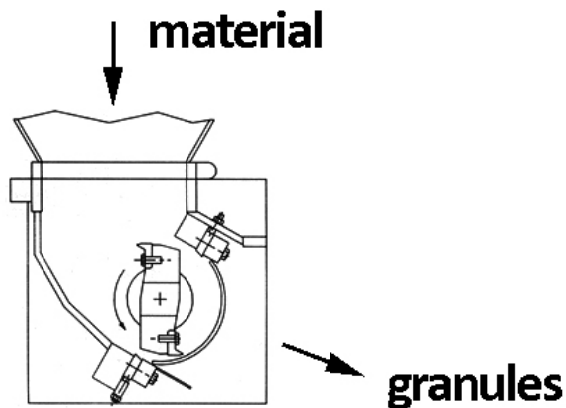


Figure 8.4: Working principle of a granulator

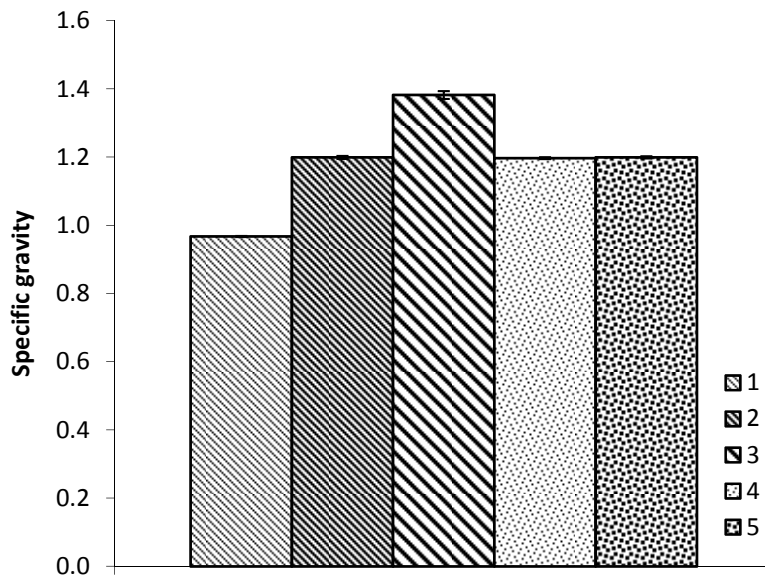


Figure 8.5: Granulator used with the recyclates

Five batches of tensile test samples were produced, which overall compositions and measured specific gravity (S.G.) after moulding are shown in Table 8.1. A chart with the S.G. values of all batches according to ISO 1183 is shown in Figure 8.6.

**Table 8.1: Recycled material batches, compositions and specific gravities**

Batch	Composition, % in weight	S.G.
1	87.6% PP, 9.4% glass, 3.0% balsa wood	0.967
2	53.0% PP, 35.5% glass, 11.4% balsa wood	1.199
3	33.2% PP, 50.5% glass, 16.3% balsa wood	1.382
4	60.3% PP, 39.7% glass	1.197
5	As 4, with 0.7% paint added	1.199



**Figure 8.6: Measured specific gravity of the recycled materials**

Batches 1-3 were all based on the granulated hull sandwich laminate, presenting different degrees of dilution in PP resin, including no dilution at all (Batch 3) to assess the manufacturability of such high fibre content material. The main processing difficulty occurred due to the presence of the fluffy lightweight balsa component, which resulted in some feeding problems leading to manual feed both into the extruder and the injection

moulding machine. This could probably have been overcome by using a twin-screw extruder with a specialised auger feed. There were also some initial wet-out problems with the balsa, which again could probably have been overcome by using more specialised compounding equipment. Batch 3, with the highest balsa and fibre content, was the most difficult to process. Despite the mentioned compounding difficulties, Batches 1-3 were processed resulting in granules that were injection moulded with relative ease.

Batch 4, which contained neither balsa nor paint, was granulated from pure laminated Twintex material (60wt.% glass). Again, the fibre content was reduced by adding virgin PP at the compounding stage, to achieve a final fibre content of 40wt.% in the moulding material. Batch 5 contained painted hull material, with a final paint content of 0.7wt.%. Both these batches processed well. The described recycling route can be seen in Figures 8.7 to 8.14.



**Figure 8.7: Hull opening on the Twintex® Atlantic 85 after material samples were cut out**



**Figure 8.8: Bow section of the boat cut (sandwich internal structure in white over black hull)**

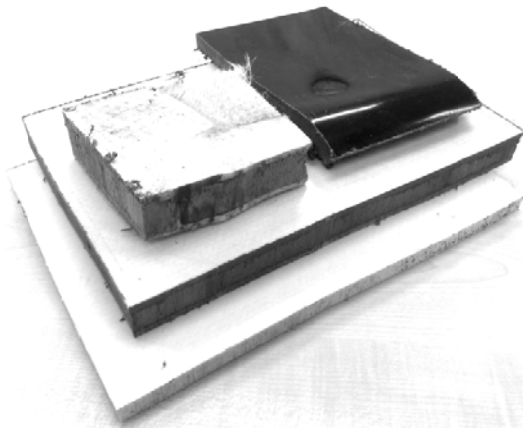


Figure 8.9: Complete set of material laminates ready for downsizing



Figure 8.10: First downsizing of material pieces prior to grinding



Figure 8.11: Ground laminate, Batch 4



Figure 8.12: Compounding of the recyclate



Figure 8.13: Resulting granules, Batch 3



Figure 8.14: Tensile bars made with the recycled materials

## Results and discussion

The specific gravities of Batches 1-3 measured after moulding were compared with calculated values, as shown in Table 8.2.

Calculations were carried out considering that, for a material containing several constituents a, b, c..., the S.G. is a function of the density of the composite, which can be expressed in terms of the volume fractions and densities of its constituents:

$$\text{S. G.} = \frac{\rho_{\text{composite}}}{\rho_{\text{water}}};$$

$$\rho_{\text{composite}} = \frac{M_a + M_b + M_c + \dots}{V} = \frac{v_a \cdot \rho_a + v_b \cdot \rho_b + v_c \cdot \rho_c + \dots}{V} = \sum V_{f_i} \cdot \rho_i \quad (8.1)$$

Where  $\rho_a$  and  $M_a$  are the density and the mass of the constituent  $a$  respectively,  $v_a$  is its volume,  $V$  is the total volume of the material, and  $V_{f_i}$  is the volume fraction of the constituent  $i$ . Also, there is a relationship between the volume and weight fractions:

$$W_{f_i} = \frac{W_i}{W} = \frac{M_i}{M} = \frac{v_i \cdot \rho_i}{V \cdot \rho} = V_{f_i} \frac{\rho_i}{\rho} \quad (8.2)$$

In the formula (8.2),  $W_{f_i}$  is the weight fraction of the constituent  $i$ ,  $W_i$  and  $M_i$  its weight and mass,  $\rho$  the density of the composite and  $W$  and  $M$  the total weight and mass of the composite, respectively. With respect to the calculations,  $\rho_{\text{water}}$  was considered to be equal to  $10^3 \text{ kg/m}^3$ . With the simple relationships (8.1) and (8.2), the final S.G. value can be calculated from the individual densities and the volume fractions of the constituents. Firstly, the balsa wood was considered to maintain its original properties during processing, hence a density of  $155 \text{ kg/m}^3$  was used, as given by the supplier. As seen in Table 8.2, the measured S.G. values are all significantly higher than those calculated this way.



Batch	S.G. (No air removed)	S.G. (Measured)	S.G. (All air removed)	Apparent S.G. (processed balsa)	Removed air
1	0.834	<b>0.967</b>	0.977	0.990	93%
2	0.684	<b>1.199</b>	1.249	1.045	90%
3	0.620	<b>1.382</b>	1.485	1.025	85%

Table 8.2: Calculated and measured specific gravity of Batches 1-3

### *Removed air*

The most probable reason for this discrepancy in S.G.'s is that the compounding and injection moulding processes removed a significant proportion of the air initially present in the wood (Figure 8.15).

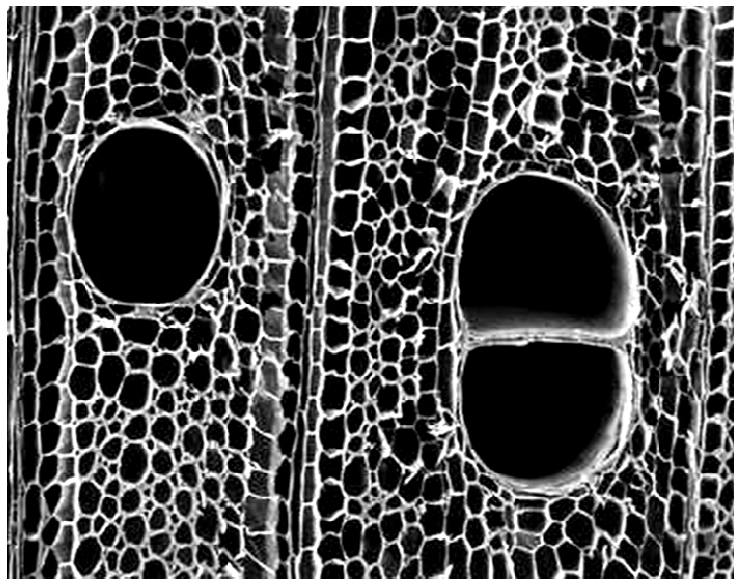


Figure 8.15: Porous structure of balsa wood, from [136]

To test this hypothesis, the S.G.'s were re-calculated, replacing the density of the balsa with a higher value of  $1,500 \text{ kg/m}^3$ , corresponding to the average density of wood fibre [135]. This second estimate would correspond to the situation where all of the air in the balsa was removed during processing. These values can be seen to agree much more closely with the measured S.G. values. A value for the apparent S.G. of the balsa wood for all three batches was calculated, by adjusting the density of the balsa in expressions (8.1) and (8.2) to match

the measured S.G. of the compounds. Finally, the resulting volume fractions were compared, showing that approximately 90% of the air enclosed in the structure of balsa wood was eliminated in the compounding and moulding processes. These calculations show a decreasing trend in the air removed from the balsa as the wood content increases. This may be due to some wood saturation that leads to some wood cells to resist to some extent the processing pressures and keep some air inside.

Some of the remaining 10% porosity in the injected balsa can be observed in the Scanning Electron Microscopy (SEM) images in Figures 8.26 to 8.29.

### Strength

A range of mechanical properties were measured for all the batches of recycled material and compared to values expected for virgin materials of similar glass content found in the literature [137, 138]. Batches 4 and 5, based on pure Twintex diluted with PP, show the highest tensile strength values, albeit with a small reduction in the case of the paint-contaminated batch (Figure 8.16).

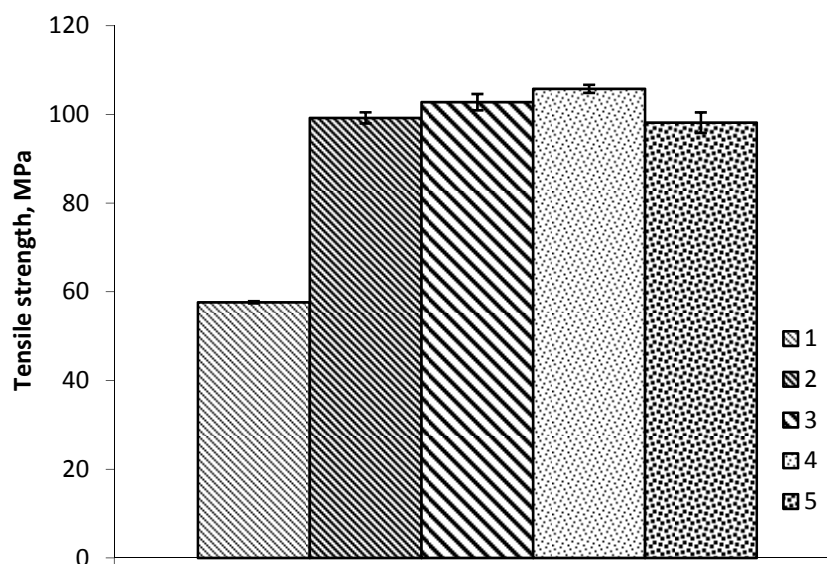
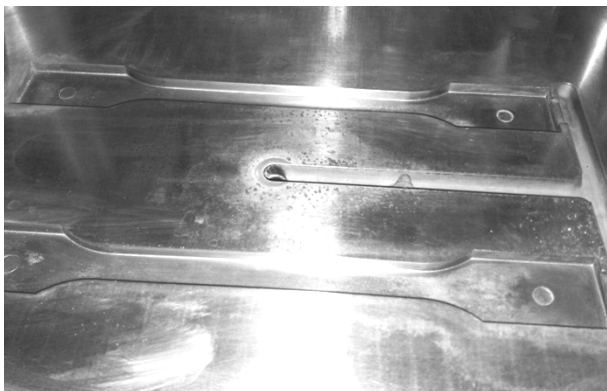


Figure 8.16: Tensile strength of recycled injection mouldings – material batch numbers correspond to those in Table 8.1

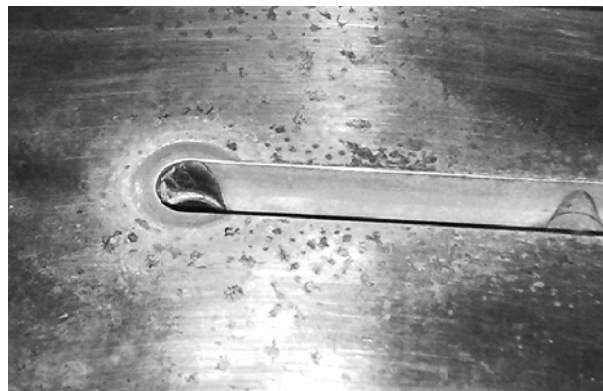
Both these batches show properties comparable with those expected of conventional virgin PP compounds of similar glass content. The reduction in the case of the paint contamination

may be due to sharp edged, low strength paint particles (SEM, Figures 8.28 and 8.29) which may not be well-bonded to the polypropylene. Hence, paint particles are acting as stress raisers in the material. It was observed that paint particles were present in all the examined fracture surfaces corresponding to Batch 5.

The batches containing the balsa show reduced, though still acceptable, strength. Although the glass content of Batch 4 (~40wt.% glass) was lower than that of Batch 3 (~50wt.% glass, ~16% wood) its strength was greater, underlining the negative effect of balsa. This could be due to the degradation of some of the balsa components. As reported by Jakab et al., wood decomposition commences at around 200°C, with decomposition of lignin and hemicellulose, accompanied by the release of water and formaldehyde [139]. Thus, partly degraded wood particles could act as stress raisers, initiating failure. All the examined samples containing wood showed wood particles on fracture surface (SEM, Figures 8.26 and 8.27). In addition, the chemical processes involved in wood degradation may lead to the presence of organic acids which may corrode the metallic mould. During these experiments, an increase in local corrosion was in fact observed (Figures 8.17 and 8.18).



**Figure 8.17: Injection mould used during the experiments**



**Figure 8.18: Detail of Figure 8.17 – corrosion spots on injection mould near the material inlet**

The tensile strengths were compared with values for virgin standard PP-glass materials [137, 138]. Figure 8.19 shows that the strength values of the recycled samples are lower than those of 'long fibre' (LF in the chart) moulding materials.

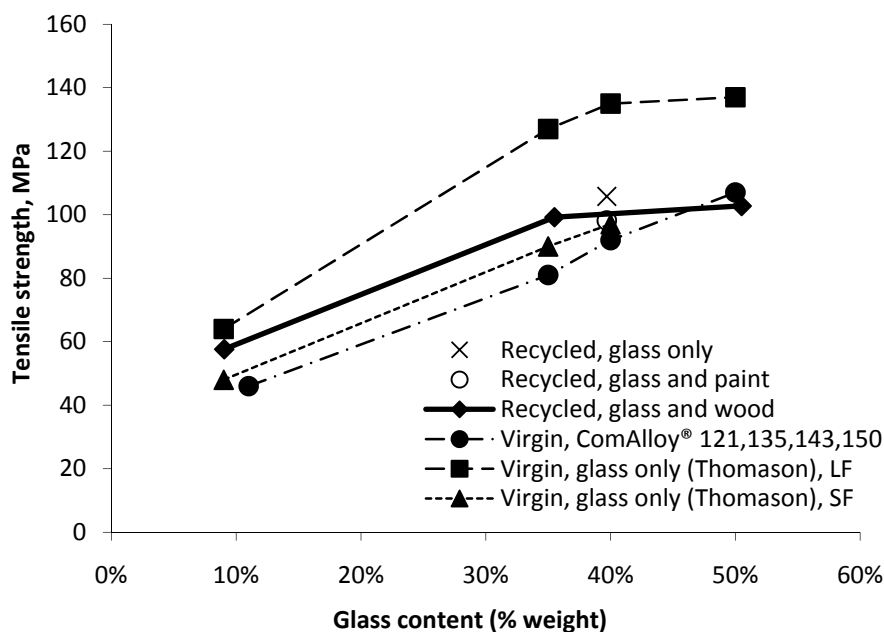


Figure 8.19: Tensile strength values for recycled laminates compared to virgin materials (Thomason from [137], ComAlloy® from [138])

This is not surprising, since the latter materials, which are manufactured by a different method, have a fibre length of the order of 1mm, which is significantly larger than in the present case. However, the strengths of the recycled materials can be seen to be comparable with those of the more widely used ‘short fibre’ (SF in the chart) materials, which are also produced by extrusion compounding, and which typically have an average fibre length of around 200 microns. These results place the properties of these mixed recycled materials well within the range that would be acceptable in the marketplace for short fibre moulding compounds.

### ***Elongation-to-break***

The values of elongation-to-break in Figure 8.20 show the expected decrease with increasing fibre content. The elongation-to-break of Batch 2 (~35wt.% glass, ~11wt.% wood) samples was lower than that of Batch 4 (~40wt.% glass), showing that the presence of balsa decreases the elongation-to-break, hence the toughness of the material. Nevertheless these values are still in the region of commercial acceptability, as can be seen from Figure 8.21.

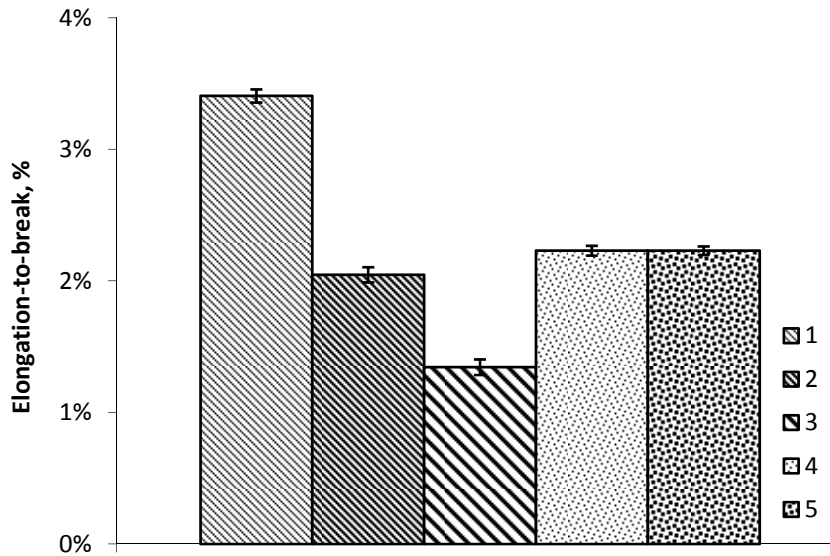


Figure 8.20: Elongation-to-break of the recycled materials

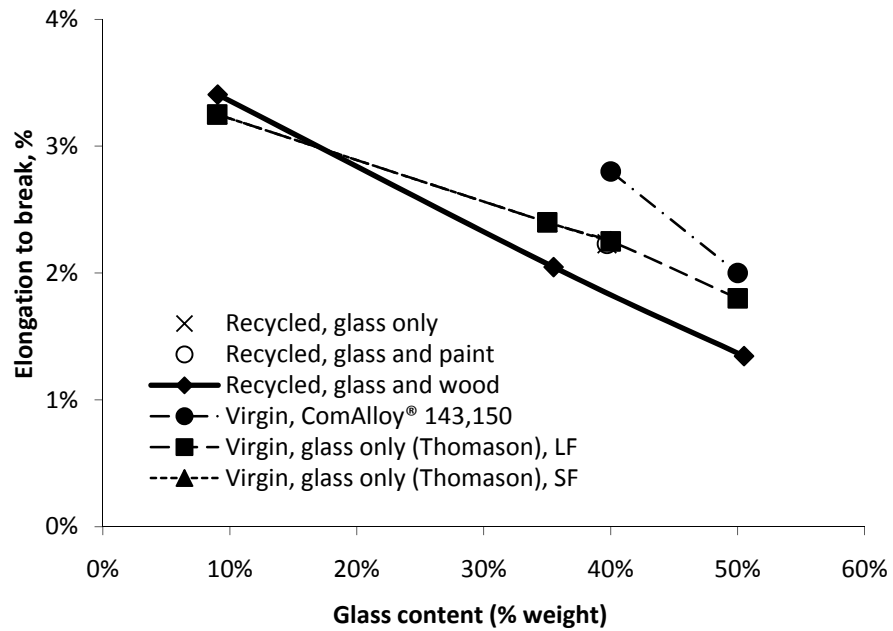


Figure 8.21: Elongation-to-break of the recycled materials compared to virgin materials

### Stiffness

Figures 8.22 and 8.23 show that, for all compounds, the Young's modulus increases with glass content. Comparing the results for Batch 2 (~35wt.% glass, ~11wt.% wood) to those for Batch 4 (~40wt.% glass) it can be inferred that wood particles do have a positive influence on modulus.

This effect seems to compensate certain loss in modulus seen in the recycled pure PP-glass and the painted batch, possibly due to the accumulated processing history of the material. By contrast, paint particles seem to have a negative effect, probably because of their own low modulus. Despite these negative influences, the moduli of the recycled batches are still remarkably similar to those of virgin injection mouldings.

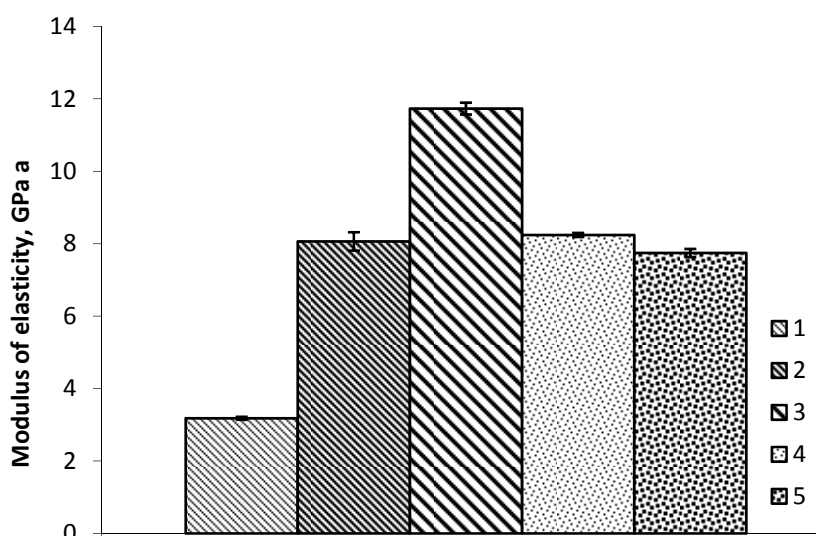


Figure 8.22: Modulus of elasticity of the recycled injection mouldings

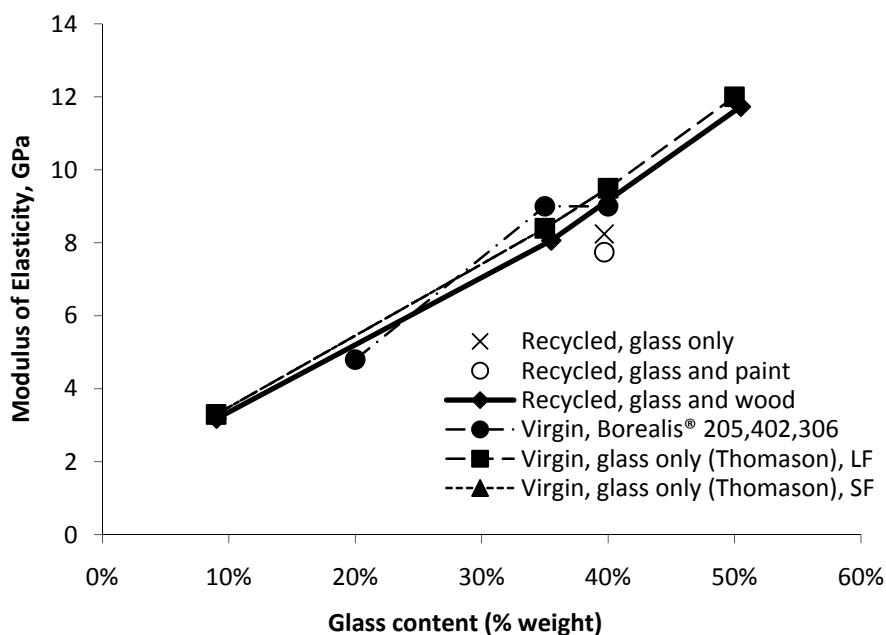


Figure 8.23: Modulus of elasticity versus glass content for recycled and virgin materials (Thomason from [137], Borealis® materials from [138])

### Impact

The low impact strength of Batch 3 samples shows that a wood content of more than 30% has a remarkable detrimental effect on impact properties, changing a slight increase into a decreasing trend, as seen in Figure 8.25. However, a small beneficial effect of the balsa wood can be observed, as ~35wt.% glass plus ~11wt.% wood (Batch 2) give higher impact strength than ~40wt.% glass (Batch 4). In contrast, commercial PP-glass shows a still increasing trend beyond 30%, as shown in Figure 8.25. Additionally, the effect of paint on impact strength is negligible (Figure 8.24).

Once more, the impact strengths of the recycled batches are in general comparable and even higher than the typical values for commercial virgin short glass fibre reinforced PP pellets for injection moulding.

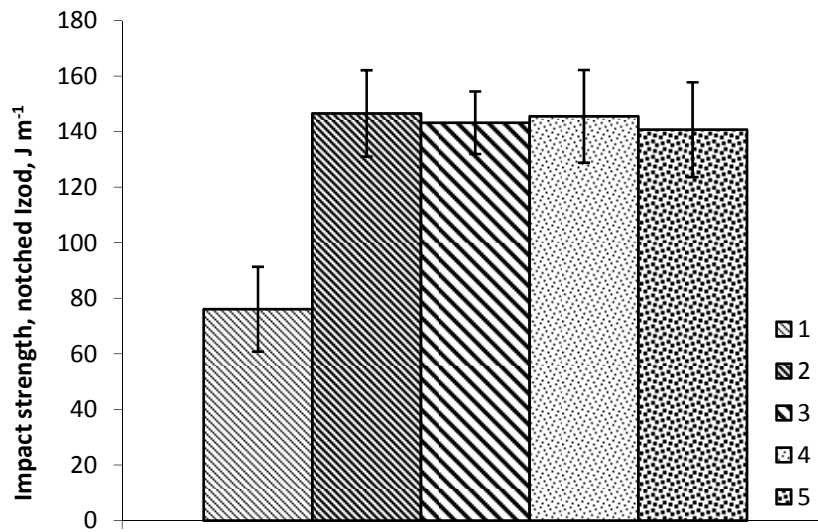


Figure 8.24: Impact strength of the recycled materials

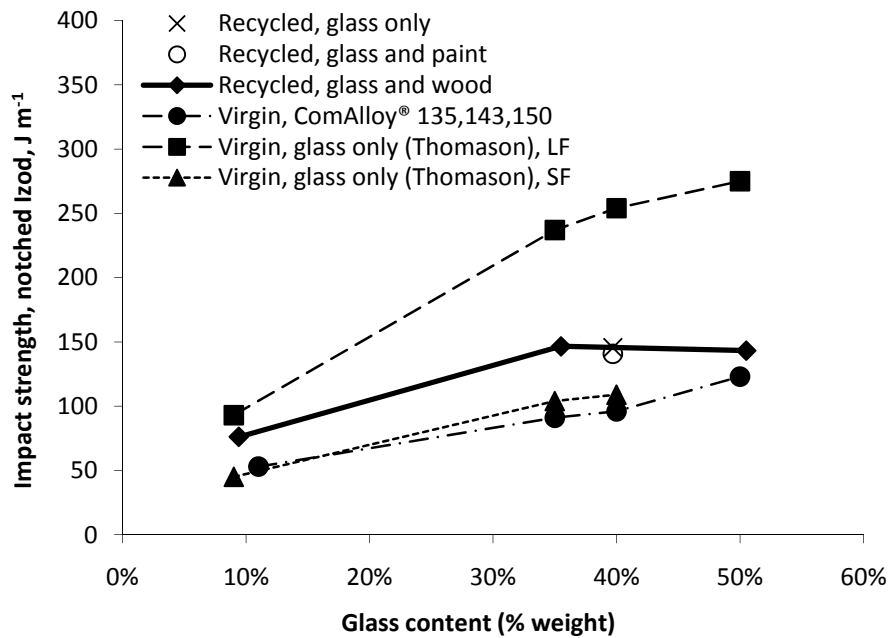


Figure 8.25: Impact strength for recycled and virgin materials



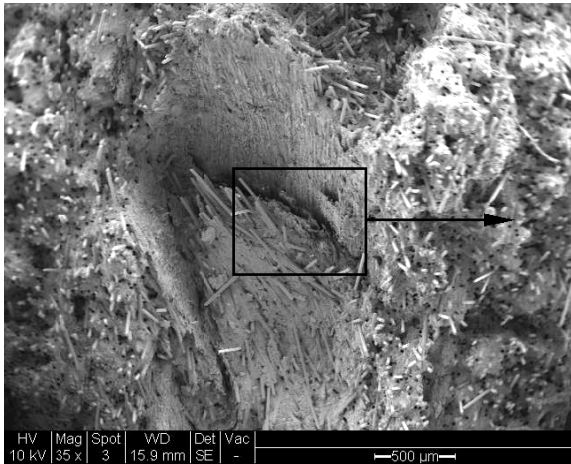


Figure 8.26: SEM image of the fracture surface of a Batch 3 sample, showing a wood chip

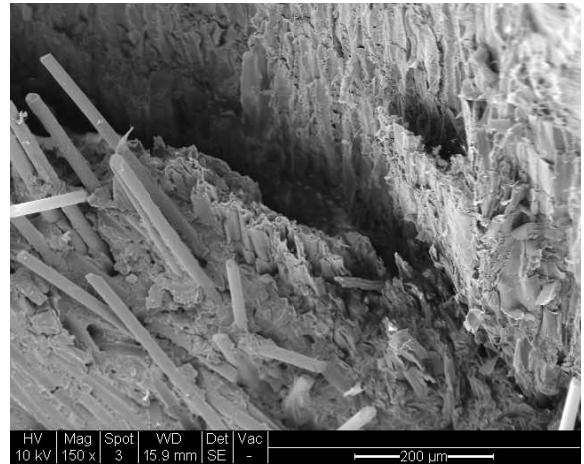


Figure 8.27: Wood chip detail from Figure 8.26

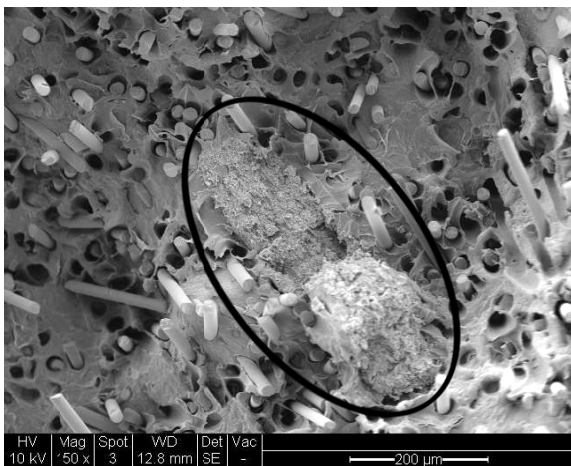


Figure 8.28: Paint particle on fracture surface, Batch 5

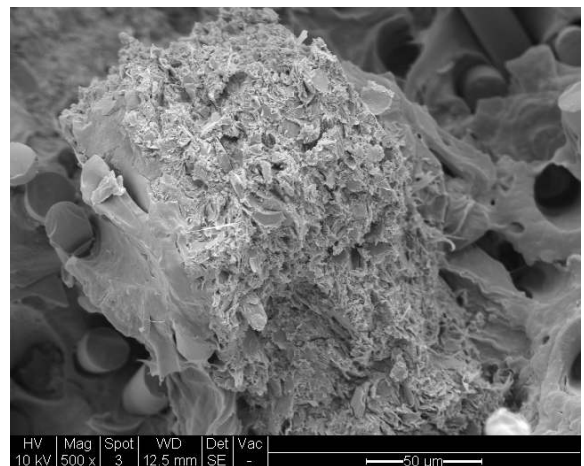


Figure 8.29: Small detail of the paint particle shown in Figure 8.28

## Conclusions

The present research results demonstrate the technical feasibility of the recycling of end-of-life thermoplastic-based composites. In particular it has been shown that the hull of a rigid inflatable boat, composed of PP-glass laminate along with balsa core material and paint, can be recycled by melt processing into injection mouldable granules which have acceptable properties when processed.

Comparison between measurements and calculations show that approximately 90% of the air is evacuated from the balsa wood during the compounding and injection moulding processes. The remaining porosity and low properties of the resulting material lead to a deleterious effect of balsa on moulded strength, elongation-to-break and impact strength above 30wt.%. However, it does have a small positive effect on modulus and impact strength up to approximately 30wt.% wood content. Recycled painted PP-glass laminates showed slightly lower strength and modulus, whereas elongation-to-break and impact properties remained virtually unaffected.

The magnitude of the mentioned beneficial and deleterious effects of the paint and the balsa lead to mechanical properties that are well-within the region of commercial interest for reinforced polypropylene moulding materials. In an industrial large-scale context, these materials could be used in non-appearance automotive applications, where talc and short glass reinforced PP are currently used, or in decking and wood imitation applications where wood-reinforced composites are currently being considered. Lately, recycled looks are welcome in traditionally banned sectors [140], which may lead to economically profitable small scale applications of such recycled materials.

## **Chapter 9 – Concluding remarks**

In the previous chapters, a number of interesting results on TPCs applied to boatbuilding have been presented and discussed. Namely, a new approach to the non-isothermal consolidation of thick laminates; the possibility of a ceramic composite mould capable of processing virtually any thermoplastic composite; a successful bonding technique for T-joints; a novel feasible emergency repair for TPC boats and interesting results on the effect of paint and balsa wood core material on the secondary recycling of a real TPC boat. Research work usually sheds light on unknown aspects of the studied subjects, in this case on TPC boatbuilding, but also raises new questions and possible future work. In this chapter, all of these are summarised and put into the context of boat construction.

### **Consolidation modelling**

The non-isothermal consolidation model reported in Chapter 4 shows that a Darcian approach can be valid for the vacuum consolidation of thick laminates, so long as it is implemented locally and finally integrated into a global consolidation rate. The model achieves a very good agreement with experimental data, using appropriate constants and sub-models found in the literature, and relying on only 4 fitting constants, 2 of which have full physical meaning.

As assumed by the model, axial resin flow may occur only after full consolidation. However, the application of the interpolated temperature profile leads to a cascading consolidation of layers, from the hot bottom side towards the top layer, much cooler. This may lead to axial flow on the layers which consolidated first, while other layers above may still be below the

resin melting point. Hence, a study focussing on such axial flow would significantly contribute to the understanding and the application of this and other models.

Also, to assess the applicability of the developed model, it would be worth trying to use it with consolidation results obtained from other fibres and resins. An analysis of the behaviour of the constants used to fit other composites would provide knowledge on the robustness and validity of the model. Especially, an assessment on the values of the kozeny constant,  $k_0$  and the initiation of the permeability decay,  $b$ , would be of particular interest.

In addition, a detailed study on the relative importance of the reduction in permeability and resin pressure during bundle impregnation would also be interesting. Such a study could be done examining partially consolidated thick laminates by optical micrography. Measurements on the bundle geometry for fully consolidated to non-consolidated regions would give an idea on to what extent and how quickly the bundle permeability decreases.

The model could potentially be implemented to predict the consolidation of a manufactured part. As a first approach towards this task, it would be of interest to assess the behaviour of the 1-D version of the model on a discretised 2-D moulded component.

## **Tooling**

From the materials review discussed in Chapter 5, it emerges that simple geometries can be moulded on a welded steel tool, whereas complex geometries need cast aluminium or high Tg epoxy moulds. However, the latter would work at their limits even with the lowest processing temperature TPC. The properties of ceramic composites make them a promising alternative, currently under development in academia and industry. The experiments reported in that chapter show that glass-reinforced ceramic composites can be a cost-effective mould material for boats and other structures, capable of processing temperatures of up to 400°C. However, their inherent porosity is still an issue. The high temperature coatings applied to the back and moulding surfaces to seal this porosity did not provide the necessary durability and reliability in the first case, and failed to secure air-tightness in the second. It is believed that a combination between surface penetration due to low viscosity,

and the possible water release during their curation could have been the reason for the unexpected remaining porosity of the coatings applied to the moulding surface.

In view of the limited durability of the naked material, it would be interesting to develop further work on the coating of the moulding surface with a suitable high temperature-resistant coating. Firstly, a study on the reason for the observed remaining porosity after moulding surface coating would be valuable, to ascertain the relative importance of the viscosity of the coating over the remaining water in the ceramic matrix, and perhaps other mechanisms. This could be addressed by trialling coatings with different viscosities, below and above 0.1 Pa·s, accompanied by a micrography study on the penetration in the surface pores. Also, an analysis on water content in Vubonite after a thorough post-curing process and also after ageing in humid air could be useful to assess the water intake after post-curation.

A highly tough coating would be advantageous, because it would probably help to maintain the integrity of the moulding surface, despite of the apparently inevitable micro-cracking which is typical of ceramic materials and particularly Vubonite. Successful PTFE coatings have been used to date on metallic and other moulds. However, this fluoroplastic stops being useful at around 260°C [141], therefore limiting the range of processable thermoplastic resins to those which melting point is well below that temperature. Therefore, depending on the desired application, other resins and coatings for the moulding surface may be worth investigating.

## **Joining**

The experiments on lap and T-joints described in Chapter 6 show that bulk-heating fusion bonding can be used to attain strong bonds in a PP-glass boat-like structural assembly. The next logical step is to actually build a boat section with this technique. Such task would require the development of tailored-to-shape and size heaters, or a careful overlapping of standard heaters. Because the hull skin would need the thermal protection of core material, it would also require the design of the sandwich configuration of that boat section. Micrography of the joints and appropriate mechanical testing of the section would help to assess the joining technique.

An undeniable influence of the melt viscosity and the crystallinity degree was observed in lap joints. However, the relative importance of one over the other is still unclear. An experiment that could be helpful in this respect could involve several manufacturing cycles at different maximum temperatures, with more thermocouples towards a better temperature resolution. Suggested maximum temperatures may be 200°C, 220°C and 240°C, although the temperature resistance of consumables and heaters must be checked. Recorded temperatures during heating and cooling would enable to apply known crystallisation kinetics models, enabling an assessment of the influence of the crystallinity degree in the strength of the lap joint.

As mentioned in Chapter 6, the number of joints, coupons and samples manufactured and tested were considered to provide sufficient reliability to the results obtained. However, the high scatter observed in the pull-out test results for non-woven T-joints and their inherent complexity would be best addressed with a number of additional samples, typically twice as many.

Additionally, a finite element simulation of the joints would enable the detailed design of actual structures using this joining technique.

## **Repair**

A successful emergency repair method was reported in Chapter 7, which attained structural integrity and water tightness by means of local fusion bonding of the edges of a flat panel to the hull scarf edges delimiting the removed damaged material. This repair could still be improved, particularly towards a cosmetic look. This could be attained for instance by sanding down the protruding material and coating the repair with the primer-topcoat system originally applied to the rest of the hull. Also, a careful study of the edge preparation and the extra layers of unprocessed material to be co-consolidated to the repair joints, could potentially deliver better mechanical properties and better appearance, requiring minimal sanding.

Another challenge in the repair of complex hulls is the repair and reconstruction of spray rails and other hull appendices. Re-consolidating the whole structure could be one way to

achieve full re-life of the boat with perfect final shape. However, with a boat like the Twintex® Atlantic 85, this would require the complete removal of the hull paint. Also, the dimensional stability of the internal structure would probably suffer from undesirable movements due to matrix reflow, compromising the re-assembling of the deck. Hence, a local repair seems to be a more feasible way to repair appendices such as spray rails. One possibility worth an experiment would be the use of a welded steel local mould with the shape of the spray rail, after the main panel has been repaired.

## **Recycling**

As described in Chapter 8, the hull material including paint and wood can be compounded with extra resin by melt extrusion and injection moulded into valuable materials which show little degradation. It was reported that the processing temperatures, if optimised for the resin, are excessively aggressive to the wood. However, lower temperatures are still possible with PP, in such way that the wood could retain more of its mechanical properties.

Such recycling route would prevent the landfilling of valuable materials that could be profitably used in other applications. Nevertheless, the actual profitability of this process largely depends on how exactly it is done, in terms of transportation of materials prior to its recycling, volume of materials available and needed for particular applications, and energy used in the process. Hence, a Life Cycle Assessment (LCA) of this recycling process would be helpful to assess its actual profitability. In particular, to find the conditions under which it would be economically viable.

As demonstrated, granulated TPCs can be remoulded into new parts. However, by shredding the boat hull, the value of continuous glass fibres is lost. Another potential way to reuse and re-manufacture is to re-form TPC panels directly, perhaps by compression moulding, without grinding into granules. This technology is still to be explored but combined with design-for-recycling could lead to a much cheaper, shorter and profitable way to replace landfilling with a more efficient use of manufactured materials.

## References

1. Greene, E., *Marine composites*. 1999, Maryland, US. Eric Greene Associates, Inc.
2. Greene, E., *Marine composites*. 1999, Maryland, US. Eric Greene Associates, Inc., p. ix.
3. Sheno, R.A. and Wellicome, J.F., *Composite materials in maritime structures*. 1993, Cambridge, UK. Cambridge University Press,
4. Greene, E., *Marine composites*. 1999, Maryland, US. Eric Greene Associates, Inc., p. 72.
5. Mouritz, A.P., Gellert, E., Burchill, P., and Challis, K., *Review of advanced composite structures for naval ships and submarines*. *Composite Structures*, 2001. Vol. 53(1), p. 21-42.
6. Lonno, A., *Frp-sandwich vessels for the swedish navy*, in *International Conference on Marine and Offshore Composites*. February, 2010. RINA Headquarters, London: Royal Institution of Naval Architects.
7. Greene, E., *Marine composites*. 1999, Maryland, US. Eric Greene Associates, Inc., p. 63.
8. Morgan, P., *Carbon fibers and their composites*. 2005, Boca Raton, US. Taylor and Francis, p. 501.
9. Campbell, F.C., *Manufacturing processes for advanced composites*. 2004, Oxford, UK. Elsevier, p. 84.
10. Daniels, C.A., *Polymers - structure and properties*. 1989, Pennsylvania, US. Technomic publishing company, p. 5.
11. Pickering, S.J., *Recycling technologies for thermoset composite materials--current status*. *Composites Part A: Applied Science and Manufacturing*, 2006. Vol. 37(8), p. 1206-1215.
12. Patnaik, P., *A comprehensive guide to the hazardous properties of chemical substances*. 2007, New Jersey, US. John Wiley and sons, p. 523.
13. Borgstedt, H.H. and Hine, C.H., *Toxicity, hazards and safe handling*, in *Epoxy resins - chemistry and technology*, C.A. May, Editor. 1988, New York, US. Marcel Dekker, p. 1173.
14. Askeland, D.R., *The science and engineering of materials*. 1984, Boston, US. Van Nostrand Reinhold International, p. 472.
15. Rymuza, Z., *Plastics*, in *Surface modification and mechanisms - friction, stress and reaction engineering*, G.E. Totten and H. Liang, Editors. 2004, New York, US. Marcel Dekker, p. 90.



16. Kilroy, J.P., *Mechanical and physical evaluation of a new high performance thermoplastic composite system for space applications*, M. Eng. Sc., Dept. of Mechanical and Biomedical Engineering. 2006, National University of Ireland: Galway.
17. Giordano, M., Borzacchiello, A., and Nicolais, L., *Pultrusion and other shaping processes*, in *Handbook of composite fabrication*, G. Akovali, Editor. 2001, Shrewsbury, UK. Rapra Technology, p. 143.
18. Béland, S., *High performance thermoplastic resins and their composites*. 1990, New Jersey, US. William Andrew Publishing/Noyes, p. 102.
19. Lauke, B., Bunzel, U., and Schneider, K., *Effect of hybrid yarn structure on the delamination behaviour of thermoplastic composites*. Composites Part A: Applied Science and Manufacturing, 1998. Vol. 29(11), p. 1397-1409.
20. Lee, W.I. and Springer, G.S., *A model of the manufacturing process of thermoplastic matrix composites*. Journal of Composite Materials, 1987. Vol. 21, p. 1017-1055.
21. Antosiewicz, F., *Firm takes rotomoulded boats to new level*, Plasticsnews.com. August 2007. [as accessed in March 2010]; <http://plasticsnews.com/headlines2.html?id=07081301702>.
22. Beall, G.L., *Rotational molding - design, materials, tooling and processing*. 1998, Cincinnati, US. Hanser/Gardner, p. 6.
23. National Research Council, *New materials for next-generation commercial transports*. 1996, Washington, US. National Academy of Sciences, p. 37.
24. Biron, M., *Thermoplastics and thermoplastic composites*. 2007, Oxford, UK. Elsevier, p. 8-9.
25. Advanced Composites Group - VTM<sup>®</sup> 260 Series Prepreg System. 2007, Heanor, UK. ACG, p. 1.
26. European Boatbuilder, *Twintex and 2win's new twincat*. March 2006. (18).
27. Owens Corning news release, *Twintex<sup>®</sup> technical fabric from owens corning chosen for innovative vacuum bag molded thermoplastic composite canoe*. 2008. [as accessed in 2010]; <http://www.ocvreinforcements.com/twintex.pdf>.
28. Gennaro, R., Greco, A., Lionetto, F., and Maffezzoli, A., *Numerical simulation of the microscale impregnation in commingled thermoplastic composite yarns*, in *ICCM 17*. 2009, Institute of Materials, Minerals and Mining: Edinburgh.
29. Bernhardsson, J. and Shishoo, R., *Effect of processing parameters on consolidation quality of gf/pp commingled yarn based composites*. Journal of Thermoplastic Composite Materials, 2000. Vol. 13(4), p. 292-313.

30. Klinkmüller, V., Um, M.K., Steffens, M., Friedrich, K., and Kim, B.S., *A new model for impregnation mechanisms in different gf/pp commingled yarns*. Applied Composite Materials, 1994. Vol. 1(5), p. 351-371.
31. Van West, B.P., Pipes, R.B., and Advani, S.G., *The consolidation of commingled thermoplastic fabrics*. Journal of Polymer Composites, 1991. Vol. 12(6), p. 417-427.
32. Ye, L., Friedrich, K., Kästel, J., and Mai, Y.W., *Consolidation of unidirectional cf/peek composites from commingled yarn prepreg*. Composites Science and Technology, 1995. Vol. 54(4), p. 349-358.
33. Cain, T.A., Wakeman, M.D., Brooks, R., Long, A.C., and Rudd, C.D., *Towards an integrated processing model for a co-mingled thermoplastic composite*, in *11th International Conference on Composite Materials*, 1997. Gold Coast, Australia, p. 366-376.
34. Bernet, N., Michaud, V., Bourban, P.E., and Manson, J.A.E., *An impregnation model for the consolidation of thermoplastic composites made from commingled yarns*. Journal of Composite Materials, 1999. Vol. 33(8), p. 751-772.
35. Long, A.C., Wilks, C.E., and Rudd, C.D., *Experimental characterisation of the consolidation of a commingled glass/polypropylene composite*. Composites Science and Technology, 2001. Vol. 61(11), p. 1591-1603.
36. Ye, L., Chen, Z., Lu, M., and Hou, M., *De-consolidation and re-consolidation in cf/pps thermoplastic matrix composites*. Composites Part A: Applied Science and Manufacturing, 2005. Vol. 36(7), p. 915-922.
37. Ijaz, M., *Vacuum consolidation of commingled thermoplastic matrix composites*, PhD Thesis, *School of Mechanical and Systems Engineering*. 2005, University of Newcastle upon Tyne: Newcastle upon Tyne, UK.
38. Ijaz, M., Robinson, M., Wright, P.N.H., and Gibson, A.G., *Vacuum consolidation of commingled thermoplastic matrix composites*. Journal of Composite Materials, 2007. Vol. 41(2), p. 243-262.
39. Gutowski, T.G., Cai, Z., Bauer, S., Boucher, D., Kingery, J., and Wineman, S., *Consolidation experiments for laminate composites*. Journal of Composite Materials, 1986. Vol. 21, p. 650-669.
40. Li, M., Gu, Y., Zhang, Z., and Sun, Z., *A simple method for the measurement of compaction and corresponding transverse permeability of composite prepregs*. Polymer Composites, 2007. Vol. 28, p. 61-70.
41. Gebart, B.R., *Permeability of unidirectional reinforcements for rtm*. Journal of Composite Materials, 1992. Vol. 26(8), p. 1100-1133.
42. Santulli, C., Gil, R.G., Long, A.C., and Clifford, M.J., *Void content measurements in thermoplastic composite materials through image analysis from optical micrographs*. Science and Engineering of Composite Materials, 2002. Vol. 10(2), p. 77-90.

43. Wysocki, M., Larsson, R., and Toll, S., *Hydrostatic consolidation of commingled fibre composites*. Composites Science and Technology, 2005. Vol. 65(10), p. 1507-1519.
44. Gibson, A.G., Ijaz, M., Dodds, N., Sharpe, A., and Knudsen, H., *Vacuum bag moulding of large thermoplastic parts in commingled glass/pet*. Plastics, Rubber and Composites, 2003. Vol. 32, p. 160-166.
45. Kamal, M.R. and Sourour, S., *Kinetics and thermal characterization of thermoset cure*. Polymer Engineering & Science, 1973. Vol. 13(1), p. 59-64.
46. Åstrom, B.T., *Manufacturing of polymer composites*. 1997, Chentelham, UK. Nelson Thornes, p. 182.
47. Strong, A.B., *High performance and engineering thermoplastic composites*. 1993, Lancaster, Pennsylvania, US. Technomic Publishing, Inc., p. 163-171.
48. Yousefpour, A., Hojjati, M., and Immarigeon, J.-P., *Fusion bonding/welding of thermoplastic composites*. Journal of Thermoplastic Composite Materials, 2004. Vol. 17(4), p. 303-341.
49. Ageorges, C., Ye, L., and Hou, M., *Advances in fusion bonding techniques for joining thermoplastic matrix composites: A review*. Composites Part A: Applied Science and Manufacturing, 2001. Vol. 32(6), p. 839-857.
50. Parlevliet, P.P., Bersee, H.E.N., and Beukers, A., *Residual stresses in thermoplastic composites - a study of the literature. Part iii: Effects of thermal residual stresses*. Composites Part A: Applied Science and Manufacturing, 2007. Vol. 38(6), p. 1581-1596.
51. Ageorges, C. and Ye, L., *Fusion bonding of polymer composites*. 2002, London. Springer-Verlag, p. 10-18.
52. Otheguy, M.E., Gibson, A.G., Findon, E., and Cripps, R.M., *Repair technology for thermoplastic composite boats, in 17th International Conference on Composite Materials*. 27-31 July, 2009. Edinburgh, UK: The British Composites Society.
53. Jouin, P., Lee, T., Vitlip, R., *Manufacture of a primary flight structure using thermoplastics, in International SAMPE Symposium, 1991: SAMPE*, p. 1014-1027.
54. Maguire, D.M., *Joining thermoplastic composites*. SAMPE Journal, 1989. Vol. 25(1), p. 11-14.
55. Todd, S.M., *Joining thermoplastic composites, in 22 International SAMPE Technical Conference*. 1990, p. 383-392.
56. Silverman, E.M. and Griese, R.A., *Joining methods for graphite/peek* SAMPE Journal, 1989. Vol. 25(5), p. 34-38.
57. Sheno, R.A. and Wellicome, J.F., *Composite materials in maritime structures - volume 2, practical considerations*. 1993, Cambridge, UK. Cambridge University Press, p. 276-278.

58. Jones, T.S., *Nondestructive evaluation methods for composites*, in *Handbook of composites*, S.T. Peters, Editor. 1982, Tonbridge, UK. Cambridge University Press, p. 851-852.
59. Mix, P.E., *Introduction to nondestructive testing*. 2005, Hoboken, US. John Wiley and sons, p. 164.
60. Royal National Lifeboat Institution - common practice, 2008. Poole, UK.
61. Greene, E., *Marine composites*. 1999, Maryland, US. Eric Greene Associates, Inc., p. 68.
62. X. Xiao , S.V.H., K.N. Street *Repair of thermoplastic resin composites by fusion bonding*, in *Composites bonding*, D.J. Damico, T.L. Wilkinson, and S.L.F. Niks, Editors. 1994, Baltimore, US. ASTM, p. 30-44.
63. BAE Systems Surface Ships - common practice, 2008. Portsmouth, UK.
64. Vinson, J.R. and Sierakowski, R.L., *The behaviour of structures composed of composite materials*. 2008, Dordrecht, Netherlands. Kluwer academic, p. 28.
65. Gramann, H. and Krapp, R.V.B., *Disposal and recycling of hsc materials*, in *6th International Conference on High-Performance Marine Vehicles*. 2008, University of Naples: Naples, Italy, p. 271 - 280
66. Conroy, A., Halliwell, S., and Reynolds, T., *Composite recycling in the construction industry*. Composites Part A: Applied Science and Manufacturing, 2006. Vol. 37(8), p. 1216-1222.
67. Hawken, P., Lovins, A.B., and Lovins, L.H., *Natural capitalism, the next industrial revolution*. 2004, London. Earthscan, p. 9-11.
68. McDonough, W. and Braungart, M., *Cradle to cradle*. 2002, New York, US. North Point, p. 92-117.
69. Mazumdar, S.K., *Composites manufacturing - materials, product and process engineering*. 2002, Boca Raton, US. CRC Press LLC, p. 377.
70. Allred, R.E. and Busselle, L.D., *Tertiary recycling of automotive plastics and composites*. Journal of Thermoplastic Composite Materials, 2000. Vol. 13(2), p. 92-101.
71. Giulvezan, G. and Carberry, B., *Composite recycling and disposal an environmental r&d issue*. Boeing Environmental Technotes, 2003. Vol. 8(4).
72. Poulakis, J.G. and Papaspyrides, C.D., *Recycling of polypropylene by the dissolution/reprecipitation technique: I. A model study*. Resources, Conservation and Recycling, 1997. Vol. 20(1), p. 31-41.

73. Siriwardena, S., Ismail, H., and Ishiaku, U.S., *Mechanical properties and recyclability of thermoplastic elastomer composites of white rice husk ash-ethylene/propylene/diene terpolymer-polypropylene*, in *International Conference on Materials for Advanced Technologies (ICMAT2001)*. Jul 01-06, 2001. Singapore, Singapore: Maney Publishing, p. 167-176.
74. Bernasconi, A., Rossin, D., and Armani, C., *Analysis of the effect of mechanical recycling upon tensile strength of a short glass fibre reinforced polyamide 6,6*. *Engineering Fracture Mechanics*, 2007. Vol. 74(4), p. 627-641.
75. Cui, Y., Lee, S., Noruziaan, B., Cheung, M., and Tao, J., *Fabrication and interfacial modification of wood/recycled plastic composite materials*. *Composites Part A: Applied Science and Manufacturing*, 2008. Vol. 39(4), p. 655-661.
76. Papanicolaou, G.C., Karagiannis, D., Bofilios, D.A., van Lochem, J.H., Henriksen, C., and Lund, H.H., *Impact strength of recycled thermoplastic composites subjected to corrosive environment*. *Polymer Composites*, 2008. Vol. 29(9), p. 1026-1035.
77. Bourmaud, A. and Baley, C., *Investigations on the recycling of hemp and sisal fibre reinforced polypropylene composites*. *Polymer Degradation and Stability*, 2007. Vol. 92(6), p. 1034-1045.
78. Adhikary, K.B., Pang, S., and Staiger, M.P., *Long-term moisture absorption and thickness swelling behaviour of recycled thermoplastics reinforced with pinus radiata sawdust*. *Chemical Engineering Journal*, 2008. Vol. 142(2), p. 190-198.
79. Ávila, A.F. and Duarte, M.V., *A mechanical analysis on recycled pet/hdpe composites*. *Polymer Degradation and Stability*, 2003. Vol. 80(2), p. 373-382.
80. Zia, K.M., Bhatti, H.N., and Ahmad Bhatti, I., *Methods for polyurethane and polyurethane composites, recycling and recovery: A review*. *Reactive and Functional Polymers*, 2007. Vol. 67(8), p. 675-692.
81. Kemmochi, K., Takayanagi, H., Nagasawa, C., Takahashi, J., and Hayashi, R., *Possibility of closed loop material recycling for fiber reinforced thermoplastic composites*. *Advanced Performance Materials*, 1995. Vol. 2(4), p. 385-394.
82. Lei, Y., Wu, Q., Yao, F., and Xu, Y., *Preparation and properties of recycled hdpe/natural fiber composites*. *Composites Part A: Applied Science and Manufacturing*, 2007. Vol. 38(7), p. 1664-1674.
83. BAE Systems Surface Ships - experience in thermoplastic composite boatbuilding, 2004. Portsmouth, UK.
84. Ehrenstein, G.W., *Polymeric materials - structure, properties, applications*. 2000, Cincinatti, Ohio, US. Hanser,
85. Liu, A.W., Bornside, D.E., Armstrong, R.C., and Brown, R.A., *Viscoelastic flow of polymer solutions around a periodic, linear array of cylinders: Comparisons of*

- predictions for microstructure and flow fields*. Journal of Non-Newtonian Fluid Mechanics, 1998. Vol. 77, p. 153-190.
86. Tripathi, A. and Chhabra, R.P., *Slow power law fluid flow relative to an array of infinite cylinders*. Industrial & Engineering Chemistry Research, 1992. Vol. 31, p. 2754-2759.
  87. Strong, A.B., *High performance and engineering thermoplastic composites*. 1993, Lancaster, Pennsylvania, US. Technomic Publishing, Inc., p. 154-155.
  88. Vasiliev, V.V., *Composite pressure vessels*, R.M. Jones, Editor. 2009, Blacksburg, US. Bull Ridge, p. 599.
  89. Fink, J.K. *Reactive polymers fundamentals and applications*, ed. S. Ebnesajjad. 2005, Norwich, US. William Andrew,
  90. Vaidya, U.K. and Chawla, K.K., *Processing of fibre reinforced thermoplastic composites*. International Materials Reviews, 2008. Vol. 53, p. 185-218.
  91. *Sr7900 product data sheet, sicomin*. 2002.
  92. *Toolfusion 2a/2b product data sheet, airtech international*. 2005.
  93. *Hx42 product data sheet, amber composites*. 2007.
  94. *El42 product data sheet, amber composites*. 2007.
  95. *Epolam 2090 product data sheet, axson technologies*. 2007.
  96. *Blendur tp-ku 3-4520/23, bayer material science*. 2006.
  97. Automation Creations, I., 1996-2010, *matweb: Material property data*, <http://www.matweb.com> (as accessed on January 2010).
  98. *Vubonite product data sheet*. [www.vubonite.com](http://www.vubonite.com) (as accessed in 2008), Symbion NV.
  99. Zweben, C., *Handbook of materials selection*, M. Kutz, Editor. 2002, New York. John Wiley & Sons, p. 393.
  100. F.L. Matthews, R.D.R., *Composite materials: Engineering and science*. 1999, Cambridge, UK. Woodhead Publishing Ltd., p. 92.
  101. Cuyppers, H. and Wastiels, J., *Thin and strong concrete composites with glass textile reinforcement: Modeling the tensile response*. American Concrete Institute - Special Publication Textile-Reinforced Concrete, 2008. Vol. SP-250, p. 131 - 148.
  102. Wastiels, J., Dannau, M., and Vanherck, J., *An absolute fire resistant matrix for composites: Vubonite*, in *Fifth International Conference on Composites in Fire*. 2008, CompositeLink Consultants Ltd: Newcastle, UK.

103. Blom, J., Itterbeeck, P.V., Ackeren, J.V., and Wastiels, J., *Inorganic phosphate textile reinforced cement composite moulds*, in *17th International Conference on Composite Materials*. 2009, Institute of Minerals, Mining and Materials: Edinburgh, UK.
104. Gao, F., Jiao, G., and Lu, Z., *Mode II delamination and damage resistance of carbon/epoxy composite laminates interleaved with thermoplastic particles*. *Journal of Composite Materials*, 2007. Vol. 41(1), p. 111-123.
105. Singh, S. and Partridge, I.K., *Mixed-mode fracture in an interleaved carbon-fibre/epoxy composite*. *Composites Science and Technology*, 1995. Vol. 55(4), p. 319-327.
106. BAE Systems Surface Ships - common practice, 2009. Portsmouth, UK.
107. W.I.Lee and G.S.Springer, *A model of the manufacturing process of thermoplastic matrix composites*. *Journal of Composite Materials*, 1987. Vol. 21, p. 1017-1055.
108. Caswell, P.A., *Influence of surface preparation on thermoplastic adhesive joints*. School of Engineering Sciences - BEng Individual Research Project IP177, 2007.
109. Kwak M., C.T., Kapadia A., *Welding techniques for reinforced thermoplastic composites*, in *Joining Plastics Conference*, 2008. Great Abington, Cambridgeshire, UK.: The Welding Institute, Welding & Joining Society, German Welding Society.
110. Závadský, E., Karniš, J., and Pechoč, V., *The time, temperature and shear dependence of the viscosity of polypropylene and its influence upon the extrusion process*. *Rheologica Acta*, 1982. Vol. 21(4), p. 470-474.
111. Ageorges, C. and Ye, L., *Resistance welding of thermosetting composite/thermoplastic composite joints*. *Composites Part A: Applied Science and Manufacturing*, 2001. Vol. 32(11), p. 1603-1612.
112. Stavrov, D. and Bersee, H.E.N., *Resistance welding of thermoplastic composites-an overview*. *Composites Part A: Applied Science and Manufacturing*, 2005. Vol. 36(1), p. 39-54.
113. Feerick, P.J., Personal conversation, Éirecomposites teo., 2008. County Galway, Ireland.
114. Lloyd's Register, *Rules and regulations for the classification of special service craft, hull construction in composite, scantling determination for mono-hull craft, part 8, chapter 3, section 1*, L.s. Register., Editor. 2009, Lloyd's Register.
115. ABS Rules for Materials and Welding – Aluminum and Fiber Reinforced Plastics (FRP), *Part 2, chapter 6, section 1*. 2006, American Bureau of Shipping.
116. Det, Norske, and Veritas, *Rules for classification of high speed, light craft and naval surface craft, pt.3 ch.4 sec. 2 and 8* D.N. Veritas, Editor. 2009, Det Norske Veritas.
117. Gibbs and Cox, I., *Marine design manual for fiberglass reinforced plastics*. 1960, New York. McGraw-Hill,

118. Dulieu-Barton, J., Earl, J., and Sheno, R., *Determination of the stress distribution in foam-cored sandwich construction composite tee joints*. The Journal of Strain Analysis for Engineering Design, 2001. Vol. 36(6), p. 545-560.
119. Sheno, R.A. and Violette, F.L.M., *A study of structural composite tee joints in small boats*. Journal of Composite Materials, 1990. Vol. 24(6), p. 644-666.
120. Stickler, P.B., Ramulu, M., and Johnson, P.S., *Experimental and numerical analysis of transverse stitched t-joints in bending*. Composite Structures, 2000. Vol. 50(1), p. 17-27.
121. Stickler, P.B. and Ramulu, M., *Investigation of mechanical behavior of transverse stitched t-joints with pr520 resin in flexure and tension*. Composite Structures, 2001. Vol. 52(3-4), p. 307-314.
122. Dodkins, A.R., Sheno, R.A., and Hawkins, G.L., *Design of joints and attachments in frp ships' structures*. Marine Structures, 1994. Vol. 7(2-5), p. 365-398.
123. Theotokoglou, E.E., *Strength of composite t-joints under pull-out loads*. Journal of Reinforced Plastics and Composites, 1997. Vol. 16(6), p. 503-518.
124. Toftegaard, H. and Lystrup, A., *Design and test of lightweight sandwich t-joint for naval ships*. Composites Part A: Applied Science and Manufacturing, 2005. Vol. 36(8), p. 1055-1065.
125. Diler, E.A., Ozes, C., and Neser, G., *Effect of t-joint geometry on the performance of a grp/pvc sandwich system subjected to tension*. Journal of Reinforced Plastics and Composites, 2009. Vol. 28(1), p. 49-58.
126. Larsson, L. and Eliasson, R.E., *Principles of yacht design*. 2007, London. Adlard Coles Nautical,
127. Kesavan, A., Deivasigamani, M., John, S., and Herszberg, I., *Damage detection in t-joint composite structures*. Composite Structures, 2006. Vol. 75(1-4), p. 313-320.
128. Theotokoglou, E.E. and Moan, T., *Experimental and numerical study of composite t-joints*. Journal of Composite Materials, 1996. Vol. 30(2), p. 190-209.
129. Gensler, R., Plummer, C.J.G., Grein, C., and Kausch, H.H., *Influence of the loading rate on the fracture resistance of isotactic polypropylene and impact modified isotactic polypropylene*. Polymer, 2000. Vol. 41(10), p. 3809-3819.
130. BARRÉ, S., CHOTARD, T., and BENZEGGAGH, M.L., *Comparative study of strain rate effects on mechanical properties of glass fibre-reinforced thermoset matrix composites*. Composites Part A: Applied Science and Manufacturing, 1996. Vol. 27(12), p. 1169–1181.
131. Greene, E., *Marine composites*. 1999, Maryland, US. Eric Greene Associates, Inc., p. 9.
132. Parlevliet, P.P., Bersee, H.E.N., and Beukers, A., *Residual stresses in thermoplastic composites--a study of the literature--part i: Formation of residual stresses*.



- Composites Part A: Applied Science and Manufacturing, 2006. Vol. 37(11), p. 1847-1857.
133. Mayer, R.M., *Design with reinforced plastics*. 1993, London. The Design Council, p. 113.
  134. van den Oever, M. and Peijs, T., *Continuous-glass-fibre-reinforced polypropylene composites ii. Influence of maleic-anhydride modified polypropylene on fatigue behaviour*. Composites Part A: Applied Science and Manufacturing, 1998. Vol. 29(3), p. 227-239.
  135. Bledzki, A.K., Reihmane, S., and Gassan, J., *Thermoplastics reinforced with wood fillers: A literature review*. Polymer-Plastics Technology and Engineering, 1998. Vol. 37(4), p. 451 - 468.
  136. Kunkel, D., *Balsa wood image at astrographics.Com*. [www.astrographics.com/GalleryPrintsIndex/GP2130.html](http://www.astrographics.com/GalleryPrintsIndex/GP2130.html), 2004.
  137. Thomason, J.L., *The influence of fibre length and concentration on the properties of glass fibre reinforced polypropylene: 5. Injection moulded long and short fibre pp*. Composites Part A: Applied Science and Manufacturing, 2002. Vol. 33(12), p. 1641-1652.
  138. Automation Creations, I.n.c., 1996-2009, MatWeb: Material Property Data. Vol. <http://www.matweb.com> (accessed on April 2009).
  139. Jakab, E., Várhegyi, G., and Faix, O., *Thermal decomposition of polypropylene in the presence of wood-derived materials*. Journal of Analytical and Applied Pyrolysis, 2000. Vol. 56(2), p. 273-285.
  140. Walker, S., *The environment, product aesthetics and surface* Design Issues, 1995. Vol. 11(3), p. 15-27.
  141. Ebnesajjad, S., *Fluoroplastics - melt processible fluoropolymers*. 2003, Norwich, NY, US. Plastics design library, p. 12.